

Changes and Causes of Rainfall Extremes over Northeast Bangladesh under the Warming World

Md. Abul Basher

DOCTOR OF PHILOSOPHY



Institute of Water and Flood Management
BANGLADESH UNIVERSITY OF ENGINEERING AND TECHNOLOGY

June 2019

Changes and Causes of Rainfall Extremes over Northeast Bangladesh under the Warming World

By

Md. Abul Basher

DOCTOR OF PHILOSOPHY



Institute of Water and Flood Management
BANGLADESH UNIVERSITY OF ENGINEERING AND TECHNOLOGY

June 2019

CERTIFICATE OF APPROVAL

We hereby recommend that the Ph.D. thesis work submitted by Md. Abul Basher, Roll No. 1014284006 F, Session: October/2014, entitled "**Changes and Causes of Rainfall Extremes over Northeast Bangladesh under the Warming World**" has been accepted as satisfactory in partial fulfillment of the requirement for the degree of Doctor of Philosophy (Ph.D.) on 29 Jun 2019.

BOARD OF EXAMINERS

- 1 

Dr. A.K.M. Saiful Islam
Professor, IWFM, BUET, Dhaka
Chairman
(Supervisor)
- 2 

Dr. Mathew Stiller Reeve
Research II, Uni Research Climate/Bjerknes
Centre for Climate Research, Bergen, NORWAY
Member
(Co-Supervisor)
- 3 

Dr. Sujit Kumar Bala
Director, IWFM, BUET, Dhaka
Member
(Ex-Officio)
- 4 

Dr. Md. Rezaur Rahman
Professor, IWFM, BUET, Dhaka
Member
- 5 

Dr. G.M. Tarekul Islam
Professor, IWFM, BUET, Dhaka
Member
- 6 

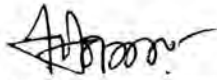
Dr. M Mozzamel Hoque
Former Professor, IWFM, BUET
92, Maszid Road, Old DOHS, Dhaka
Member
(External)
- 7 

Dr. Md. Mizanur Rahman
Superintending Engineer
BWDB, MOWR, WAPDA Building (2nd Floor)
Member
(External)

CANDIDATE'S DECLARATION

This is to certify that this work entitled “**Changes and Causes of Rainfall Extremes over Northeast Bangladesh under the Warming World**” has been done by me under the supervision of Dr. A.K.M. Saiful Islam, Professor, Institute of Water and Flood Management (IWFM), Bangladesh University of Engineering and Technology (BUET), Dhaka. I do hereby declare that this thesis or any part of it has not been submitted elsewhere for the award of any degree or diploma from any other institution.

Signature of the candidate



(Md. Abul Basher)

DEDICATED
TO MY BELOVED FAMILY

ACKNOWLEDGEMENT

Undertaking this Ph.D. has been a truly life-changing experience for me, and it would not have been possible without the support and guidance that I received from many people.

Firstly, I would like to express my heartiest gratitude to my supervisor, Dr. A.K.M Saiful Islam, Professor, IWFM, BUET, for providing me an ample opportunity to conduct my Ph.D. under his supervision. He always kept me focused on my research objectives. I appreciate Dr. A.K.M Saiful Islam for his patience and high efficiency in guiding me in a proper way of conducting this research.

Next, I would like to express my gratitude to my co-supervisor, Dr. Mathew Stiller Reeve, Uni. Research Climate, Norway, for his continuous assistance towards methodological issues needed for the success of this work. He was so patient in reading my thesis and making insightful comments.

Sincere thanks go to all members of the Doctoral Committee and Board of examiners - Dr. M. Mozzammel Hoque, former Professor, IWFM, BUET; Dr. Md. Rezaur Rahman, Professor, IWFM, BUET; Dr. Sujit Kumar Bala, Professor, IWFM, BUET, Dr. G.M. Tarekul Islam, Professor, IWFM, BUET, and Dr. Md. Mizanur Rahman, Superintending Engineer, BWDB for their insightful comments, encouragement, and the critical question which encouraged me to widen my research from various perspectives.

I want to thank my colleagues of Climate Modeling and Simulation lab, IWFM, BUET for the stimulating discussions and for all the memories we have had in the last three years. This dissertation would not have been possible without the intellectual contribution of Dr. Mohan Kumar Das and Mr. Jamal Uddin Khan, a research associate in the lab.

I am also very grateful for the TRACKS (TRansforming Climate Knowledge with and for Society) project sponsored by the Research Council of Norway for providing me all kinds of financial support for conducting this research.

The author would like to convey special thanks to the authority of the Bangladesh Water Development Board (BWDB) for giving me 3-year deputation for pursuing the Ph.D. in IWF, BUET.

I am indebted to many individuals without whose assistance, this research could not have been completed in time. I want to thank everyone who has helped me along the way.

Finally, I would like to thank my beloved parents, wife, son, and other family members for their endless love and kind support during this journey.

ABSTRACT

Northeast Bangladesh is located in the Meghna basin. The local community of northeast Bangladesh is very much concerned about the flash flood as it damages the Boro rice during the pre-monsoon season. Hence, long-term or seasonal flood prediction is essential for many management decisions in agriculture and food security, water and disaster risk reduction. El Niño–Southern Oscillation (ENSO) can be significant concerning seasonal flood prediction. They are also apprehensive about the impact of climate change on the long-term rainfall pattern, which could influence the hydro-climatic extremes like floods, droughts, and other extreme events. Therefore, this study focused on determining the changes of future rainfall extremes under the warming world and to find out if there exist any teleconnections between the pre-monsoon rainfall and large scale process e.g., ENSO.

The trends of extreme rainfall indices over northeast Bangladesh during the pre-monsoon and monsoon seasons were analyzed for the period 1984-2016. With access to the highest number of available rainfall stations in northeast Bangladesh, the trends of extreme rainfall events were investigated using the Mann-Kendall trend test and Sen's slope estimator. The Standard Normal Homogeneity and the Pettitt tests were used in appraising the quality of the data. Among seven stations, the rainfall of Sunamganj station was found inhomogeneous and was not considered for trend analysis. Most of the rainfall extremes indices showed a decreasing trend during the pre-monsoon as well as monsoon season, with the most significant reduction during the monsoon season. The total seasonal rainfall and consecutive wet days showed a decreasing trend in both seasons. The consecutive dry days (CDD) showed an increasing trend in the monsoon season only. Moreover, a decreasing trend was observed in one-day maximum rainfall (RX1), five-day maximum rainfall (RX5), the intensity of the daily rainfall over 25 mm (R25) during the pre-monsoon and 50 mm (R50) during the monsoon.

The future trend and changes in rainfall extremes for northeast Bangladesh were examined for the periods of 2041-2070 and 2071-2099. Six regional climate models (RCMs) over the coordinated regional downscaling experiment (CORDEX) South Asia domain considering two representative concentration pathways (RCPs), namely

RCP4.5 and RCP8.5, were used for this purpose. The multi-model ensemble mean of the extreme rainfall indices was generated using the Bayesian model averaging (BMA) approach. The BMA mean is a weighted average related to each RCM's predictive skill during the training period.

Most of the extreme indices showed an increasing trend during the pre-monsoon season for all future time slices except 2071-2099 for RCP4.5, while they showed a decreasing trend for the baseline period (1976-2005) for the same season. Most of the extreme indices showed a decreasing trend during the monsoon season for all future time slices, which is similar to the baseline period.

The seasonal rainfall, together with other extreme indices, is expected to increase in the future relative to the baseline period, except for a decrease of CDD during both pre-monsoon and the monsoon season. The average pre-monsoon rainfall of the study area is projected to increase by 12.93% and 18.42% under RCP4.5 for the period 2041-2070 and 2071-2099, respectively. The increase of the pre-monsoon rainfall for those periods will be 18.18%, and 23.85%, respectively under RCP8.5. The average monsoon rainfall of the study area is projected to increase by 4.96% and 2.27% under the RCP4.5 for the period 2041-2070 and 2071-2099, respectively. These increases in monsoon rainfall for that period will be 6.56% and 6.40%, respectively for RCP8.5. It was also noted that all the extreme indices except consecutive wet days (CWD) are expected to increase significantly at the 95% confidence level during the pre-monsoon season. Therefore, the study area is expected to experience more frequent floods in the future in both the pre-monsoon and monsoon seasons as a consequence of climate change. In particular, the intensity and the magnitude of the flash flood in the pre-monsoon are expected to increase in the future as the extreme indices are likely to increase significantly in the pre-monsoon season.

The present study also examined the relationship between El Niño Southern Oscillation (ENSO) and pre-monsoon rainfall, particularly in April over the Meghna basin and its response under the warming world. Firstly, the relationship between April rainfall over the Meghna basin and the heat low over central India during April was determined. The heatwave creates a low-pressure system (Cyclonic) in central India and the high-pressure system (Anticyclonic) in the Bay of Bengal. These two-systems trigger the south-westerly moisture flow from the Bay of Bengal towards the Meghalaya Mountain

region and cause heavy rainfall over the Meghna basin. The result showed that there is a high inverse correlation ($\rho > 0.55$) between April rainfall over the Meghna basin and heat low over central India during April. Considering these findings, the relationship of different ENSO indices (e.g., ESOI, SOI, ONI, MEI) for several months (e.g., January, February, and March) with April rainfall was determined. It was found that the Oceanic Niño Index (ONI) during January has the highest correlation value ($\rho=0.52$) and the maximum spatial coverage of the correlation value for which it is statistically significant ($\rho=0.32$ at the 95% confidence level) with April rainfall. It was also found that in most of the cases, floods in April occurred either during El Niño events or even neutral events but not during the La-Nina events during January. Finally, the relationship between ONI index during January and the heat low over central India during April was determined and found that there is a high inverse correlation of heatwave over central India in April with ONI index during January ($\rho=-0.55$). This infers that if the ENSO index during January is positive, there is a possibility of heat low over central India during April. On the other hand, it was shown that the heat low over central India has an impact over heavy rainfall during April over the Meghna basin. Therefore, it can be stated that the El Niño during January is related to heavy rain during April over the Meghna basin.

As ENSO would impact flash floods over the Meghna basin, how ENSO would be influenced under the warming world was also studied. The result showed that the intensity of El Niño event increases with global warming under extreme scenario while it is opposite in the case of a La Niña event. However, there is no significant change in ENSO amplitude under the warming climate. Hence, Northeast Bangladesh would experience more frequent flooding in April as the El Niño event is expected to increase remarkably in the future.

TABLE OF CONTENTS

ACKNOWLEDGEMENT.....	vi
ABSTRACT.....	viii
TABLE OF CONTENTS	xi
LIST OF TABLES	xiv
LIST OF FIGURES	xvi
ABBREVIATIONS AND ACRONYMS.....	xx
1. CHAPTER 1 INTRODUCTION.....	1
1.1. Background.....	1
1.2. The Rationale of the Study	1
1.3. Objectives and Outcomes	3
1.4. Outline of the Thesis	3
2. CHAPTER 2 LITERATURE REVIEW.....	4
2.1. Global Warming.....	4
2.2. Emission Scenario	7
2.3. GCMs and RCMs for Impact Studies	9
2.4. Uncertainties Associated in Regional Climate Projection	10
2.5. CORDEX Experiment	11
2.6. Bias Correction of RCMs	12
2.7. Observed Trends of Rainfall in Bangladesh	13
2.8. Impact of Climate Change.....	14
2.9. Mechanism of Pre-monsoon rainfall in Northeast Bangladesh	15
2.10. Flash Flood in Northeast Bangladesh	16
2.11. El Niño–Southern Oscillation (ENSO)	17
3. CHAPTER 3 STUDY AREA AND DATA.....	20
3.1. Study Area	20
3.2. Data.....	22
3.2.1. Observed data.....	22
3.2.2. Gridded data.....	22
3.2.3. Selection of the RCP scenario	23
3.2.4. Climate model data	23
3.2.5. ENSO data	25
4. CHAPTER 4 METHODOLOGY.....	26
4.1. Trend Analysis of Observed Rainfall Extremes	26

4.1.1.	Quality control of data.....	26
4.1.2.	Selection of extreme rainfall indices.....	27
4.1.3.	Identification and quantification of trends.....	29
4.2.	Projection of Future Rainfall Extremes.....	30
4.2.1.	Performance Evaluation of RCMs.....	30
4.2.2.	Bias correction of RCMs.....	31
4.2.3.	Multi-model ensemble mean.....	32
4.3.	Relationship between El Niño Southern Oscillation (ENSO) and Pre- monsoon Rainfall and its Response under the Warming World.....	34
5.	CHAPTER 5 TREND ANALYSIS OF OBSERVED RAINFALL EXTREMES.....	36
5.1.	Introduction.....	36
5.2.	Spatial Distribution of Annual and Seasonal Rainfall.....	36
5.3.	Quality control of the data.....	38
5.3.1.	Homogeneity test.....	38
5.3.2.	Autocorrelation test.....	39
5.4.	The trend of Indices of Rainfall Extremes.....	40
5.4.1.	Pre-monsoon.....	40
5.4.2.	Monsoon.....	42
5.5.	Summary.....	43
6.	CHAPTER 6 PROJECTION OF FUTURE RAINFALL EXTREMES UNDER THE WARMING WORLD.....	45
6.1.	Introduction.....	45
6.2.	Performance Evaluation of RCMs.....	45
6.3.	Quantile Mapping Bias Correction of RCMs.....	48
6.4.	Bayesian Model Averaging.....	49
6.5.	The trend of future rainfall extremes.....	53
6.6.	Changes of Future Rainfall Extremes.....	57
6.7.	Summary.....	62
7.	CHAPTER 7 RELATIONSHIP BETWEEN EI NINO SOUTHERN OSCILLATION (ENSO) AND PRE-MONSOON RAINFALL AND ITS RESPONSE UNDER THE WARMING WORLD.....	64
7.1.	Introduction.....	64
7.2.	Relationship between ENSO and pre-monsoon rainfall.....	65
7.3.	Impact of global warming on ENSO.....	71
7.4.	Summary.....	73

8. CHAPTER 8 DISCUSSIONS AND IMPLICATION OF THE RESULTS	75
8.1. Introduction	75
8.2. Implication of the results	75
9. CHAPTER 9 CONCLUSIONS AND RECOMMENDATIONS	78
9.1. Conclusions	78
9.2. Limitations of the study	80
9.3. Recommendations	81
REFERENCES	82
APPENDICES	101
Appendix A: Theory	101
Appendix B: Supplementary Figures	109

LIST OF TABLES

Table 2.1 Description of the RCPs [130].	8
Table 2.2 CORDEX domain and their zone.	11
Table 2.3 Projected change in global mean surface temperature and global mean sea level rise for the mid- and late 21st century, relative to the 1986–2005 period [78].	14
Table 2.4 Geographic extent within which different SST based indices are calculated.	18
Table 3.1 List Rainfall stations and their location.	22
Table 3.2 List of RCMs and their driving models.	24
Table 3.3 Description of the GCMS and their institution.	24
Table 4.1 List of indices of rainfall extremes used for trend analysis.	29
Table 5.1 The first order Autocorrelation coefficient for the indices of rainfall extreme for seven stations of northeast Bangladesh for the period of 1984 to 2016.	40
Table 5.2 The Sen’s Slop estimator (Q) for indices of rainfall extremes for six stations of northeast Bangladesh for the period of 1984 to 2016. The slopes corresponding to statistically significant Zs in Fig 5.4 are underlined.	41
Table 6.1 Seasonal rainfall for Sylhet station before and after bias correction.	49
Table 6.2 Normalized Root Mean Square Error (NRMSE) for seasonal rainfall of different RCMs, Arithmetic Ensemble Mean (AEM) and BMA during the historical period (1976-2005).	52
Table 6.3 Sens’s slope estimator of rainfall extremes considering all model ensemble mean derived by BMA for two future time slices (2041-2070 and 2071-2099 under RCP 4.5 and RCP 8.5 scenarios for Pre-monsoon. The corresponding Sen's slopes of the extreme indices which were significantly increased or decreased in Fig 6.8 were made bold and underlined.	55
Table 6.4 Sense slope estimator of rainfall extremes considering all model ensemble mean derived by BMA for two future time slices (2041-2070 and 2071-2099 under RCP 4.5 and RCP 8.5 scenarios for monsoon. The corresponding Sen's slopes of the extreme indices which were significantly increased or decreased in Fig 6.9 were made bold and underlined.	57

Table 6.5 p-values of average changes of rainfall extremes over the study area considering all model ensemble mean in different RCP scenarios using Mann–Whitney U test. The extreme indices which changed significantly at 95 % confidence level (p-value ≤ 0.05) are bold and underlined.61

LIST OF FIGURES

Fig 2.1 Observed global mean combined land and ocean surface temperature anomalies, from 1850 to 2012 from three data sets. Top panel: annual mean values. Bottom panel: decadal mean values, including the estimate of uncertainty for one dataset (black). Anomalies are relative to the mean of 1961–1990. (b) Map of the observed surface temperature change from 1901 to 2012 derived from temperature trends determined by linear regression from one dataset (orange line in panel a) [77].	5
Fig 2.2 Maps of observed precipitation change from 1901 to 2010 and from 1951 to 2010 [77].	6
Fig 2.3 Global mean sea level relative to the 1900–1905 mean of the longest-running dataset, and with all datasets aligned to have the same value in 1993, the first year of satellite altimetry data. All time-series (colored lines indicating different data sets) show annual values, and were assessed, uncertainties are indicated by colored shading [77].	7
Fig 2.4 Representative Concentration Pathways. (a) Changes in radiative forcing relative to pre-industrial conditions and (b) Energy and industry CO ₂ emissions for the RCP candidates [130].	9
Fig 2.5 Schematic description of the large-scale ocean-atmosphere interactions during the development of ENSO Phases. (a) El Niño, (b) Normal condition and (c) La Niña [60].	17
Fig 3.1 Study area with rainfall stations.	20
Fig 3.2 Meghna river system.	21
Fig 3.3 Different ENSO indices used for this study.	25
Fig 4.1 Histogram and gamma pdf for monthly rainfall of Sylhet station (a) Pre-monsoon and (b) monsoon.	33
Fig 5.1 Spatial distribution of mean rainfall of the study area for (a) Pre-monsoon, (b) Monsoon and (c) Annual.	37
Fig 5.2 The Box-and-Whisker plot of the spatiotemporal variation of rainfall of northeast Bangladesh for the period of 1984 to 2016.	38

Fig 5.3 The Test statistics of homogeneity test for annual rainfall for seven stations in the northeast of Bangladesh for the period of 1984 to 2016 (a) SNHT test (b) Pettit test.	39
Fig 5.4 The normalized test statistic (Z_s) for the Mann-Kendall test of the indices of rainfall extremes of six stations of northeast Bangladesh for the period of 1984 to 2016: (a) Pre-Monsoon and (b) Monsoon. The absolute Z_s value which, is higher than the critical value ($Z_c=1.96$) are considered as statistically significant at 95% confidence level.....	41
Fig 6.1 Normalized bias for different RCMs with respect to observed station rainfall during the period of 1976-2005 for (a) Pre-monsoon and (b) monsoon.....	46
Fig 6.2 Normalized RMSE for different RCMs with respect to observed station rainfall during the period of 1976-2005 for (a) Pre-monsoon and (b) monsoon.....	47
Fig 6.3 Q-Q Plot for Sylhet station during 1976-2005 for (a) Pre-monsoon and (b) Monsoon.	47
Fig 6.4 Quantile-quantile plots for the uncorrected (colored marker) and corrected (black marker) of simulated daily rainfall by RCMs against observed daily rainfall for Sylhet: (a) Pre-monsoon and (b) Monsoon.....	48
Fig 6.5 Marginal posterior pdf of the DREAM derived BMA weights of monthly rainfall totals for pre-monsoon of Sylhet station. The MCMC derived solution is separately indicated in each panel with symbol 'X'.....	50
Fig 6.6 Marginal posterior pdf of the DREAM derived BMA weights of monthly rainfall totals for the monsoon of Sylhet station. The MCMC derived solution is separately indicated in each panel with symbol 'X'.....	50
Fig 6.7 BMA weights of each RCM for monthly rainfall totals of different stations during the historical period (1976-2005): (a) Pre-monsoon and (b) Monsoon.....	51
Fig 6.8 The normalized test statistic (Z_s) of the Mann-Kendall test of the indices of rainfall extremes considering all model ensemble mean derived by BMA for pre-monsoon: (a) RCP 4.5(2041-2070),(b)RCP4.5(2071-2099),(c)RCP8.5(2041-2070),(d) RCP8.5(2071-2099). (The absolute Z_s value which is higher than the critical value ($Z_c=1.96$) are considered as statistically significant at 95% confidence level.	54
Fig 6.9 The normalized test statistic (Z_s) of the Mann-Kendall test of the indices of rainfall extremes considering all model ensemble mean derived by BMA for monsoon: (a) RCP 4.5(2041-2070),(b)RCP4.5(2071-2099),(c)RCP8.5(2041-2070),(d)	

RCP8.5(2071-2099). (The absolute Zs value which is higher than the critical value ($Z_c=1.96$) are considered as statistically significant at 95% confidence level.	56
Fig 6.10 Box and whisker plots for changes of rainfall extremes of Sylhet station considering all RCMs for two future time slices (2041-2070 and 2071-2099) relative to the baseline period (1976-2005) under RCP 4.5 and RCP 8.5 scenarios: (a) Pre-monsoon and (b) Monsoon.	58
Fig 6.11 Box and whisker plots for changes of rainfall extremes over the study area considering all model ensemble mean derived by BMA for two future time slices (2041-2070 and 2071-2099) relative to the baseline period (1976-2005) under RCP 4.5 and RCP 8.5 scenarios: (a) Pre-monsoon and (b) Monsoon.....	59
Fig 6.12 Average changes of rainfall extremes over the study area considering all model ensemble mean derived by BMA for two future time slices (2041-2070 and 2071-2099) relative to the baseline period (1976-2005) under RCP 4.5 and RCP 8.5 scenarios: (a) Pre-monsoon and (b) Monsoon.	60
Fig 7.1 Average Wind flow direction during some flooding event in April: (a) April 9 to April 19, 2004; (b) April 1 to April 4, 2010; (c) April 20 to April 30, 2016, and (d) April 1 to April 4, 2017. The low-pressure zone is marked with a solid red circle, and the high-pressure zone is marked with a dashed red circle.....	66
Fig 7.2 Average Wind flow direction during some non-flooding event in April: (a) April 1 to April 30, 2008, and (b) April 1 to April 30, 2014.	67
Fig 7.3 Correlation between MSL pressure and April rainfall over Cherrapunji during the year 1979 to 2017.....	67
Fig 7.4 Correlation between April rainfall and different ENSO index for the period 1979 to 2017: (a) SOI for December; (b) SOI for January; (c) SOI for February; (d) ESOI for December; (e) ESOI for January; (f) ESOI for February; (g) ONI for December; (h) ONI for January; (i) ONI for February; (j) MEI for December; (k) MEI for January and (l) MEI for February. The study area in which the correlation value is statistically significant ($p\text{-value} \leq 0.05$) is shaded with red color.	69
Fig 7.5 Normalized rainfall anomaly for Cherrapunji during April and ONI Index for January during the year 1979 to 2017. The red level of the points indicates the flooding year in April.	70
Fig 7.6 Correlation between ONI during January and EHF over central India during April.....	71

Fig 7.7 Relative change of ENSO intensity for all month under warming world with respect to the baseline.	72
Fig 7.8 Relative change of ENSO intensity for January under the warming world with respect to the baseline.	72
Fig 7.9 Relative change of ENSO amplitude under warming world with respect to the baseline.	73

ABBREVIATIONS AND ACRONYMS

AEM	Arithmetic Ensemble Mean
AGCM	Atmospheric General Circulation Model
AOGCM	Atmosphere-Ocean General Circulation Model
AR5	Fifth Assessment Report
BMA	Bayesian Model Averaging
BMD	Bangladesh Meteorological Department
BR	Buishand Range
BWDB	Bangladesh Water Development Board
CDD	Consecutive Dry Days
CDF	Cumulative Distribution Functions
CMIP5	Coupled Model Inter-comparison Project Phase 5
CORDEX	Coordinated Regional Downscaling Experiment
CWD	Consecutive Wet Days
DREAM	Differential Evolution Adaptive Metropolis
ECMWF	European Centre for Medium-Range Weather Forecasts
EHF	Excessive Heat Factor
ENSO	El Niño–Southern Oscillation
eQM	Empirical Quantile Mapping
ESOI	Equatorial Southern Oscillation Index
FFWC	Flood Forecasting and Warning Center
GCM	General Circulation Model
GDP	Gross Domestic Product
GHGs	Greenhouse Gases
gpQM	Gamma and Generalized Pareto Distribution
gQM	Gamma Quantile Mapping
IPCC	Intergovernmental Panel on Climate Change
IS92	1992 IPCC scenario
JMA	Japan Meteorological Agency
LOCI	Local Intensity Scaling
MEI	Multivariate ENSO Index
NRMSE	Normalized Root Mean Square Error
OGCM	Oceanic General Circulation Model
ONI	Oceanic Niño <i>Index</i>
PDFs	Probability Density Functions
PRCPTOT	Total Precipitation
RCD	Regional Climate Downscaling
RCMs	Regional Climate Models
RCPs	Representative Concentration Pathways
RMSE	Root Mean Square Error
RX1	One-day maximum Rainfall
RX5	Five-day maximum Rainfall
SA90	1990 IPCC scenario A

SDII	Daily Intensity Index
SNHT	Standard Normal Homogeneity Test
SOI	Southern Oscillation Index
SRES	Special Report on Emission Scenarios
SST	Sea Surface Temperature
TNI	Trans- Niño Index
TRACKS	Transforming Climate Knowledge with and for Society
UNFCC	United Nations Framework Convention on Climate Change
VNR	Von Neumann Ratio
WCRP	World Climate Research Program

CHAPTER 1

INTRODUCTION

1.1. Background

Climate change is a significant concern and should be considered as one of the most critical environmental issues faced in the world today [78]. Anthropogenic and natural factors contribute to variations in climate. Combustion of fossil fuels and land-use change are the primary anthropogenic activities responsible for changes in atmospheric concentrations of greenhouse gases (GHGs) and the energy balance in the climate system. On the other hand, the natural factor such as El Niño-Southern Oscillation (ENSO), volcanic eruptions, and variation of solar radiation as well as the orbital change of the earth also contribute to climate change [78].

Greenhouse gases such as carbon dioxide (CO₂), methane (CH₄) and nitrous oxide (N₂O) have increased in the atmosphere in significant quantities during recent centuries [77,112,207]. Therefore, the average atmospheric temperature and sea levels have been rising since the 19th century. Several observations have confirmed the increase in ocean surface temperature; shrinkage of polar ice; the development of polar glaciers and icebergs since the 1950s [181,196].

Global climate change is arguably changing rainfall patterns in different regions of the world, with far-reaching environmental, social, and economic impacts for the local communities. One of the notable change can be to the frequency and severity of the extreme rainfall events, which can exacerbate the risks of climate-related damages in a region. As rainfall patterns are specific to different regions, any changes in rainfall brought by the global climatic change will be similarly specific [198]. For this reason, communities need high-quality scientific information on historical trend and future trend in rainfall extremes. They can use this information for adapting to changes in the rainfall relative to both current climate variability and future climatic change [131].

1.2. The Rationale of the Study

Among the meteorological variables, rainfall is a significant concern for northeast Bangladesh [20]. Heavy rainfall in the adjacent mountainous region of India causes a flash flood during pre-monsoon and prolongs riverine flood during the monsoon. During the pre-monsoon season, the region receives more than 900 mm rainfall, which is three times higher than the average rainfall of the whole country. The pre-monsoon

rainfall is also characterized by severe local storms known as nor' Westers (*Kalbaishaki*). These storms bring heavy rain, hail, gusty wind, lightning, and sometimes tornadoes [133,214]. The sudden intrusion of the flash flood may damage the agricultural production from about 0.33 million ha, worth TK 3486 million or 3% of the national agricultural contribution to the gross domestic product (GDP) [62]. The pre-monsoon flash floods can damage the seasonal Boro rice, which is the main crop of the region [6]. Such events severely impact individual farmers, families, communities, and the region's food security. Therefore, a dedicated early flash flood warning system is not only urgent for the survival of the people living here but also necessary for saving the economy of the country.

At present, the Flood Forecasting and Warning Center (FFWC) of the Bangladesh Water Development Board (BWDB) produce only short-term forecasts with (3-day lead time). The short-term flash flood forecast may be very useful in harvesting the crop early even before full maturity to capture at least part of it by the farmers. Seasonal flood forecasts can be helpful in many management decisions in agriculture and food security, water, and disaster risk reduction. To find a teleconnection between the weather of a region and ENSO can be significant concerning to seasonal flood forecast. Several studies on the relationship between the Indian summer monsoon and ENSO have been conducted over the years [34,79,83,92,94,103,107,108,173,192]. However, no study has been conducted to determine the relationship between ENSO and pre-monsoon rainfall in the Meghna Basin, which includes northeast Bangladesh. If there is a teleconnection between ENSO and the pre-monsoon rainfall over the Meghna basin, it will help provide seasonal flash flood forecasting of the region.

Bangladesh is ranked as one of the most climate-vulnerable countries in the world. It is at extreme risk of floods, tropical cyclones, sea-level rise, and drought, all of which could drive millions of people to migrate [53]. Bangladesh is already experiencing climate-induced hazards like storm surge, flood, and drought. Northeast Bangladesh is experiencing a remarkable decreasing trend of annual precipitation during the last decades [15]. Climate change is likely to influence the hydrological cycle in northeast Bangladesh. If the policy-makers and local communities want to plan for changes in extreme rainfall, they need knowledge about future rainfall variability. Therefore, it is

essential to understand the pattern of the regional rainfall variation and its past and future trend.

1.3. Objectives and Outcomes

The main objective of this study is to understand how the rainfall extremes in northeast Bangladesh may change in the future and how this rainfall is connected to large-scale processes like ENSO.

To accomplish the main objective, the following specific objectives will be achieved by this study:

- To analyze the trend of observed rainfall extremes in the northeast of Bangladesh;
- To investigate the performance of regional climate models (RCMs) to reproduce characteristic rainfall patterns;
- To generate multi-model ensemble mean of the future rainfall extremes from RCMs under the newly developed representative concentration pathways (RCPs) for the study area;
- To determine the relationship between El Niño Southern Oscillation (ENSO) and pre-monsoon rainfall over the Meghna basin and its response under the warming world.

The possible outcomes of this study will be to understand how the rainfall extremes in the study area are expected to be impacted due to climate change. It will be helpful to understand how the large-scale process like ENSO is connected to pre-monsoon rainfall over the Meghna basin, particularly in northeast Bangladesh. It will also be beneficial for seasonal flood forecasting.

1.4. Outline of the Thesis

This thesis contains nine chapters. The organization of the chapters is as follows:

Chapter 1 provides the background and rationale of the study. It also mentions the objectives of the study. A literature review on global warming, emission scenarios, the previous studies on historical trend & the future projection of rainfall of the study area, ENSO is discussed in Chapter 2. The study area & data and the methodologies are described in Chapter 3 and 4, respectively. Chapters 5 to 7 details the results and discussions found in this study. Chapter 8 presents the discussions and implications of the results of the study. Finally, Chapter 9 draws the conclusions and limitations of the study. It also provides recommendations for further studies.

CHAPTER 2

LITERATURE REVIEW

2.1. Global Warming

Global warming or climate change is defined as the long-term changes in weather condition. It may be observed in both average conditions and extreme events [76]. The world climate is mainly determined by solar radiation. When the amount of incoming solar radiation (shortwave) equals the outgoing radiation (longwave), the earth surface temperature remains the same. The key driver of the climate change is the trapping of the outgoing solar radiation into the atmosphere because of increased concentrations of aerosols, clouds, and greenhouse gases in the atmosphere while the incoming solar radiation has remained the same [77].

Both the anthropogenic (such as greenhouse gas emissions from fossil fuel burning, land-use change, waste management, deforestation) and natural (such as solar radiation, volcanic eruption, ENSO) sources are responsible for global warming. However, the anthropogenic sources have been found more responsible than other sources for climate change [72,75]. The most significant human influence has been the emission of greenhouse gases such as carbon dioxide, methane, and nitrous oxide. Carbon dioxide is a crucial GHGs, which has increased significantly since the industrial revolution primarily for increased consumption of fossil fuels and rapid land-use change. The atmospheric concentration of CO_2 in 2005 was higher than experienced in the past 6,50,000 years, and its growth rate is continuously increasing every year [75].

The effect of climate change mostly occurs in the atmosphere, on land surfaces, in the oceans, and on land glaciers. In situ observations and glacier explorations reveal the significant increase of greenhouse gases in the atmosphere during recent centuries [77, 78,112,207]. Several observations have revealed an increase in temperatures on land and ocean surfaces that started over one hundred years ago. The global (land and ocean) surface temperature has increased by $0.85^{\circ}C$ over the period 1880-2012 confirmed by multiple independently produced datasets [77,78] (Fig 2.1).

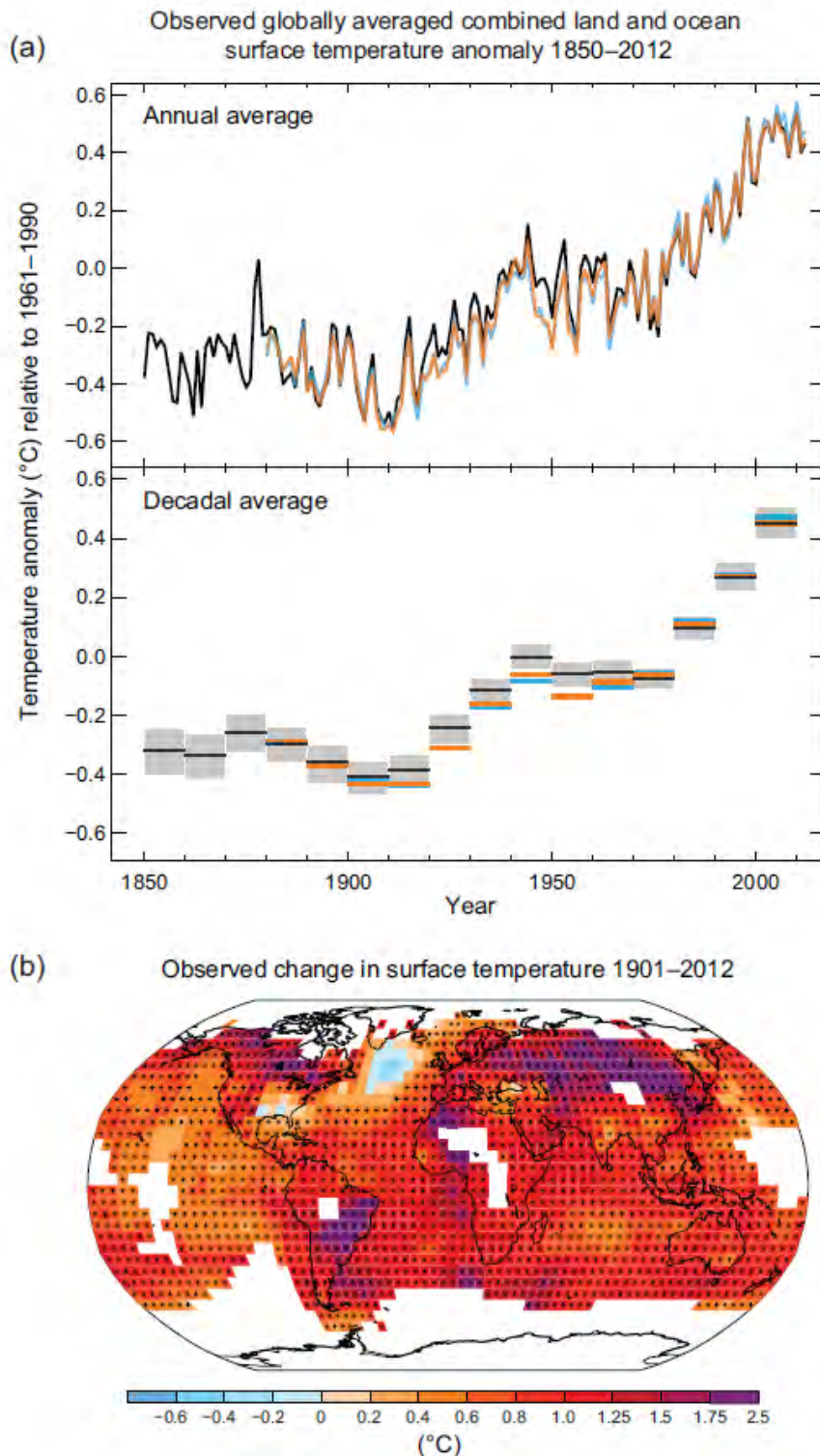


Fig 2.1 Observed global mean combined land and ocean surface temperature anomalies, from 1850 to 2012 from three data sets. Top panel: annual mean values. Bottom panel: decadal mean values, including the estimate of uncertainty for one dataset (black). Anomalies are relative to the mean of 1961–1990. (b) Map of the observed surface temperature change from 1901 to 2012 derived from temperature trends determined by linear regression from one dataset (orange line in panel a) [77].

Earth's average surface temperature rose by 0.74 ± 0.18 °C in the period from 1906 to 2005. The rate of warming almost doubled in the last half of that period (0.13 ± 0.03 °C per decade, against 0.07 ± 0.02 °C per decade) [75]. Several observations have confirmed the increase of ocean surface temperature, shrinkage of polar ice, and development of polar glaciers and icebergs since the 1950s [181,196].

Precipitation has increased over the mid-latitude land areas of the Northern Hemisphere since 1901 (medium confidence before and high confidence after 1951 (Fig 2.2). There is an area-averaged long-term positive or negative trends have low confidence for other latitudes [77]. The extreme weather and climate events have changed since 1950. It is very expected that the number of cold days and nights has reduced while the number of hot days and nights has increased on the global scale. It is expected that the frequency of heatwaves has increased in large parts of Europe, Asia, and Australia. There are expected heavy precipitation events has increased in most of the land region [77]. The frequency or intensity of heavy precipitation events has likely increased in North America and Europe, while in other continents, there is medium confidence in changes of it [77].

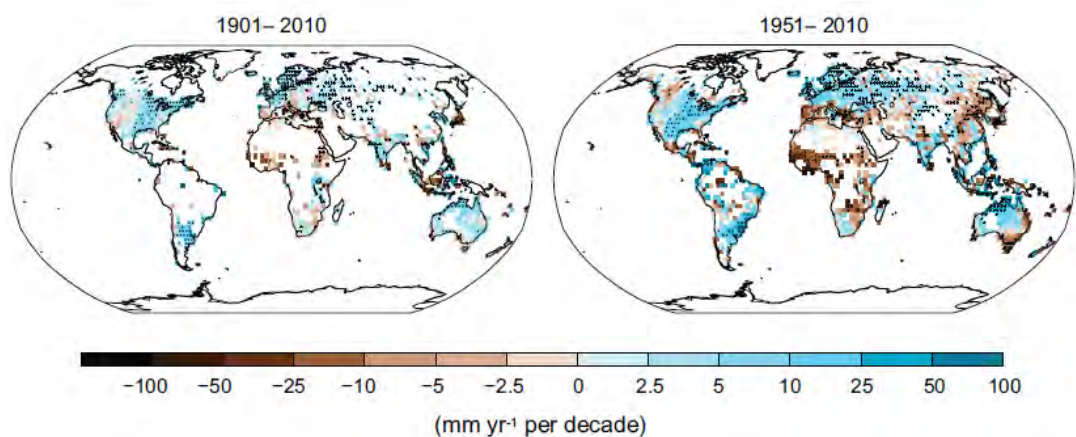


Fig 2.2 Maps of observed precipitation change from 1901 to 2010 and from 1951 to 2010 [77].

The sea level has risen at a higher rate since the mid-19th century than the previous two millennia. It rose by 1.7 mm/year, 2.0 mm/year and 3.2 mm/year between 1901 and 2010, between 1971 and 2010 and between 1993 and 2010, respectively (Fig 2.3). The frequency of the flood and drought event has also been reported to change. Since 1950, the frequency of the drought has increased in Southern Europe and West Africa, while

it has decreased in central North America and northwestern Australia [76]. Though the impact of climate change on the trend on historical flooding has not been identified yet, the shift in the timing of spring peak flows is observed. Moreover, global and continental-scale studies project an increase in flood hazard worldwide. However, it is expected to decrease for central to western Eurasia and northern parts of North America [40, 68].

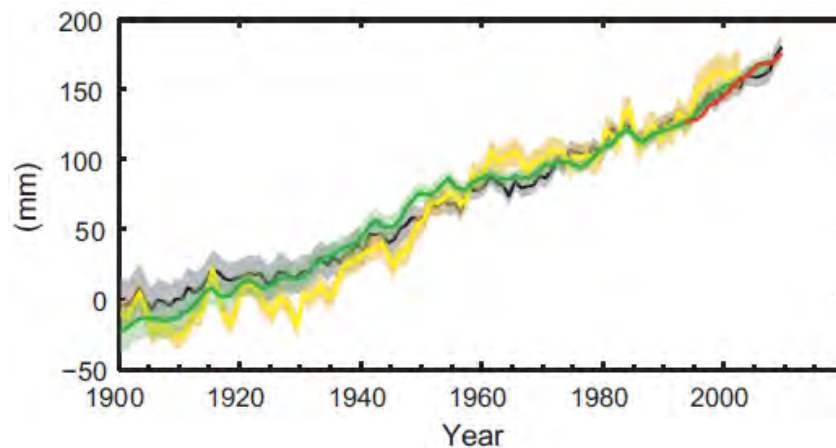


Fig 2.3 Global mean sea level relative to the 1900–1905 mean of the longest-running dataset, and with all datasets aligned to have the same value in 1993, the first year of satellite altimetry data. All time-series (colored lines indicating different data sets) show annual values, and were assessed, uncertainties are indicated by colored shading [77].

2.2. Emission Scenario

Climate change impact assessment involves the simulation of future climate generated by climate models using different scenarios of socio-economic and physical processes [125]. The objective of generating a scenario is to better understand the uncertainties for reaching a robust decision under a wide range of future climates [115]. The development of scenarios in climate change research based on socio-economic scenarios such as projections of population, demographics, economic growth, energy supply and demand, land use, and technological developments. These socio-economic scenarios are used as input for complex socio-economic models to estimate emissions scenarios of GHGs.

Intergovernmental Panel on Climate Change (IPCC) established several emissions scenarios over the times such as the 1990 IPCC scenario A (SA90), the 1992 IPCC scenario (IS92), the Special Report on Emission Scenarios (SRES) and Representative

Concentration Pathways (RCP). RCP is the new emission scenarios adopted in 2014 by the IPCC for its Fifth Assessment Report (AR5). These new emission scenarios define four possible future climates based on the amount of greenhouse gases are emitted in the upcoming years. The four RCPs such as RCP2.6, RCP4.5, RCP6, and RCP8.5, are named after a possible range of radiative forcing values in the year 2100 relative to pre-industrial values [209]. A detail description of the four RCPs is provided in Table 2.1 and Fig 2.4. They illustrate how the selected RCPs represents the literature in terms of radiative forcing.

RCPs use a parallel approach in the development of its scenarios. In a parallel approach, the socio-economic scenarios are not the starting point for the RCPs. It begins with the identification of essential characteristics for scenarios of radiative forcing for climate modeling. The most prominent of which is the level of radiative forcing in the year 2100 [130]. This parallel approach allows for socio-economic, emissions, and climate scenarios to be developed in parallel with each other. In this way, changes can be made to one individual scenario without having to restart the whole sequence. RCP emission scenarios are used in the Coupled Model Inter-comparison Project Phase 5 (CMIP5) multi-model experiment under the World Climate Research Program (WCRP) for projecting the future climate scenarios.

Table 2.1 Description of the RCPs [130].

Scenario	Radiative forcing (Wm^{-2})	CO_2 equivalent Concentration (p.p.m.)	Pathway	Model providing RCP*
RCP2.6	3.0	490	Peak before 2100 and then decline	MESSAGE
RCP4.5	4.5	650	Stabilization after 2100	AIM
RCP6	6.0	850	Stabilization after 2100	GCAM
RCP8.5	8.5	1370	Rising	IMAGE

* MESSAGE, Model for Energy Supply Strategy Alternatives and their General Environmental Impact, International Institute for Applied Systems Analysis, Austria; AIM, Asia-Pacific Integrated Model, National Institute for Environmental Studies, Japan; GCAM, Global Change Assessment Model, Pacific Northwest National Laboratory, USA (previously referred to as MiniCAM); IMAGE, Integrated Model to Assess the Global Environment, Netherlands Environmental Assessment Agency, The Netherlands.

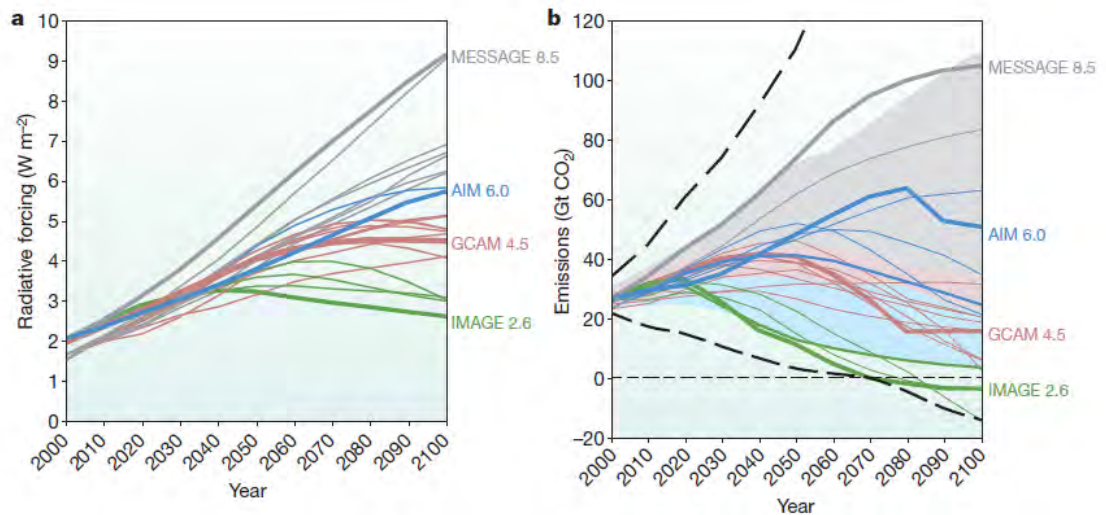


Fig 2.4 Representative Concentration Pathways. (a) Changes in radiative forcing relative to pre-industrial conditions and (b) Energy and industry CO₂ emissions for the RCP candidates [130].

2.3. GCMs and RCMs for Impact Studies

The general circulation model (GCM) represents the physical processes in the atmosphere, ocean, cryosphere, and land surface [139]. It uses the Navier–Stokes equations on a rotating sphere with thermodynamic terms of various energy sources (radiation, latent heat). Atmospheric and Oceanic GCMs (AGCM and OGCM) are vital components along with sea ice and land-surface components. It simulates the climate using a 3-dimensional grid over the globe with a horizontal resolution of between 250 and 600 km and 10 to 20 vertical layers in the atmosphere [199]. It is an essential tool for projecting future climate variables using emission scenarios. However, because of the coarse spatial resolution, the direct use of GCMs output is limited since it cannot adequately model many physical processes related to clouds [223]. Instead, their known properties must be averaged over the larger scale in a technique known as parameterization. GCMs has a limitation to simulate various feedback processes such as water vapor and warming; clouds and radiation; ocean circulation and ice and snow albedo [113].

The regional climate model (RCM) is dynamically downscaled from GCM, and it uses GCM grid-point data as the boundary conditions [13]. Dynamic downscaling provides information at a much better spatial resolution (0.5 degrees) which can be used as inputs to basin-scale hydrological models. RCMs represent an advantage over GCM data for representing small-scale processes since RCM simulations are more realistic when

scaled, in comparison to GCM simulation data [32]. However, the spatial resolution of RCMs remains too coarse for some applications and still represents spatial averages, rather than local extremes [13].

2.4. Uncertainties Associated in Regional Climate Projection

There are three key sources of uncertainty in climate projection, such as GHG emission scenarios, Atmosphere-Ocean General Circulation Model (AOGCM) configuration, and AOGCM internal variability [59]. Uncertainty in GHG emission scenarios can be examined by simulating different emission scenarios; uncertainty in AOGCM configuration can be explored by using different AOGCMs or different model configurations (e.g., physics parameters) within the same modeling system; and uncertainty in AOGCM internal variability can be examined by executing different realizations of the same scenario each using different initial conditions [59]. However, for regional climate projections, there arise four additional sources of uncertainty such as regional climate downscaling (RCD) configuration, RCD internal variability, RCD method, and region of interest. The uncertainty in RCD configuration can be explored in a similar way to AOGCM configuration. The uncertainty in RCD internal variability can be examined in a similar way to AOGCM internal variability. The uncertainty in the region of interest can be tested by applying the RCD models to different regions.

AOGCM configuration is one of the most significant sources of uncertainty in climate projections since it accumulates all sources of uncertainties such as GHG emission scenarios, model internal variability, and non-linearities in the climate system and for the choice of RCD method [1]. Several studies have shown that the uncertainty in AOGCM configuration and GHG emission scenarios are the primary sources of uncertainty in climate change projections for longer timescales whereas the uncertainty in AOGCM internal variability is most vital on shorter timescales [59].

The uncertainties in regional climate change projections need to be described entirely to provide useful information for impact assessment studies. Sometimes it needs to be reduced where possible. All the relevant uncertainty dimensions can be scrutinized by generating ensembles of simulations. The probability density functions (PDFs) of climatic variables of interest can be generated in order to capture all ranges of uncertainty. The spread of the PDF gives a measure of uncertainty. The uncertainty space of climate change projection can be sampled and examined more effectively if

the ensembles are relatively larger. However, it is a challenging task to capture all the ranges of uncertainties since it needs the completion of a large number of a multidimensional matrix of experiments [1,58].

2.5. CORDEX Experiment

The Coordinated Regional Climate Downscaling Experiment (CORDEX) initiated by the World Climate Research Program (WCRP) to guide a coordinated international framework for producing improved regional climate change projections [136]. The CORDEX framework aims to provide a benchmark for evaluating and possibly improving models (model evaluation framework) together with exploring the maximum range of the source of uncertainties through a set of experiments to produce climate projections for impact and adaptation studies [136].

Table 2.2 CORDEX domain and their zone.

Domain	Zone
1	South America
2	Central America
3	North America
4	Africa
5	Europe (EURO)
6	South Asia
7	East Asia
8	Central Asia
9	Australasia
10	Antarctica
11	Arctic
12	Mediterranean (MED)
13	Middle East North Africa (MENA)
14	South-East Asia (SEA)

Initially, in the CORDEX framework, there were twelve regions, covering the majority of the populated land areas worldwide, plus both the Arctic and Antarctic [138] (Table 2.2). Afterward, WCRP included two new CORDEX domains for Arab and South-East Asia. This selection of a domain is based partly on physical processes in different regions, resources needed for the simulations and the availability of ongoing programs. Initially, about 50 km (or 0.5 degrees) standard horizontal resolution was selected for the first phase CORDEX simulations in order to allow worldwide participation [138]. However, at present, many groups are simulating RCMs with substantially higher grid spacing (up to ~10 km).

In the model evaluation framework, similar boundary condition was used for a selected domain to evaluate the performance RCMs. Initially, the CORDEX framework utilized the European Centre for Medium-Range Weather Forecasts (ECMWF) ERA-Interim re-analysis covering the period of 1989-2007. The climate projection framework is based on the set of new GCMs supporting the IPCC Fifth Assessment Report (i.e., GCMs from CMIP5). A large number of experiments were included in this simulation setup considering new GHG scenarios for the 21st century, decadal prediction experiments, experiments, including the carbon cycle and experiments aimed at investigating specific feedback mechanisms [184].

2.6. Bias Correction of RCMs

The state-of-the-art climate data from RCMs have been used for climate change impact studies. However, it is well established that the precipitation data from RCMs are biased because of limited process understanding or insufficient spatial resolution [106]. Therefore, the output from RCMs needs to be corrected before applying for climate change impact studies [35,106,119,187,208]. In recent years, extensive studies have investigated different bias correction methods for providing a reliable estimate of observed precipitation climatology given RCM output [27,74,106,171,188,191,194].

The simplest method is the delta correction method, in which an average bias (delta) for a specified period is used to correct the bias [120]. This bias correction can be done either as one delta for the whole period considered or for different steps like seasonal or monthly deltas. Another approach calculates monthly correction factors that are based on the ratio between observed and simulated values in the past [120].

A linear transformation function between one or more predictors and the predictand is used in multiple linear regression methods [65, 70,189]. This method is used to adjust mean and variance only of the observed and simulated rainfall. The Local Intensity Scaling (LOCI) method can adjust the mean as well as both wet-day frequencies and wet-day intensities of precipitation time series [171,189].

The power transformation method corrects the mean and variance of precipitation by applying a non-linear correction in an exponential form [101,102,189]. Here, the observed long-term monthly mean is mapped on the monthly mean of the corrected daily simulated precipitation series.

A somewhat modern approach called distribution mapping in which the distribution of RCM simulated climate data is matched with the distribution of the observed climate data to correct the distribution of the RCM simulated climate data. A transfer function is generated to shift the occurrence distributions of precipitation and temperature [22,168,174]. In the literature, it can be found in several other names such as ‘probability mapping’ [18, 74], ‘quantile-quantile mapping’ [19, 44, 82,168,182], ‘Statistical downscaling’ [146] and ‘histogram equalization’ [161,174,211]. Based on adjusting the probability distribution, the quantile mapping method is sub-classed as Empirical Quantile Mapping (eQM), Parametric Quantile Mapping (gamma distribution, gQM) and a Special case of Parametric Quantile Mapping (gamma and Generalized Pareto Distribution, gpQM).

Among various methods, distribution mapping-based methods are getting more popular lately and have been applied to the downscale and correct temperature and precipitation data from RCMs [11, 45, 47,146, 168, 190], particularly in hydrological studies.

2.7. Observed Trends of Rainfall in Bangladesh

Trend analysis of observed rainfall is essential for water resources planning and management [183]. Therefore, trend analysis of extreme rainfall events is getting importance in recent years [17,106]. Studies in different parts of the world indicate that climate change has altered precipitation patterns resulting with resulting frequent extreme weather events, such as floods, droughts, and rainstorms [39,170,183, 218]. Studies on historical rainfall record show that annual and seasonal rainfall in India has decreased [14,109].

Previous studies have either considered Bangladesh [2,154] or India [80,127,143] separately. These studies often consider trends in seasonal (including pre-monsoon and monsoon) or annual rainfall. The trends vary between positive [42, 98] and negative [41,99,127], depending on the region and the time period analyzed, but none has been statistically significant. All the studies in northeast Bangladesh used rainfall for the Sylhet station only. These studies have shown increasing trends for pre-monsoon and a decreasing trend for the monsoon [92,176], which is similar to most studies over India. However, total seasonal or annual rainfall is just one rainfall characteristic that can change. Fewer studies have looked at changes in other characteristics. For example, [176] found an insignificant increase of one-day maximum rainfall while a decrease of

five-day maximum rainfall, consecutive wet day and consecutive dry day for the Sylhet station for the last sixty years (1958-2007). Over the border in India, [150] found that low-intensity rainfall has decreased and high-intensity rainfall had increased in Cherrapunji, but only during the pre-monsoon. These results imply less, but more intense rainy days over the region. By comparison, the Barak Basin further east seems to have experienced an increase in the number of pre-monsoon rainy days [98].

2.8. Impact of Climate Change

Average global surface temperature and mean sea level rise are likely to increase over the 21st century under all emission scenarios (see Table 2.3). Heat waves will occur more often and last longer, and extreme precipitation events will become more intense and frequent in many regions [78]. Multi-model projections of global climate model indicate that there is likely to be frequent severe hydro-climatic extremes like floods, droughts, and other extreme events in the future because of climate change [71,103,135,167].

Table 2.3 Projected change in global mean surface temperature and global mean sea level rise for the mid- and late 21st century, relative to the 1986–2005 period [78].

Scenarios		2046-2065		2081-2100	
		Mean	Likely range	Mean	Likely range
Global Mean Surface Temperature Change (°C)	RCP2.6	1.0	0.3-1.7	1.0	0.3-1.7
	RCP4.5	1.4	1.1-2.6	1.8	1.1-2.6
	RCP6.0	1.3	1.4-3.1	2.2	1.4-3.1
	RCP8.5	2.0	2.6-4.8	3.7	2.6-4.8
Global Mean Sea Level Rise (m)	RCP2.6	0.24	0.17-0.32	0.40	0.26-0.55
	RCP4.5	0.26	0.19-0.33	0.47	0.32-0.63
	RCP6.0	0.25	0.18-0.32	0.48	0.33-0.63
	RCP8.5	0.3	0.22-0.38	0.63	0.45-0.82

Several studies about future climate change on a global perspective concluded that the extreme event would become intense and more frequent; the wet region will become wetter and dry region will be drier during the 21st century [185, 33]. The high-intensity rainfall event is likely to increase over the East Asia region under a global warming scenario [26, 220,204,103]. Global warming is likely to intensify monsoon precipitation over a broad region encompassing South Asia [25, 96,100]. However, there are lots of uncertainty in projecting future rainfall due to wide variations among the model

projections [8, 50, 93, and 98,165]. The India summer monsoon rainfall is likely to increase moderately due to atmospheric warming. However, it is slightly counterbalanced by weakening large-scale monsoon circulation [177]. Seasonal mean rainfall and rainfall extreme over Bangladesh are likely to increase due to climate change [98,141,158]. In recent years, India has suffered from significant heatwaves during March-June. The rising trend of the number of intense heat waves in recent decades has been vaguely attributed to global warming [154]. Several studies suggest delaying the onset of the Indian summer monsoon due to global warming [46].

2.9. Mechanism of Pre-monsoon rainfall in Northeast Bangladesh

A substantial amount of rainfall occurs in northeast Bangladesh and the adjacent hilly region of India during the months of March-May and causing a flash flood in this region. However, this early summer rainfall is not completely understood by the research community. A number of researchers [57, 61, 66, 104, 121, 159, 186] have proposed different theories to explain the possible causes of pre-monsoon heavy rainfall over Northeast Bangladesh. However, most of the theories related to the convection mechanism triggered by the orography around the northeast region and others are related to the diurnal convective maximum. A brief description of these theories is given below.

Orographic lifting

The warm, moist southwesterly air from the Bay of Bengal is blowing towards the Meghalaya Plateau and causes heavy rainfall on the windward side of the Meghalaya Plateau resulting from the orographic uplifting of the moist air [176, 133, 66]. A heat low over central India adjacent to the western border of Bangladesh resulting from strong heating of the landmass triggered this southwesterly moisture flow from the Bay of Bengal towards the Meghalaya Plateau [59,195].

Nocturnal jet

The strong low-level southerly or southwesterly jet from the Bay of Bengal is termed as the nocturnal jet. It occurs when daytime convection ceases [59]. The nocturnal low-level jet is responsible for the development of the convective systems by intersecting with fronts or outflow boundaries that cause the late night or early morning rainfall peak and flash floods in northeast Bangladesh [121].

Katabatic convergence

The katabatic wind or mountain breeze is the denser cool air that flows downslope as a gravity current. Some researchers have suggested that the night-time convective maximum in northeast Bangladesh could be triggered when the katabatic wind from the Meghalaya converge with the moisture prevailing wind off the Bay of Bengal [59].

Cold Pool convergence

A cold pool can be defined as a block/region of cold air that is cooler than the surrounding air. The evaporative cooling of falling precipitation is responsible for the development of a cold pool. The convergences of the cold pool air over northeast Bangladesh at 925 hPa and warm moisture from the Bay of Bengal likely to be another mechanism of pre-monsoon rainfall of this region.

2.10. Flash Flood in Northeast Bangladesh

The river system in northeast Bangladesh originates from adjacent hilly areas of Assam, Meghalaya, and Tripura of India. The main tributary is the Barak River, which has a considerable part of its catchment area located in India. When it enters Bangladesh at Amalshid, it bifurcates into Surma and the Kushiya rivers. Some other rivers originate in India and pass-through this area such as Manu, Dhalai, Khowai. All these river systems are fed mainly from the rainfall in the upstream catchment and some additional local drainage systems within Bangladesh. If it rains heavily in the adjacent hilly areas of the catchments, the run-off quickly accumulates and flows into Bangladesh. Flash flood starts in these areas from mid-April i.e., before the onset of the southwesterly monsoon. It can occur within a time-period between few minutes to a few hours.

Pre-monsoon flash flood, particularly in April, is a major concern for the community since it destroys Boro rice, fisheries, and other livelihoods. The return period of a severe flash flood is five years [164]. The most notable severe flash flood occurred in 1980, 1985, 1990, 2002, 2004, 2010, 2016, and 2017. Flash floods in the latter part of March or early April are not a regular occurrence in the haor region as it happened in 2017. A severe heatwave over central India caused heavy rainfall at the Meghalaya mountain region at the end of March 2017. A total of 1,262mm of rain fell at Cherrapunji during the period between March 28 and April 4 in 2017, which was 5.5 times greater than the amount of rainfall during the same period in 2016. It devastated the Boro rice in six haor districts that were worth TK 13,000.

2.11. El Niño–Southern Oscillation (ENSO)

ENSO is used to quantify and measure the variability of the large-scale process since it reduces a climate process into a single number [180,193]. It is a complex interaction between the atmosphere and ocean in the eastern and central equatorial Pacific that reoccurs on average every four years [67,149]. It is a dominant mode of inter-annual variability in the tropics and can significantly affect the climate of tropical and extratropical [28].

The warm phase of it is termed as El Niño, and the cold phase is termed as La Niña [49]. During the El Niño event, the above-average sea surface temperature (SST) weakens the easterly trade wind or sometimes starts blowing in another direction (Fig 2-5). This results in slowing down the ocean current that moves away the surface water from the western coast of South America, which in turn keeps the water of the coast of Peru and Ecuador relatively warmer [38].

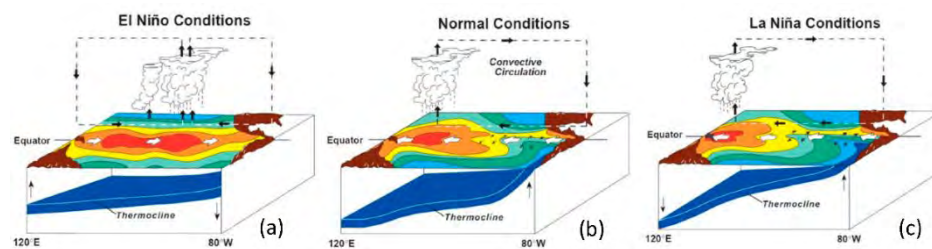


Fig 2.5 Schematic description of the large-scale ocean-atmosphere interactions during the development of ENSO Phases. (a) El Niño, (b) Normal condition and (c) La Niña [60].

ENSO is the most prominent year-to-year climate fluctuation on Earth, alternating between anomalously warm (El Niño) and cold (La Niña) sea surface temperature (SST) conditions in the tropical Pacific. ENSO exerts its impacts on the remote regions of the globe through atmospheric teleconnections, affecting extreme weather events worldwide. However, these teleconnections are inherently nonlinear and sensitive to ENSO SST anomaly patterns and amplitudes. In addition, teleconnections are modulated by variability in the oceanic and atmospheric mean state outside the tropics and by land and sea ice extent.

In an early sixteenth century, the fishermen in Peru and Ecuador first noticed this unusual warming of eastern equatorial Pacific which typically began after Christmas and referred to as El Niño or Christ child or little boy. While during the La Niña event,

the below-average SST makes the normal easterly trade wind even stronger (Fig 2.5). This results in a large-scale cooling of the eastern equatorial Pacific and termed as a little girl. The ENSO affects the global climate, though it originates in the equatorial Pacific. The countries in the eastern part of the Pacific like Peru and Chile experience the vast amount of rainfall, whereas countries in the western side of the Pacific like India, Australia, and Indonesia suffers from a severe drought during El Niño. La Niña causes droughts in the eastern equatorial Pacific and floods in the western equatorial Pacific.

Table 2.4 Geographic extent within which different SST based indices are calculated.

Index	Longitude range	Latitude range
Niño-1+2	90°W- 80°W	0°-10°S
Niño-3	150°W- 90°W	5°N-5°S
Niño-4	160°E- 150°W	5°N-5°S
Niño-3.4	170°E- 120°W	5°N-5°S
JMA	150°W- 90°W	4°N-4°S
TNI	90°W- 80°W and 160°E- 150°W	0°-10°S and 5°N-5°S

Several indices are used to measure the phase and strength of ENSO events. However, the application of a particular index is based on the purpose and the geographical location of the region of interest. The most commonly used indices are generally classified based on pressure and sea surface temperature (SST) [205]. The Southern Oscillation Index (SOI) and the Equatorial Southern Oscillation Index (ESOI) are pressure-based indexes. The SOI is calculated by subtracting atmospheric pressure at sea level of Darwin from Tahiti. Therefore, during El Niño, SOI is negative while during La Niña, SOI is positive. The limitation of SOI is that the ENSO phenomena are mainly concentrated close to the equator while both Tahiti and Darwin are located slightly south of the equator. To overcome this limitation, ESOI is introduced in which the pressure difference between two places centered on the equator (5°S to 5°N) over Indonesia and the eastern equatorial Pacific. The SST based indexes are Niño-1+2, Niño-3, Niño-4, Niño-3.4, and Japan Meteorological Agency (JMA) [63,205]. These indices are calculated by averaging sea surface temperature anomalies over the particular region over the equatorial Pacific Ocean described in Table 2.4. Besides indices mentioned above, Trans- Niño Index (TNI) and the Multivariate ENSO Index (MEI) are also used for measuring the phase and strength of the ENSO event. The TNI is calculated by subtracting normalized anomalies of the SST of the Niño-4 region from

the Niño-1+2 region. On the other hand, the MEI is calculated as the first principle component analysis of the six main observed variables such as sea level pressure, zonal and meridional components of the surface wind, SST, surface air temperature and total cloudiness fraction of the sky [9,210].

The El Niño Southern Oscillation (ENSO) controls the strength and position of the Indian Summer Monsoon through modulation of the stationary Rossby wave of the midlatitude [24]. Several studies [73,94,192] found that there is a decrease of Indian monsoon rainfall during the warm phase of ENSO, but no such a relationship during the cold phase of ENSO. However, preceding winter La Niña reduces the strength of the following Indian Summer Monsoon, which reduces the monsoon rainfall over India [24]. The monsoon rainfall over northeast India tends to be higher in the years in which the ENSO phase (warm to cold) transition occurred rapidly than other years [185]. Some studies over Bangladesh show weak or no correlation between ENSO and monsoon rainfall [92,134]. There is some significant negative relationship between monsoon rainfall at some stations in the northeastern parts of Bangladesh and ENSO [175]. However, no study has been conducted to determine the relationship between ENSO and pre-monsoon rainfall in Meghna Basin, which includes northeast Bangladesh.

CHAPTER 3 STUDY AREA AND DATA

3.1. Study Area

The study area is in northeast Bangladesh located approximately between $24^{\circ}N$ to $25^{\circ}N$ and $90.62^{\circ}E$ to $92.50^{\circ}E$ (Fig 3.1). Northeast Bangladesh encompasses seven administrative districts of Bangladesh such as Sunamganj, Sylhet, Netrokona, Moulvibazar, Habiganj, Kishorganj and Brahmanbaria. It is located within the basin of the Meghna River. The total catchment area of the Meghna is 6500 square kilometers of, which roughly 33% lies in northeast Bangladesh and 67%, lies in India [122].

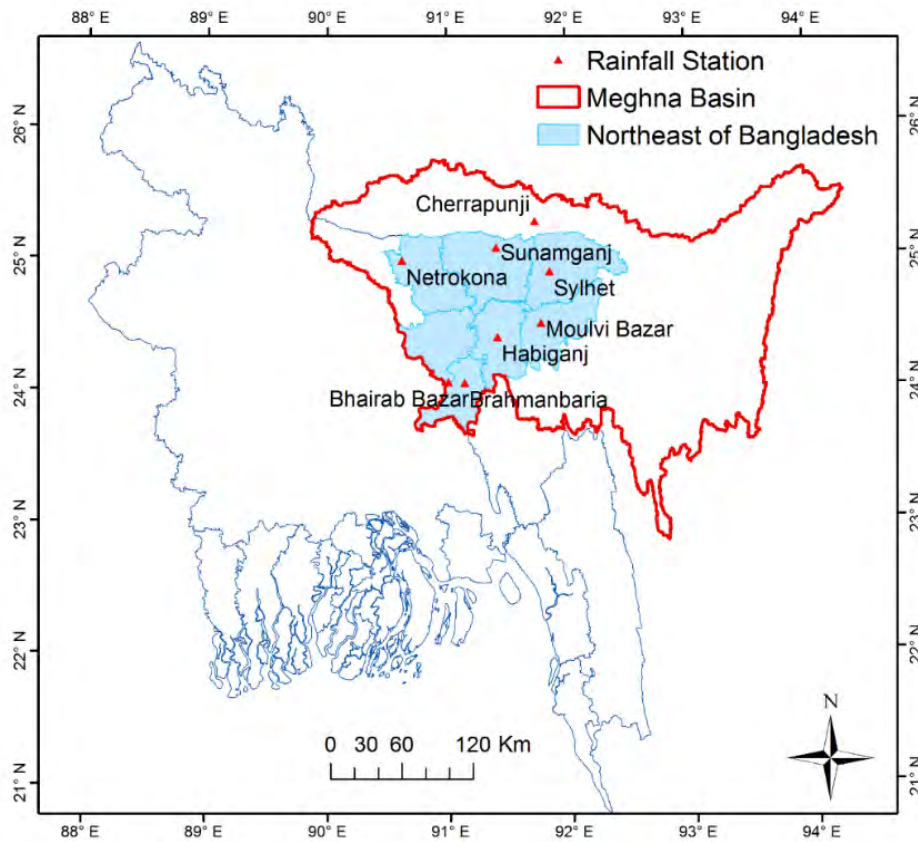


Fig 3.1 Study area with rainfall stations.

The upper portion of the basin is the mountainous regions of Asam, Meghalaya and Tripura states of India, while the lower portion of the basin is the flat and low-lying areas of northeast Bangladesh. The Cherrapunji, well known as one of the wettest places on Earth, is located very proximity to the study area. As a result, the rainfall pattern of the adjacent hilly part of India has a significant influence on flooding in this region. Therefore, in some cases, this study has been extended to the upper part of the Meghna basin.

From the climatic perspective, northeast Bangladesh is categorized by sub-tropical humid conditions [64]. The dry winter (December to February), the pre-monsoon (March to May), the monsoon (June to September) and the post-monsoon (October to November) are the predominant seasons of this area [151]. The mean annual monsoon and pre-monsoon rainfall varies from 2000mm to 6000mm, 1000mm to 4000mm, respectively. The average pre-monsoon and monsoon rainfall of Cherrapunji is about 1700 mm and 7400 mm, respectively.

Northeast Bangladesh is known as the “haor region”, which is bowl-shaped, low-lying floodplains. They have unique characteristics which are dry in the winter months and flooded during the monsoon. There are over 400 small or large haors in northeast Bangladesh [164]. The prominent haors are the Hakaloki haor, Sumir haor, Dakhar haor, Tanguyar haor, Gungiajuri haor, Mukhar haor, Kaowadighir haor. Around 70% of northeast Bangladesh is under haor in which 80% of the area is covered by Boro rice, and 10% is covered by T.aman [6]. The biodiversity of the haor region makes it a unique wetland ecosystem [164].

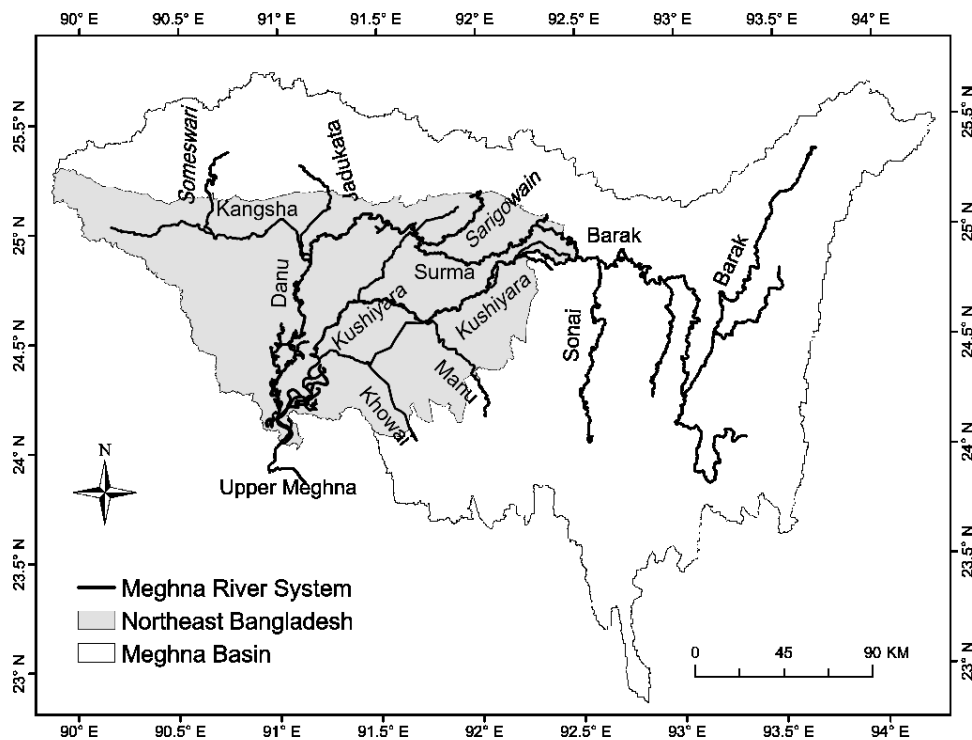


Fig 3.2 Meghna river system.

The river system of the Meghna basin originates from the hills of Shillong and Meghalaya, India. The Barak is the primary source of the Meghna river system, which has a considerable catchment in the ridge and valley terrain of eastern Assam bordering

Myanmar [52]. It crosses the Bangladesh border at Amalshid point of Sylhet and bifurcates into Surma and Kushiya rivers (Fig 3.2). The Surma and Kushiya rivers are flashy and receive water from rainfall at Cherrapunji and Tripura, respectively. The two rivers rejoin at the Markuli point of Sylhet and flow via Bhairab as the Meghna to join the Padma at Chandpur.

The haors are mostly dry from December to May, therefore, Boro rice is extensively cultivated during this time. Boro rice is harvested during the pre-monsoon, which accounts for most agricultural output and contributes significantly to the country's total rice production [6]. Pre-monsoon rainfall is, therefore, a significant concern for this region. Heavy rainfall in April and May can cause flash floods, and that can damage entire crops as it was seen in many places in April 2017. Between June to November, the haors remain underwater and therefore fisheries play a significant role in the livelihoods of many local communities.

3.2. Data

3.2.1. Observed data

The observed dataset comprises of daily rainfall data from seven weather stations in northeast Bangladesh. Among the stations, only Sylhet station is maintained by the Bangladesh Meteorological Department (BMD) and others are maintained by the Bangladesh Water Development Board (BWDB). The observed rainfall data for the period 1976-2016 were used in this study. A list of the observation stations, their names, and their locations are shown in Fig 3.1 (also shown in Table 3.1).

Table 3.1 List Rainfall stations and their location.

Station ID	Station Name	District	Latitude	Longitude
CL128	Sylhet	Sylhet	24.90°N	91.88°E
CL63	Netrokona	Netrokona	24.98°N	90.62°E
CL127	Sunamganj	Sunamganj	25.00°N	91.44°E
CL122	Moulvi Bazar	Moulvi Bazar	24.49°N	91.70°E
CL110	Habiganj	Habiganj	24.39°N	91.41°E
CL103	Brahman Baria	Brahman Baria	24.00°N	91.14°E
CL101	Bhairab Bazar	Kishoreganj	24.00°N	91.00°E

3.2.2. Gridded data

In this study, ERA-Interim re-analysis gridded (0.5⁰ spatial resolution) data of daily rainfall, T_{max} , T_{min} , mean sea level pressure(MSLP), U and V component of wind for

the period 1979-2017 were used. Hadley Centre Global Sea Surface Temperature (HadISST) with 1° spatial resolution was also used in this study.

3.2.3. Selection of the RCP scenario

Four representative concentration pathways (RCPs) are used as a basis for long-term climate modeling experiments. The four RCPs together span the range of radiative forcing values for the year 2100, as found in the literature, from 2.6 to 8.5 W/m² (Fig 2.4). Among them, there is one mitigation scenario (RCP2.6), two medium stabilization scenarios (RCP4.5/RCP6), and one very high baseline emissions scenario (RCP8.5). RCP2.6 is the lowest emission scenario which aims to limit the increase of global mean temperature below 2°C. Often these scenarios show negative emissions from energy use in the second half of the 21st century. The scenario is very optimistic, as it requires full participation and commitment of all countries in the world. However, outcomes of recent climate summits at the highest level, and the annual Conferences of Parties to the United Nations Framework Convention on Climate Change (UNFCCC) do not point in that direction. As this study aims to develop a robust and realistic rainfall projection, RCP2.6 was not included in this study. This leaves the choice to two medium stabilization scenarios (RCP4.5 and RCP6) and one very high baseline emission scenario (RCP8.5). The best choice, in that case, is to include RCP4.5 and RCP8.5, thus including one medium stabilization scenario and the high emissions scenario, and covering the entire range of radiative forcing resulting from RCP4.6, RCP6, and RCP8.5.

3.2.4. Climate model data

Daily rainfall data from six RCMs over the Coordinated Regional Climate Downscaling Experiment (CORDEX) South Asia domain (Table 3.2) was used for this study. The historical run from six RCMs for the 30 years (1976-2005) was taken for the baseline period. Daily rainfall from RCMs for RCP4.5, as well as RCP8.5 for the period 2041-2070 and 2071-2099, were used for projecting the future rainfall extremes for the study area. The output of RCMs is available at the spatial resolution of 0.5°x0.5°. The locations of weather stations do not match RCM grid points exactly. In this situation, the RCM output was calculated at a weather station's location by interpolating (Inverse distance weighting method) four RCM grid points within which that station lies.

Table 3.2 List of RCMs and their driving models.

RCM	Driving GCM	Institute	GCM Model description
ACCESS	ACCESS1-0	CSIRO-Australia	MOSES land surface model of UK Met Offices.
CCSM4	CCSM4	CSIRO-Australia	Community Climate System Model, NCAR of USA.
CNRM	CNRM-CM5	CSIRO-Australia	Earth system model by National Centre for Meteorological Research of French.
MPI	MPI-ESM-LR	CSIRO-Australia	Max Planck Institute Earth System Model at base resolution, Germany.
MPI-REMO	MPI-M-MPI-ESM-LR	MPI-CSC	Max Planck Institute for Meteorology (MPI-M) based on the MPI-ESM-LR model.
SMHI	ICHEC, EC-EARTH	SMHI-Sweden	Irish Centre for High-End Computing Earth System Model, Irish Centre for High-End Computing (ICHEC), European Consortium ESM (EC-EARTH).

Table 3.3 Description of the GCMS and their institution.

GCMS Name	Institution
ACCESS1-0	Commonwealth Scientific and Industrial Research Organization (CSIRO) and Bureau of Meteorology (BOM), Australia.
CSIRO-Mk3-6-0	Australian Commonwealth Scientific and Industrial Research Organization (CSIRO) Marine and Atmospheric Research (Melbourne, Australia) in collaboration with the Queensland Climate Change Centre of Excellence (QCCCE) (Brisbane, Australia).
EC-EARTH	European Earth System Model
GFDL-CM3	Geophysical Fluid Dynamics Laboratory (GFDL) of National Oceanic and Atmospheric Administration (NOAA).
HadGEM2-AO	National Institute of Meteorological Research, Seoul, South Korea
MIROC-ESM	Japan Agency for Marine-Earth Science and Technology, Kanagawa, Japan (JAMSTEC); Atmosphere and Ocean Research Institute, The University of Tokyo, Chiba, Japan (AORI); and National Institute for Environmental Studies, Ibaraki, Japan (NIES).
MPI-ESM-LR	Max Planck Institute for Meteorology.
MPI-ESM-MR	Max Planck Institute for Meteorology.
MRI-CGCM3	Meteorological Research Institute, Tsukuba, Japan.
NorESM1-M	Norwegian Climate Centre.

Monthly SST data from 10 General Circulation Model (GCM) under CMIP5 for Representative Concentration Pathway, RCP4.5, and RCP8.5 for the period 2041-2070 and 2071-2100 were used for projecting the future ENSO index over Nino 3.4 region. The SST data of control run from these GCMs ranges for the period 1976-2005 were

chosen as the base period. The spatial resolution of these GCMs is varied between 0.25° to 2° . Details of the GCMs and their institutes are presented in Table 3.3

3.2.5. ENSO data

Different ENSO indices such as Southern Oscillation Index (SOI), NOAA Oceanic Niño Index (ONI) at Niño-3.4 region and Multivariate ENSO Index (MEI) were collected from National Oceanic & Atmospheric Administration (NOAA) web portal (<https://www.esrl.noaa.gov/psd/enso/data.html>). The plots of the monthly ENSO Index for SOI, ESOI, ONI, and MEI for the period January 1961 to February 2018 are presented in Fig 3.3.

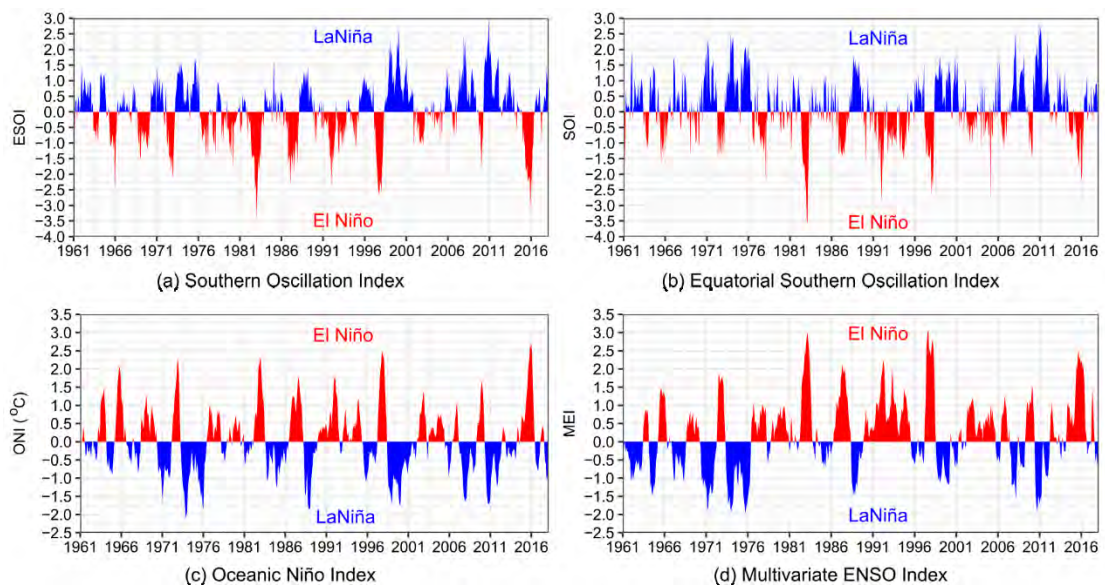


Fig 3.3 Different ENSO indices used for this study.

CHAPTER 4 METHODOLOGY

This chapter outlines the methodology used in this study, which can be subdivided into four major sections. Section 4.1 describes the methods applied for trend analysis of observed rainfall extremes for seven rainfall stations in the study area. Section 4.2 and Section 4.3 present the brief descriptions of RCMs performance assessment and projection rainfall of extremes, respectively. Finally, Section 4.4 details the connection between large-scale processes such as ENSO and pre-monsoon rainfall and how ENSO is likely to be impacted under the warming world.

4.1. Trend Analysis of Observed Rainfall Extremes

The trend analysis was performed for several different indices of rainfall extremes using the Mann-Kendall trend test and Sen's slope estimator. Though more extended data period is better for trend analysis, the minimum length of the data period needs to be at least 30 years [11]. Therefore, observed rainfall for the latest 33 years (1984-2016) was used for trend analysis in this study. Before applying the trend analysis, the Standard Normal Homogeneity Test (SNHT) and the Pettitt test was applied to check the homogeneity of the data. The randomness of the index of rainfall extremes was checked using an autocorrelation test. A brief discussion of the above mentioned statistical tests was given following sub-sections.

4.1.1. Quality control of data

Homogeneity test

Homogeneity test is used to check if there is an error in the data series because of several reasons such as station relocations, equipment changes, equipment drifts, and changes in the method of data collection [2]. If the data series is subjected to any kind of error other than climatic factors, the data series is called inhomogeneous. These inhomogeneous data series needs to be either adjusted or discarded from further analysis. The homogeneity test can be classified as absolute homogeneity and relative homogeneity [2,54]. Data series from different stations are tested individually in absolute homogeneity tests, while they are compared with neighboring reference stations in relative homogeneity tests. However, it is tough to find a reference station

with a high correlation and a homogeneous structure. Hence, in this study, the absolute homogeneity test was applied to check the reliability of the data series.

Four homogeneity tests are generally used to test the homogeneity of the rainfall data, such as Standard Normal Homogeneity Test (SNHT), Buishand Range (BR) test, Pettitt test, and Von Neumann Ratio (VNR) test [126]. In the homogeneity test, the series is considered as homogeneous if the annual values of Y_i of the testing variables, Y are independent and identically distributed under the null hypothesis [84]. Under the alternative hypothesis, SNHT, BR test, and Pettitt test assume that the series comprised of a break in the mean and considered as inhomogeneous. These three tests are capable of detecting the year where the break occurs. However, VNR test cannot give information on the year break because the test assumes that the series is not randomly distributed under the alternative hypothesis. Among SNHT, BR test and Pettitt test, SNHT is sensitive in detecting the breaks near the beginning, and at the end of the series; BR test and Pettitt test are sensitive to identify the break in the middle of the series [84]. Moreover, the SNHT and BR are parametric, whereas the Pettitt test is a non-parametric rank test. Within this test category, in this study, the Standard Normal Homogeneity [7] and the Pettitt tests [145] were chosen since these two tests are more widely used for the homogeneity test [126]. These two tests are discussed in Appendix A (A.1 & A.2).

Autocorrelation test

The indices of rainfall extreme obtained from observed data series must be a series of random events to get reliable trends from the trend analysis [221]. The autocorrelation is generally performed to check the randomness of the data series. If the data series is positively auto-correlated, then it is not a random event, and the resulting trend may not be realistic [129]. In this study, first-order auto-correlation was applied to check the randomness of the data. The theory of the above mentioned statistical tests is discussed in Appendix A (A.3).

4.1.2. Selection of extreme rainfall indices

The decision to focus on extreme rainfall indices was guided by the collaborative research-framing phase, as part of the TRACKS project approach to co-produce knowledge of climate variability for adaptation, with communities in northeast

Bangladesh. This framing, or co-design, of the research, sought to identify those weather phenomena most important to local people and emerged over several rounds of interaction between scientific project partners and different actors in communities in northeast Bangladesh. The identification of the most critical weather phenomena began with a large scoping meeting in Sylhet city September 2014, bringing together local government officials, representatives of non-governmental organizations, scientists at local universities and research institutes, and other groups such as teachers and journalists. This scoping meeting identified local Sylhet communities vulnerable to climate variability and change and led to the second round of interaction; conducting 234 interviews in Sunamganj Sadar, Jamalganj, Barlekha, and Hakaluki haor in December 2014, with diverse ‘grassroots’ actors. The third round of interaction brought together a subset of those people interviewed in workshops in Sunamganj Sadar and Barlekha in March 2016. Through this interaction, communities were able to make precise the weather information that was more important to support local adaptation efforts, and scientists were able to make clear limitations of the science, and what information it is possible to provide. This interaction also allowed for discussion across different knowledge systems, with climate and meteorological information discussed relative to other local and traditional ways of knowing the weather and seasons, using traditional calendars and natural signs for instance. The framing of this research also drew on the published literature.

These interactions showed us that the local communities are particularly concerned about the pre-monsoon rainfall, particularly its amount and distribution. For instance, heavy rain at this time can cause flash floods that can damage or destroy the year’s main Boro rice. The damages of Boro rice can have a substantial economic impact on the local society. Once the importance of rainfall in the pre-monsoon season is understood, the analysis had been split between both the pre-monsoon and monsoon seasons. Though, the onset of the monsoon changes from year-to-year [159], however, a static definition of the monsoon and pre-monsoon seasons was applied here in order to facilitate comparison with previous studies [154,176].

In this study, the pre-monsoon and monsoon were defined as the months of March-May and June-September, respectively. Next, appropriate rainfall indices had to be identified. The selected indices (Table 4.1) reflect rapid flash floods, wet and dry

periods, and seasonal totals. The selection of indices is therefore meant to reflect some challenges the local people told us about, but also be compared to previous and future climate studies.

Table 4.1 List of indices of rainfall extremes used for trend analysis.

Index	Descriptive name	Definition	Unit
RX1DAY	Daily maximum rainfall	Seasonal maximum 1-day rainfall	mm
RX5DAY	5-day maximum rainfall	Seasonal maximum 5-day rainfall	mm
R25mm	Frequencies in days	Number of extremely heavy rainfall days ($RR \geq 25\text{mm}$) during pre-monsoon	days
R50mm	Frequencies in days	Number of extremely heavy rainfall days ($RR \geq 50\text{mm}$) during monsoon.	days
PRCPTOT	Seasonal total wet day precipitation	Seasonal total precipitation in wet days ($RR \geq 1\text{mm}$)	mm
CWD	Consecutive wet days	Maximum number of consecutive wet days in a season with $RR \geq 1\text{mm}$	days
CDD	Consecutive dry days	Maximum number of consecutive dry days in a season with $RR < 1\text{mm}$	days
SDII	Simple daily intensity index	Seasonal total precipitation divided by the number of wet days in the season	mm/day

Through considerable discussion, eight indices of rainfall extremes were selected as also proposed by Frich and Alexander [7,55]. These indices are presented in Table 4.1 with their respective definitions. Both the RX1DAY and RX5DAY represent extremely heavy rainfall, RX1DAY causes flash flooding, while RX5DAY is more likely to cause long-term riverine flooding. Through several discussions with the locals, it is understood that the amount and distribution of PRCPTOT, especially during pre-monsoon are significant in Boro rice production since it influences the seasonal water levels in the haor.

4.1.3. Identification and quantification of trends

The trend of extreme rainfall indices listed in Table 4.1 was identified and quantified using the Mann–Kendall test [88,118] and Sen’s Slope estimator [173], respectively. The Mann-Kendall test is widely used for trend analysis of rainfall and other

climatologic events [56,140,148,212,216,217]. It is a non-parametric test and is less sensitive to a non-homogeneous time series. It can be applied to non-normally distributed data and for data that contain outliers and non-linear trends [21]. According to this test, the null hypothesis H_0 indicates that there is no trend and an alternative hypothesis H_1 indicates that there is a trend [142].

Sen's Slope method [173] was then applied to estimate the magnitude of the trend. A time series of equally spaced data is required for this method and is not influenced by missing values or gaps in the input data. Among the rainfall station considered, Sylhet station has less missing values (0.5%), and Netrokona has more missing values (3.9%). There are several methods used for filling missing values of daily rainfall values. The most common methods used in the filling of the missing data include the closest station, simple arithmetic averaging, inverse distance weighting, multiple regression, and the normal ratio [117,128,213]. In this study, Inverse Distance Weighting (IDW) method was applied for filling the missing values as this widely used method is suitable for rainfall stations that are closely spaced and the orographic features of the stations are almost similar to each other [16,128]. For more information about the theory, please see Appendix A (A.4 & A.5).

4.2. Projection of Future Rainfall Extremes

In this study, changes of extreme rainfall indices (listed in Table 4.1) for the scenario periods (2041-2070 & 2071-2099) regarding the reference period (1976-2005) were estimated for RCP4.5 and RCP8.5 from six RCMs. However, beforehand, bias correction of RCMs was performed, and the multi-model ensemble mean of extreme indices was generated followed by the performance evaluation of the RCMs which were discussed in following sub-sections.

4.2.1. Performance Evaluation of RCMs

The performance of RCMs was evaluated in terms of bias, root mean square error (RMSE) and quantile-quantile (Q-Q) plot. The bias and RMSE are quantitative and directional measure, while the Q-Q plot is a qualitative measure. The bias and RMSE were calculated over average pre-monsoon and monsoon rainfall over the period 1976-2005. The equation of bias and RMSE was discussed in Appendix A (A.6).

Q–Q plot is a probability plot in which the quantiles of the two data set are plotted each other. If the two distributions being compared are similar, the points in the Q–Q plot will approximately lie on the line $y = x$. In this study, the quantile of the daily rainfall from RCMs was plotted on the Y-axis, and the quantile of the observed rainfall was plotted on the X-axis. If a particular point is below the $y = x$ line, then it is underestimated and vice versa. Therefore, in this way, the Q-Q plot can tell us which rainfall intensity of RCMs is underestimated /overestimated or correctly matched with observed rainfall.

4.2.2. Bias correction of RCMs

The downscaled rainfall data from the RCMs are affected by biases inherited from the forcing GCMs [86]. Even within a single geographic region, different RCMs may produce different results due to their model fundamentals, and climate forcing [44, 48,124,219]. The biases in the RCMs include too much drizzle, errors in the mean and failing to simulate heavy rainfall events [146]. Therefore, without removing or reducing bias, multi-model means cannot be used for impact assessments.

In this study, the quantile mapping bias correction method was used since it has been successfully and widely applied in climate change studies [106,155,187,188,197]. In this method, cumulative distribution functions (CDF) were generated for both the observed and RCM simulated rainfall firstly and then the CDF from an RCM simulated value was matched to the observed value at the same CDF over a specified base period [23,91]. All the daily rainfall values from the RCMs are scaled up or down according to the adjusted CDF.

Though both parametric and nonparametric quantile mappings are widely used to correct the bias of climate model output, a parametric method yields a better result [91]. This is because the parametric method is able to adjust the distributions of the model output to agree with observed distributions. In this study, gamma distribution was chosen since it represents rainfall data well, particularly for monthly and seasonal values [87,91,146]. This method was applied to both the reference (1976-2005) and scenario periods (2041-2070 and 2071-2099). A brief procedure of the quantile mapping bias correction method is discussed in Appendix A (A.7).

4.2.3. Multi-model ensemble mean

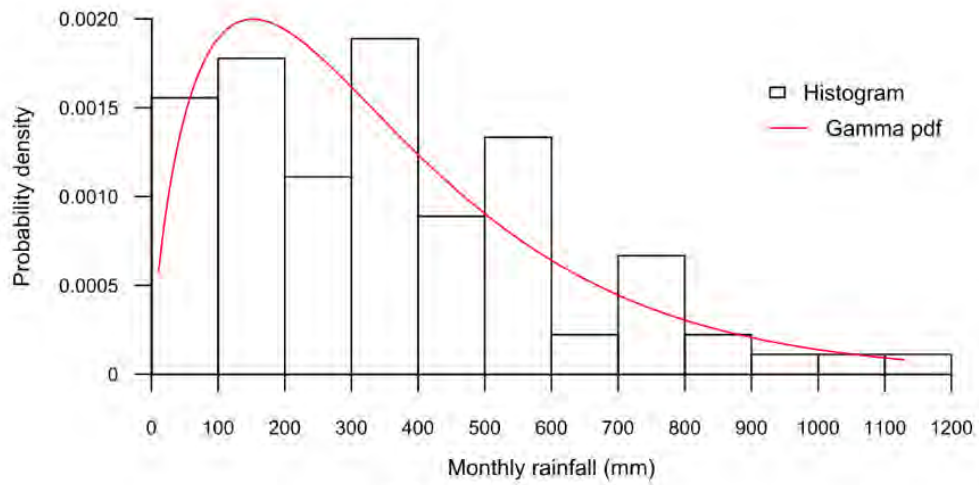
With the corrected RCM simulations, a multi-model ensemble mean was taken to analyze possible future changes. Multi-model ensemble means have been shown to outperform individual model output at the regional level [147,51]. Among several methods, the Bayesian Model Averaging (BMA) method provides a more reasonable ensemble mean [152,202,223] since it gives higher weight to the RCM with better predictive skills in the training period. This study used the RCMs output under the CORDEX framework, and the observational data from seven rainfall station for the first time.

Bayesian model averaging (BMA) produces a complete probability density function (PDF) of the ensemble mean and quantifies the associated uncertainty of forecasts. The BMA method has become increasingly popular since it produces a more reliable multi-model ensemble mean [4,137,153]. In this approach, the PDF of the ensemble mean is the weighted average of the conditional PDF of an individual model where the weights are posterior probabilities of the models generating the forecasts and reflect the relative contributions of each model to the overall predictive skill.

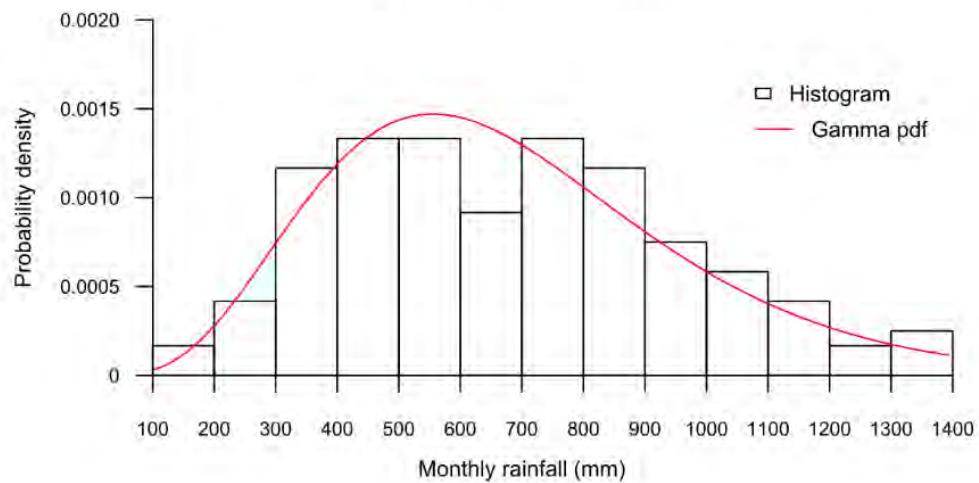
At first, the monthly values of extreme rainfall indices from daily time series were derived to determine the BMA weight of it for each model. Then, the indices of the pre-monsoon and monsoon seasons were separated. By doing so, three values for the pre-monsoon and four values for the monsoon season for each index were obtained. In this way, for a 30-year period, time series comprising 90 values for the pre-monsoon and 120 values for the monsoon season was obtained for the BMA computation.

However, beforehand, it was needed to know the distribution of the indices according to the above discussions. For example, monthly rainfall totals of a particular season were fitted for different distributions (e.g., normal, gamma, exponential) to determine for which a specific distribution data sample is best fitted. Using the Kolmogorov–Smirnov test and graphical techniques (histograms and density estimate), it was found that the monthly rainfall data for the study area are best fitted by the gamma distribution. As an example, a data histogram and the corresponding fitted gamma PDF for monthly rainfall of Sylhet station are shown in Fig 4.1. As expected, rainfall data are positively skewed with a long tail to the right of the distribution. This is the case for both the pre-monsoon and monsoon seasons. The gamma distribution, while being asymmetric and

bounded on the left by zero, provides a good fit to the empirical data, particularly in the extreme left and right tails of the distribution. Therefore, the gamma distribution was considered for generating the conditional PDF.



(a) Pre-monsoon



(b) Monsoon

Fig 4.1 Histogram and gamma pdf for monthly rainfall of Sylhet station (a) Pre-monsoon and (b) monsoon.

The maximum likelihood function for the BMA multi-model ensemble mean was optimized using the Differential Evolution Adaptive Metropolis (DREAM) Markov Chain Monte Carlo algorithm for estimating the BMA weights and variance [200,201,203]. Finally, the DREAM scheme was used to search for the optimal global solution of BMA weight [203]. A detail description of BMA is discussed in Appendix A (A.8).

4.3. Relationship between El Niño Southern Oscillation (ENSO) and Pre-monsoon Rainfall and its Response under the Warming World.

The relationships between ENSO and pre-monsoon rainfall in the Meghna basin was performed in three steps. Firstly, the relationship between pre-monsoon rainfall and heat low in central India during the pre-monsoon particularly, in April was determined. Because the Southwesterly moisture flows from the Bay of Bengal is triggered by the low-pressure system in central India which brings moist air towards the foothills of the Meghalaya Mountain that feeds deep convection over the Meghna basin. Before determining the relationship between heat low over India and ENSO, it is essential to know the answer of two questions: firstly, does there exist any significant relationship between pre-monsoon rainfall and ENSO? Secondly, if there is a significant relationship between pre-monsoon rainfall and ENSO then among different ENSO index (e.g., ESOI, SOI, ONI, and MEI) which is the best suited ENSO index for the study area? Therefore, the relationship between the pre-monsoon rainfall and different ENSO indexes (e.g., ESOI, SOI, ONI, MEI) with different monthly lags was determined in the second step. Since the heatwave produces heat low, the relationship between the heatwave in central India during April and best suited ENSO index (identified in the second step) was determined in the third step. Among different indices, Excessive Heat Factor (EHF) can define heatwave more effectively since it considers the existing moisture content, weather condition of two days before, and climatological anomaly [160]. Therefore, in this study, Excessive Heat Factor (EHF) was used to define heatwave, which is based on the Excess Heat Index and Heat Stress. A brief discussion of the heatwave is given in Appendix A. Finally, the relationship between heatwave (in terms of EHF) in central India during April and best suited ENSO index (identified in the second step) was determined in the third step. If a link between the Indian heat low and pre-monsoon rainfall can be developed, this could be helpful for short-term (monthly or seasonal scale flood forecasting. If a relationship between ENSO and pre-monsoon rainfall (either directly or via a connection with the Indian heat low) can be shown, this could be helpful for seasonal flood forecasting of the region. It is noted here that the Spearman's Rank Order Correlation was used to establish the above-mentioned relationship. The advantage of using Spearman's Rank Order Correlation over Pearson correlation is that Spearman's Rank Order Correlation is a non-parametric method, and therefore, it does not require to follow any distribution of the data.

Using the sea surface temperature (SST) from the GCMs, the monthly oceanic niño index (ONI) was calculated for the Nino 3.4 region for the control and the scenario period. The ONI index was calculated by subtracting the SST values from the 30 years average SST over the Nino 3.4 region [110]. Until February 2013, the Climate Prediction Center of National Oceanic and Atmospheric Administration used a 30-year average of the three most recent complete decades, updated in each new decade. For example, they used the 1961-1990 average for the 1990s and 1971-2000 average for the 2000s. However, in this study, the average SST value was calculated according to the latest guidelines of the Climate Prediction Center. According to this guideline, for each 5-year period, the 30-year period was selected in such a way that the first year of the 5-year period falls in the center of the 30-year period. For example, SST values for the year 1956-1960 are compared to the average of 1941-1970. Similarly, SST values for the year 1961-1965 are compared to the average of 1946-1975. The advantage of this new method over the previous method is that it does not distort the ENSO climatic record due to warming up or cooling down the past three decades in the tropical Pacific [110]. The response to ENSO under warming world was studied in terms of ENSO frequency (number ENSO event) and ENSO amplitude (standard deviation of the SST anomaly). It was done by using the output (monthly SST data) of the latest available GCMs under CMIP5 for RCP4.5 and RCP8.5 during 2041-2070 and 2071-2100.

CHAPTER 5

TREND ANALYSIS OF OBSERVED RAINFALL EXTREMES

5.1. Introduction

Rainfall extremes are one of the major causes of natural disasters, such as flash floods, urban waterlogging, landslides, and crop damage [212]. Because of global climate change and alteration of Earth's hydrological, the heavy rainfall event has increased in the past and likely to continue [10]. Hence, trends in extreme rainfall events for historical record and future have received considerable attention in recent years because of the many extreme events such as hurricanes, droughts, and floods observed.

Therefore, this chapter presents the trend analysis of observed rainfall extremes over northeast Bangladesh for the period 1984-2016. This study extends on previous studies of rainfall in northeast Bangladesh. Many of the previous studies on rainfall in northeast Bangladesh were limited to Sylhet station only. A single rainfall station might not represent the surrounding climate [212], as it may be influenced by a particular local climate [81]. This study, therefore, performed on the observed dataset from seven rainfall stations located across northeast Bangladesh. The trend was identified on seasonal totals and seven other rainfall indices depicting different rainfall characteristics. This study considers trends in the pre-monsoon and monsoon seasons separately. Rainfall in these seasons can have different convective triggering mechanisms, but can also impact the lives of the local communities in very different ways. The detail descriptions of the data and the methodology were presented in Chapter 3 and Chapter 4, respectively.

At first, the rainfall climatology of northeast Bangladesh was described using a new dataset. After that, the results from the homogeneity and the auto-correlation tests were discussed. In the final section, the results of the trend analysis were presented.

5.2. Spatial Distribution of Annual and Seasonal Rainfall

For the seven stations combined, the mean annual, monsoon, and pre-monsoon rainfall of the study area was 3232mm, 1765mm and 780mm, respectively. The spatial distribution of annual mean rainfall (Fig 5.1) shows that the north receives higher rainfall than the south. The same pattern emerges throughout the year where the mean

annual rainfall ranges from 6000mm along in the north to 2000mm in the south (Fig 5.1c). The mean pre-monsoon and monsoon rainfall increase, respectively from 590mm to 950mm and from 1000mm to 3700mm between the north and south of northeast Bangladesh (Fig 5.1a and Fig 5.1b).

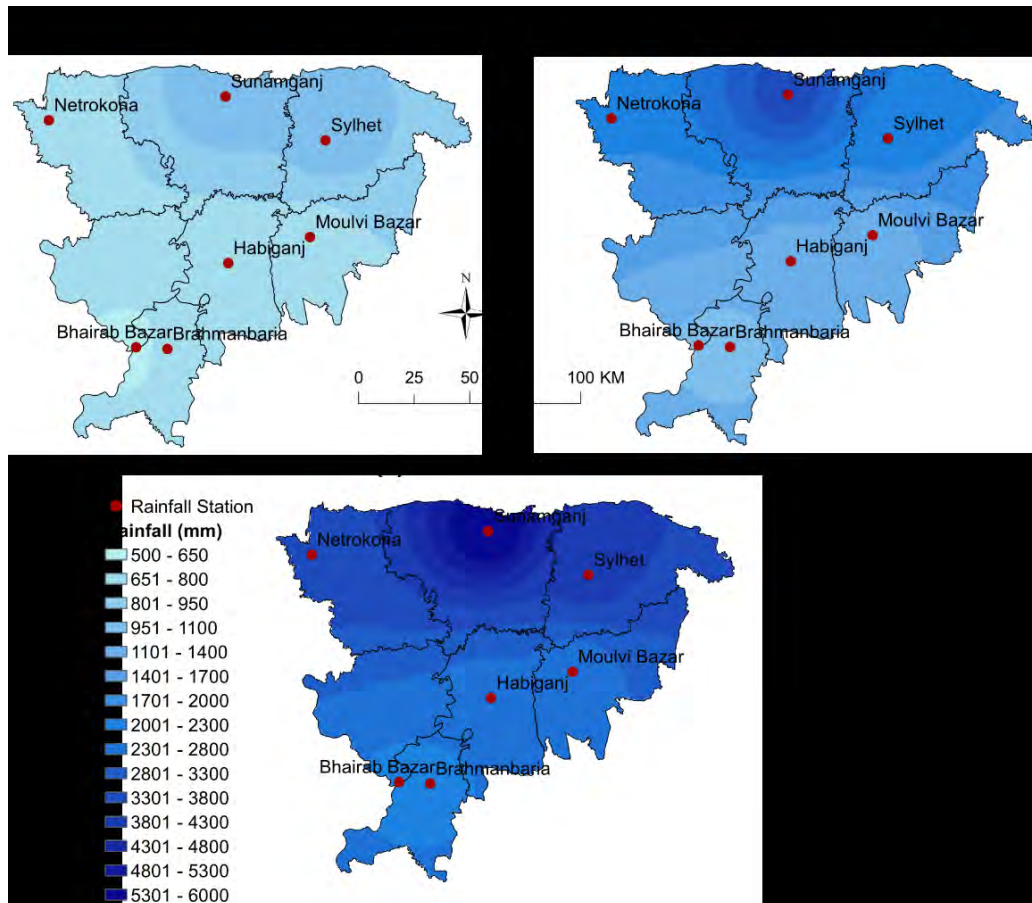


Fig 5.1 Spatial distribution of mean rainfall of the study area for (a) Pre-monsoon, (b) Monsoon and (c) Annual.

The mean annual, monsoon and pre-monsoon rainfall of Sunamganj was higher than the other stations. This is understandable because of the station's proximity to the Meghalaya foothills and Cherrapunji, India, one of the wettest weather stations in the world. The long-term variation of annual, pre-monsoon and monsoon rainfall for each station is presented as a Box-and-Whisker plot in Fig 5.2. The variability of rainfall is high in Sunamganj for the pre-monsoon and the monsoon seasons. Other stations showed much lower inter-annual variability. These results show how detailed the local meteorology of the northeast region can be varied.

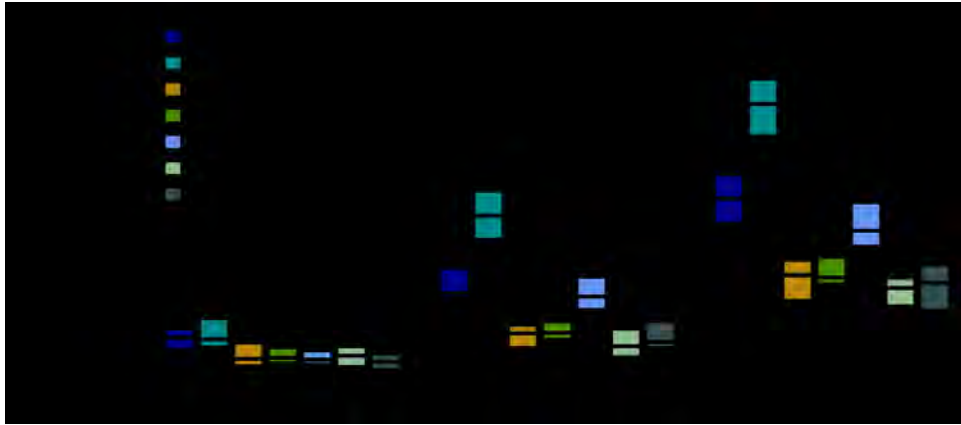


Fig 5.2 The Box-and-Whisker plot of the spatiotemporal variation of rainfall of northeast Bangladesh for the period of 1984 to 2016.

5.3. Quality control of the data

5.3.1. Homogeneity test

The result of the homogeneity test was presented in Fig 5.3. In this figure, it was observed that the test statistics for most of the stations decreased from 1992 to 2000 and remained below the critical line while the Sunamganj it remained above the critical line for the same period. For the data sets to be considered homogeneous, the value of the “test statistic” needs to remain below the critical value [89,145]. The maximum values of test statistics for annual rainfall for all seven stations except Sunamganj stayed below the critical value for the 95% confidence level. Since the null hypothesis for the SNHT as well as Pettit test was accepted at the 95% confidence level, these stations were considered homogeneous at this confidence level. Whereas, the rainfall at Sunamganj station was said to be inhomogeneous since the null hypothesis was rejected

Before deciding whether to discard the Sunamganj data, an attempt was taken to find out what was wrong with the data set. It was started by trying to identify any change points in the time series using the Student t-test at the 95% confidence level. It was found that the trend in the Sunamganj data changed in 2005 (Fig B.1a in Appendix B). The field officer who was responsible for data collection confirmed that there were irregularities in the data collection for some years before 2005. The comparison of the de-trending annual rainfall of Sunamganj with the nearest and meteorologically similar station of Sylhet also justified the argument of field office (Fig B.1b in Appendix B). It was found that the de-trending annual rainfall pattern of these two stations was similar before 1998 and after 2005, which was not the case in between 1998 and 2005.

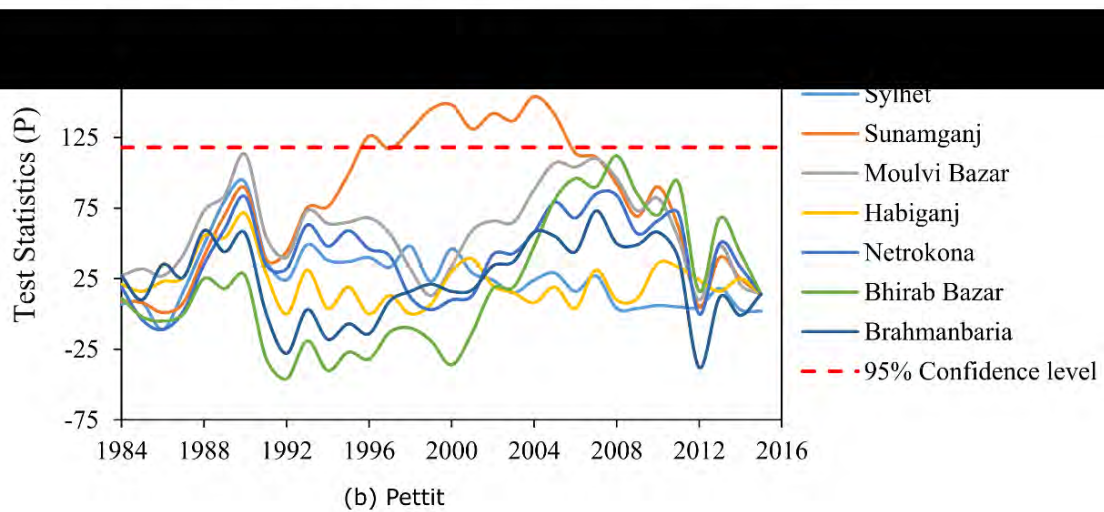
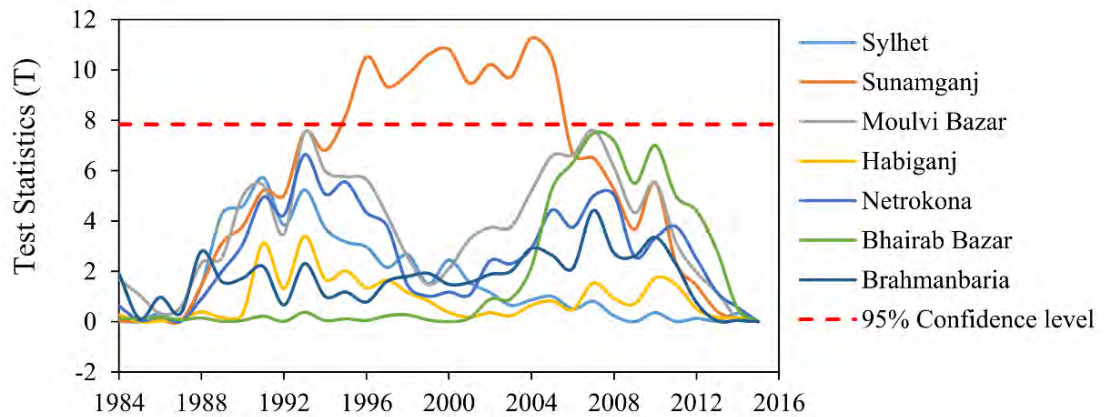


Fig 5.3 The Test statistics of homogeneity test for annual rainfall for seven stations in the northeast of Bangladesh for the period of 1984 to 2016 (a) SNHT test (b) Pettit test.

5.3.2. Autocorrelation test

Autocorrelation test is necessary to determine the randomness of the data. If the data is not random, the result of trend analysis may give false information. The first order autocorrelation coefficient for the indices of rainfall extreme for seven stations of northeast Bangladesh for the period of 1984 to 2016 was presented in Table 5.1. The co-efficient which is within the 95% confidence interval is considered as independent or random event. The interval of the autocorrelation coefficient at the 95% confidence limit depends on sample size and the order of lag. In this study, the sample size is 33, and hence, for a two-sided test, the interval of the auto co-relation coefficient at the 95% confidence limit is -0.37 to 0.31. The lag 1 autocorrelation coefficient of rainfall extreme for the pre-monsoon and monsoon season was within the range of 95% confidence limit so the indices were not auto-correlated either random event (Table 5.1). Therefore, the selected indices can be used for trend analysis.

Table 5.1 The first order Autocorrelation coefficient for the indices of rainfall extreme for seven stations of northeast Bangladesh for the period of 1984 to 2016.

	Station	RX1	RX5	R25 (R50)	PRCPTOT	CWD	CDD	SDII
Pre-monsoon	Sylhet	-0.02	-0.10	-0.15	-0.30	-0.08	-0.05	0.06
	Habiganj	0.10	0.03	-0.19	0.00	-0.13	-0.19	-0.01
	Moulvibazar	0.18	0.15	-0.10	0.05	-0.06	-0.28	0.10
	Netrokona	0.17	0.21	0.05	0.15	-0.13	0.17	0.24
	Brahmanbaria	-0.17	-0.09	-0.17	-0.13	-0.11	0.00	-0.30
	Bhairab Bazar	-0.01	-0.01	0.06	0.00	-0.10	-0.33	0.14
Monsoon	Sylhet	-0.02	0.00	-0.27	-0.19	0.22	-0.17	-0.02
	Habiganj	-0.14	0.16	-0.32	-0.29	-0.03	-0.07	-0.21
	Moulvibazar	-0.10	-0.27	-0.10	-0.11	-0.22	-0.22	0.01
	Netrokona	0.22	-0.07	0.18	0.09	0.16	0.10	0.03
	Brahmanbaria	-0.09	-0.17	-0.24	-0.23	0.10	0.14	-0.15
	Bhairab Bazar	-0.11	0.10	0.03	0.08	0.04	-0.24	-0.06

5.4. The trend of Indices of Rainfall Extremes

The trend analysis was performed on those stations that passed the quality control tests. All the stations passed the autocorrelation test while the Sunamganj station failed to pass the homogeneity test. Hence, the Sunamganj station was not considered for trend analysis. The trend of extreme indices for the pre-monsoon and monsoon season are discussed separately in the following sections.

5.4.1. Pre-monsoon

Fig 5.4 (a) showed that the one-day maximum rainfall (RX1) for all stations except Sylhet and the five-day maximum rainfall (RX5) for all stations was decreased. However, none of the stations showed a significant change in these two indices at the 95% confidence level. The most substantial decreases of RX1 (1.17 mm/year) and RX5 (2.0 mm/year) were at Moulvibazar (Table 5.2). The R25, PRCPTOT, and SDII also decreased in most of the stations but not statistically significantly anywhere in Fig 5.4 (a). The most substantial decreases of R25, PRCPTOT, and SDII was 0.1 days/year at Habiganj, 7.64mm/year at Moulvibazar and 0.24 mm/day/year at Bhairab Bazar, respectively (Table 5.2). The CWD of most of the stations showed a decreasing trend, and the CDD of most of the stations showed an increasing trend. However, these indices were not statistically significant in any of the stations.

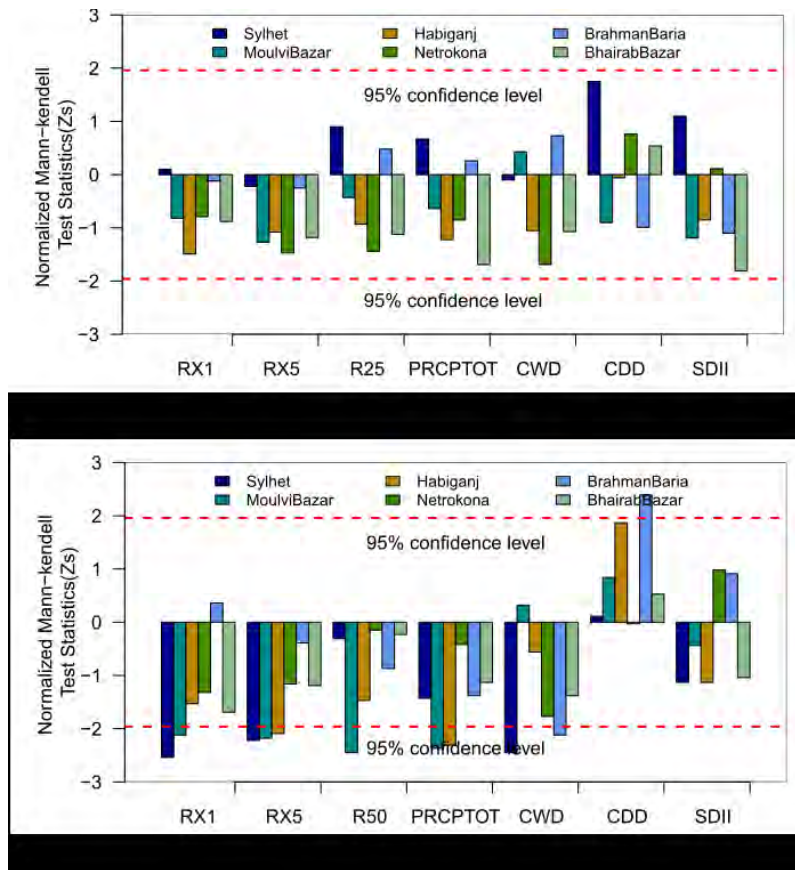


Fig 5.4 The normalized test statistic (Z_s) for the Mann-Kendall test of the indices of rainfall extremes of six stations of northeast Bangladesh for the period of 1984 to 2016: (a) Pre-Monsoon and (b) Monsoon. The absolute Z_s value which, is higher than the critical value ($Z_c=1.96$) are considered as statistically significant at 95% confidence level.

Table 5.2 The Sen's Slope estimator (Q) for indices of rainfall extremes for six stations of northeast Bangladesh for the period of 1984 to 2016. The slopes corresponding to statistically significant Z_s in Fig 5.4 are underlined.

Station	RX1	RX5	R25/R50	PRCPTOT	CWD	CDD	SDII
Pre-monsoon							
Sylhet	0.06	-0.36	0.09	4.32	-0.02	0.17	0.15
Netrokona	-0.69	-1.91	-0.02	-2.74	0.04	-0.16	-0.12
MoulviBazar	-1.17	-2	-0.09	-7.64	-0.03	-0.03	-0.17
Habiganj	-0.64	-1.57	-0.1	-2.98	-0.04	0.13	0.01
Brahman Baria	-0.17	-0.27	0.05	1.62	-0.09	-0.19	-0.12
Bhairab Bazar	-0.74	-1.59	-0.07	-6.85	-0.01	0.1	-0.24
Monsoon							
Sylhet	<u>-2.76</u>	<u>-4.00</u>	-0.02	-13.61	<u>-0.33</u>	-0.03	-0.11
Netrokona	<u>-1.90</u>	<u>-3.43</u>	<u>-0.25</u>	<u>-25.35</u>	0.04	0.05	-0.13
MoulviBazar	-1.82	<u>-3.33</u>	-0.11	<u>-17.02</u>	-0.08	0.09	-0.09
Habiganj	-1.03	-1.95	-0.09	<u>-3.79</u>	-0.11	-0.01	0.10
Brahman Baria	0.25	-0.76	-0.04	-10.93	-0.14	<u>0.20</u>	0.10
Bhairab Bazar	-1.19	-2.54	0.02	-12.02	-0.06	0.03	-0.15

5.4.2. Monsoon

The RX1 at most of the stations exhibited downward trends in which Sylhet and Netrokona decreased statistically significant at the 95% confidence level (Fig 5.4 b). The RX1 decreased at a rate of 2.76 mm/year at Sylhet and 1.90 mm/year at Netrokona (Fig 5.4 b). The RX5 decreased at all stations in which it decreased significantly at Sylhet, Netrokona, and Moulvibazar. The decreasing rates of these three stations are 4.0mm/year, 3.43mm/year and 3.33mm/year, respectively. The PRCPTOT also showed falling trends at every station, in which it decreased significantly at Netrokona and Moulvibazar stations 25.35mm/year and 17.02mm/year, respectively. At all stations, the R50 showed a decreasing trend in which one station decreased significantly. The trend of CWD and CDD during monsoon season had an almost similar trend like pre-monsoon season where most of the station showed a negative trend for CWD and the positive trend of CDD. The CWD decreased significantly at Sylhet and Brahmanbaria 0.33days/year and 0.14days/year, respectively. The CDD increased significantly at Brahmanbaria only 0.2days/year. Among the six stations, the SDII showed a falling trend at four stations while rising trend at two stations. However, none of them was statistically significant.

Several of the stations show decreasing (but not significant) trends in total pre-monsoon rainfall, which agrees with previous studies [42,176]. Overall, the pre-monsoon climate does not seem to change very rapidly since it was observed no significant trends for any rainfall index during this season. Regarding the monsoon season, previous studies have concluded that long-term monsoon rainfall over the Assam and Meghalaya state of India has decreased, but not significantly [42,98,99,134,179]. The results show that the monsoon rainfall has decreased in all stations, most significantly at Netrokona. Significantly decreasing trends in RX1 and RX5 at the same station, including Sylhet, was also observed. These results do not align with the narrative that total rainfall can decrease, but extremes can increase. Overall, the results vary from the index to the index and station to station. This shows how the local climate can be even in a relatively small region like northeast Bangladesh.

Being in the downstream part of the Meghna Basin, northeast Bangladesh receives a significant portion of water from the adjoining part of India. As the observed rainfall data from India was not accessible, the trend was identified using observed data from

Bangladesh only. This trend analysis can, therefore, not directly show any changes in a flash flood, riverine flood, or drought occurrence over the entire basin.

5.5. Summary

In this chapter, the trends of rainfall extremes of northeast Bangladesh for the period 1984 to 2016 for the pre-monsoon and monsoon seasons were explained. The daily rainfall data of seven stations representing the seven administrative districts of this region were used for this study. The trend analysis considered a number of different indices of rainfall extremes and was performed using the Mann-Kendall trend test and Sen's slope estimator.

Before applying the trend test, the Standard Normal Homogeneity Test (SNHT) and the Pettitt test was applied to check the homogeneity of the data. The randomness of the index of rainfall extremes was checked using an autocorrelation test. Among the seven stations, all stations were found to be homogeneous except Sunamganj, which was found to be inhomogeneous, and all the stations passed the correlation test meaning the index of rainfall extremes resulted from random events. The irregularities in data of the Sunamganj station from 1998 to 2005, causing inhomogeneity of rainfall data were identified using change-point analysis, comparing de-trending annual rainfall with the nearby station and information from the field office. Hence, the Sunamganj station was not considered for the trend analysis.

In general, all the extremes rainfall indices showed a decreasing trend in both seasons over the region, with most of them decreased significantly during the monsoon. The most significant finding is that over this region, the seasonal total rainfall and the consecutive wet day exhibited a decreasing trend whereas the consecutive dry day saw an increasing trend. The decreasing trend of one-day maximum rainfall, five-day maximum rainfall, the intensity of the daily rainfall over 25mm during the pre-monsoon, and 50mm during the monsoon, indicate a decrease in the magnitude and intensity of rainfall, with implications for seasonal and flash-floods. While these trends were observable over most stations, the trends were not always found to be statistically significant, demanding continued research into rainfall extremes. If these decreasing trends of rainfall extreme continue in the future, northeast Bangladesh may suffer from significant water stress. While extreme flooding can be harmful to these communities,

they have learned to live with the phases of ‘normal’ flooding. For example, the reduction of pre-monsoon rainfall and an increase in consecutive dry days could affect Boro rice production. Likewise, flooding brings a significant amount of coarse sand, stone, and boulders from the surrounding mountains, with the harvesting of this valuable resource employing many people. Similarly, the monsoon floods are necessary for fertilizing the paddy field and replenishing fish stocks in the haor. Hence, the findings from this study, together with future climate projections from climate models, will be helpful for future planning and management of water resources in the region. In the next chapter, the future trend and possible changes in rainfall extremes considering climate change were discussed.

CHAPTER 6

PROJECTION OF FUTURE RAINFALL EXTREMES UNDER THE WARMING WORLD

6.1. Introduction

In Chapter 5, it was observed that most of the extreme rainfall indices showed a decreasing trend in both seasons, with the most significant decrease during the monsoon. Now it is essential to know how these rainfall extremes are likely to change in future considering climate change. Therefore, in this chapter, the trend of rainfall extremes over northeast Bangladesh for the period 2041-2070 and 2071-2099 as a consequence of climate change was presented first. After that, the changes in rainfall extremes for the same period regarding baseline (1976-2005) was analyzed. For these purposes, six RCMs over the CORDEX South Asia domain considering two RCPs, namely RCP4.5 and RCP8.5, were used. Multi-model ensemble means were generated using a Bayesian Model Averaging (BMA) approach. In this approach, individual RCM was assigned a weight according to its predictive skill during the training period. Beforehand, the quantile mapping bias correction was performed after evaluating the RCMs performance in simulating the present-day climate. The detail descriptions of the data and the methodology were presented in Chapter 3 and Chapter 4, respectively.

6.2. Performance Evaluation of RCMs

The performance of RCMs over CORDEX South Asia domain was evaluated to determine the ability to reproduce historical rainfall over northeast Bangladesh. It was evaluated against observed station data in terms of bias, RMSE, and Q-Q plot for the period of 1976-2005. The bias indicates the wetness or dryness of the model, while the RMSE indicates the overall accuracy. The Q-Q plot shows if RCMs can simulate a particular rainfall intensity or not. Therefore, bias and the RMSE were estimated on monthly rainfall totals, while the Q-Q plot was drawn on daily rainfall.

In this study, only the pre-monsoon and monsoon season was considered as the study area is subjected to pre-monsoon flash flood and monsoon flood, which cause enormous damage to lives and livelihood of the region. The bias and RMSE of RCMs needed to be normalized for comparing them during the pre-monsoon and monsoon season. Therefore, the actual bias and RMSE were normalized by mean seasonal rainfall and standard deviation, respectively, from observed data. The normalized bias was negative

for most of RCMs during the pre-monsoon and all RCMs during the monsoon (Fig 6.1). Therefore, the average bias of the RCMs was also negative for both seasons. This means that RCMs always underestimate in simulating present-day average rainfall for the study area. It was also noted here that the normalized bias was higher for the monsoon than pre-monsoon.

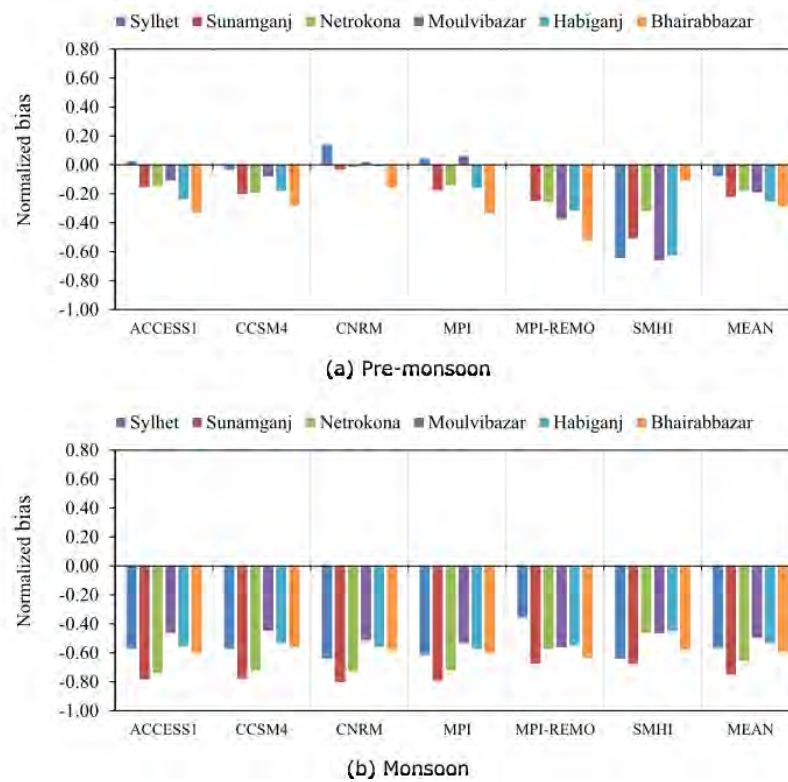


Fig 6.1 Normalized bias for different RCMs with respect to observed station rainfall during the period of 1976-2005 for (a) Pre-monsoon and (b) monsoon.

The normalized RMSE of the RCMs were also higher during the monsoon than the pre-monsoon (Fig 6.2). Therefore, it can be inferred that RCMs were less efficient in simulating the higher amount of rainfall. The reasons for higher bias and RMSE of the RCMs could be because of a lack of good quality high-resolution observed data. Another reason could be the sparse observation because of the complex geography of the study area. Lack of proper knowledge to use point measurement data in evaluating the grid-based RCMs, particularly for sparse station networks with complex topography could also be another reason.

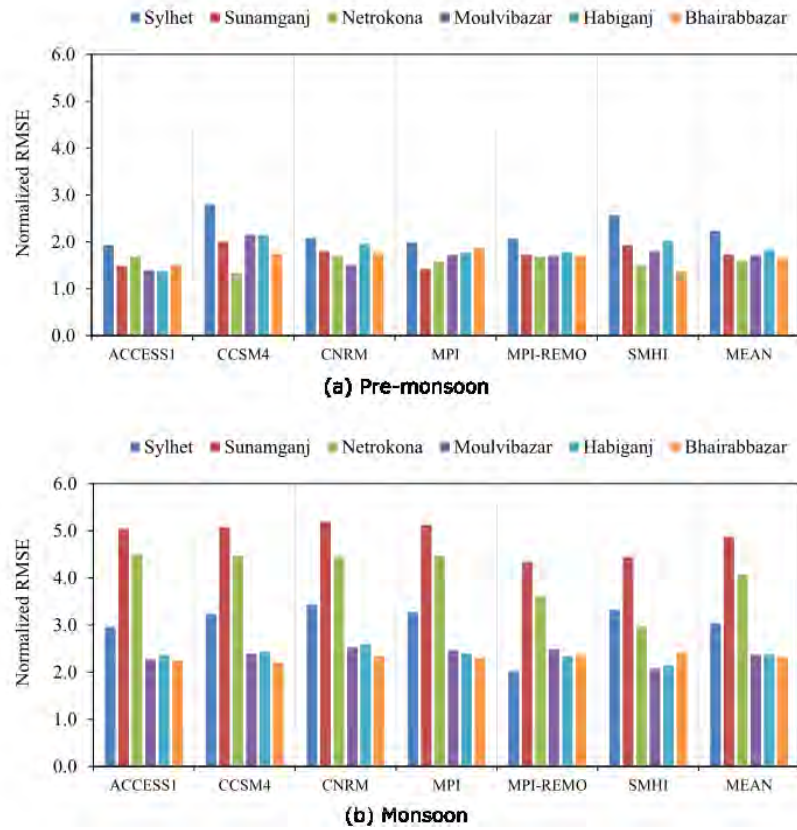


Fig 6.2 Normalized RMSE for different RCMs with respect to observed station rainfall during the period of 1976-2005 for (a) Pre-monsoon and (b) monsoon.

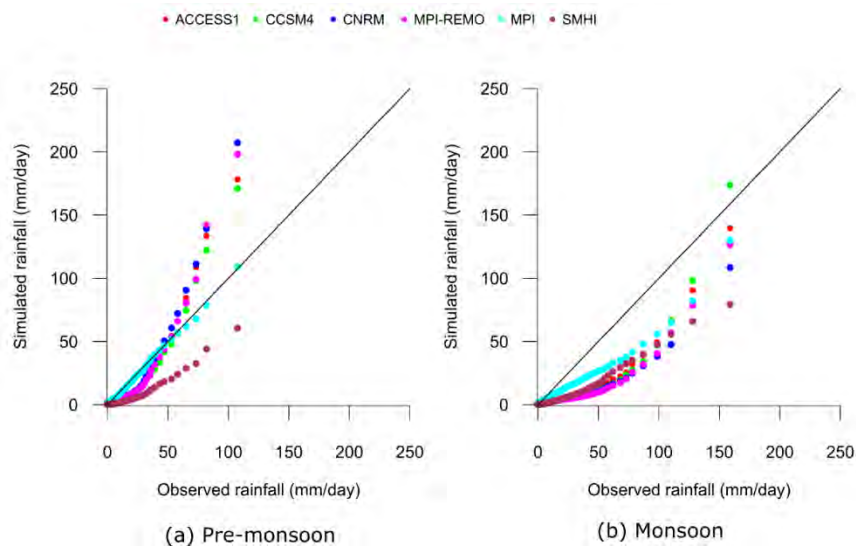


Fig 6.3 Q-Q Plot for Sylhet station during 1976-2005 for (a) Pre-monsoon and (b) Monsoon.

The Q-Q plot for Sylhet station showed that all the RCMs underestimated the low-intensity rainfall and overestimated the high-intensity rainfall during the pre-monsoon

(Fig 6.3). RCMs always underestimated the observed rainfall during the monsoon. Other stations also showed similar behavior like Sylhet in simulating present-day climate (see Fig B.2 and Fig B.3 in Appendix B).

6.3. Quantile Mapping Bias Correction of RCMs

The bias correction was performed on daily rainfall data for the pre-monsoon and monsoon season independently after modifying wet-day frequencies of the RCMs simulated rainfall as discussed in methodology in Chapter 4. However, the result of Sylhet station only was presented here as an example (Fig 6.4).

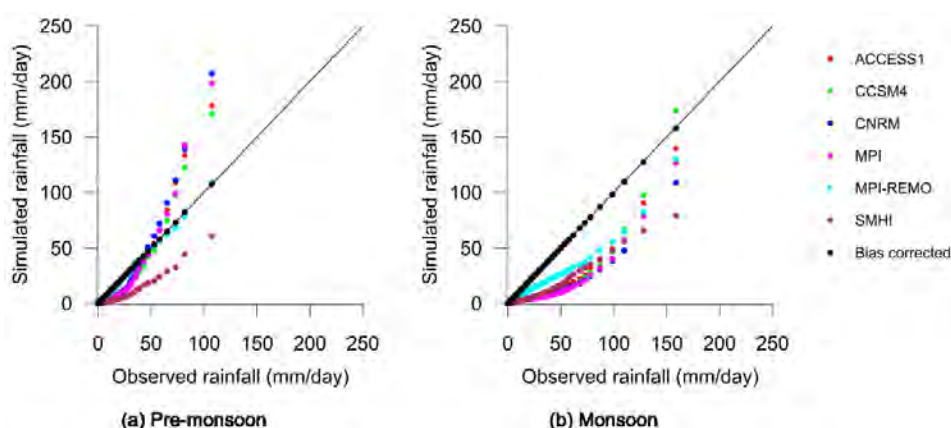


Fig 6.4 Quantile-quantile plots for the uncorrected (colored marker) and corrected (black marker) of simulated daily rainfall by RCMs against observed daily rainfall for Sylhet: (a) Pre-monsoon and (b) Monsoon.

The result of this bias correction for other stations was similar to that shown in Fig 6.4 (see Fig B.3 and Fig B.4 in Appendix B). Seasonal total rainfall of the Sylhet station before and after bias correction was shown in Table 6.1 as an example. Most of the uncorrected RCMs overestimate the observed rainfall at high intensity but, underestimated at low-intensity rainfall and also produce too many drizzle days during the pre-monsoon season (Fig 6.4). In terms of total seasonal rainfall also for Sylhet, as listed in Table 6.1, all RCMs simulate the almost equal amount of pre-monsoon rainfall except SMHI. Also, it was noteworthy that the simulated seasonal rainfall from four (ACCESS, CCSM4, MPI, and MPI-REMO) out of six RCMs was close to the observed amount (1087 mm). After bias correction, the RCM simulation was closer to the observed seasonal rainfall, and this improvement is evident for SMHI and CNRM RCMs. Among all six RCMs, the most considerable seasonal rainfall difference between simulation and observation is only 28 mm after bias correction.

Table 6.1 Seasonal rainfall for Sylhet station before and after bias correction.

		Observed	ACCESS	CCSM4	CNRM	MPI	MPI-REMO	SMHI
Pre-monsoon	Before bias correction	1087	1116	1050	1239	1134	1088	386
	After Bias correction	1087	1090	1072	1079	1081	1059	1076
Monsoon	Before bias correction	2733	1171	1168	976	1049	1760	982
	After Bias correction	2733	2707	2700	2710	2719	2712	2712

During the monsoon season, all six RCMs underestimated the observed daily rainfall considerably from low to high intensity (Fig 6.4). As a result, all the RCMs underestimate the seasonal rainfall (Table 6.1). The RCM rainfall for the other stations was also shown similar behavior like Sylhet. However, after the bias correction, the RCM rainfall distributions and total amounts were similar to those of the observed rainfall. The most substantial seasonal rainfall difference between RCMs and the observation is only 33 mm.

6.4. Bayesian Model Averaging

With the corrected RCM simulations, the multi-model ensemble mean was generated using the BMA method. Among several methods, the BMA method provides more reasonable ensemble mean [152,202,222] since it gives higher weight to the RCM with better predictive skills in the training period. Though BMA weights were calculated for all extreme rainfall indices, the result of monthly rainfall in the pre-monsoon and monsoon was presented here, for example. Histograms of the posterior marginal probability density functions of the BMA weights of the monthly rainfall totals for the individual ensemble members during the training period of Sylhet station for pre-monsoon and monsoon respectively were presented in Fig 6.5 and Fig 6.6 (see Fig B.6 to Fig B.15 Appendix B for the other stations). In those figures, it was found that all the histograms exhibit gamma distribution, as explained earlier. This means that there is high confidence in the weights applied to each of the individual models. The optimal values derived with the MCMC algorithm were separately indicated in each panel with the 'x' symbol.

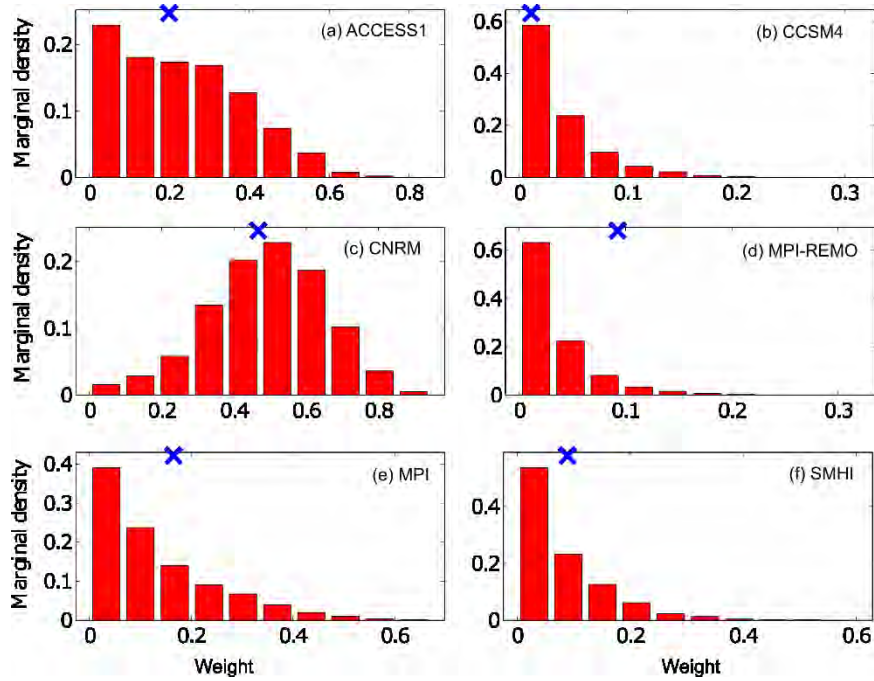


Fig 6.5 Marginal posterior pdf of the DREAM derived BMA weights of monthly rainfall totals for pre-monsoon of Sylhet station. The MCMC derived solution is separately indicated in each panel with symbol 'X'.

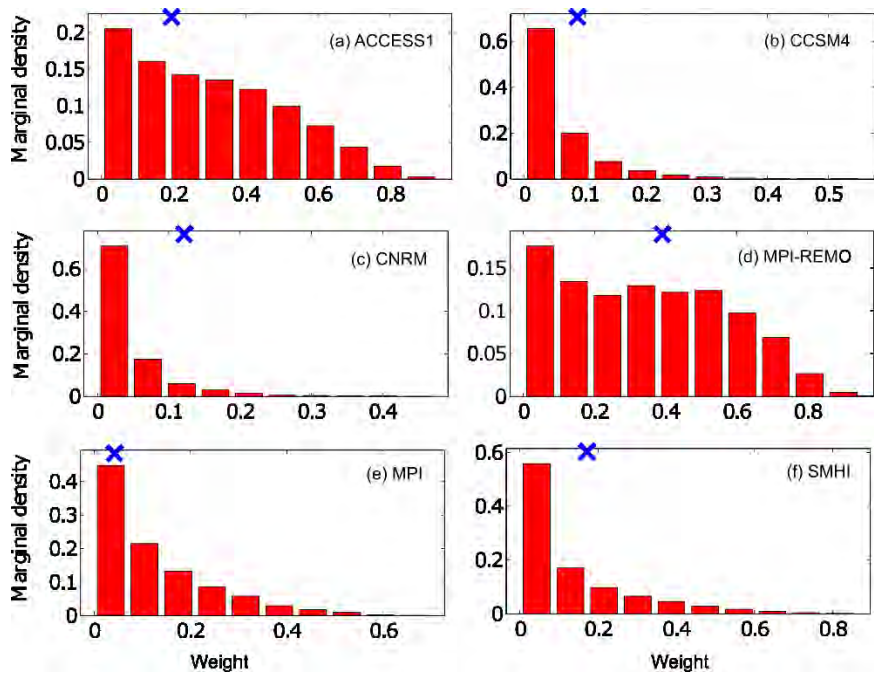


Fig 6.6 Marginal posterior pdf of the DREAM derived BMA weights of monthly rainfall totals for the monsoon of Sylhet station. The MCMC derived solution is separately indicated in each panel with symbol 'X'.

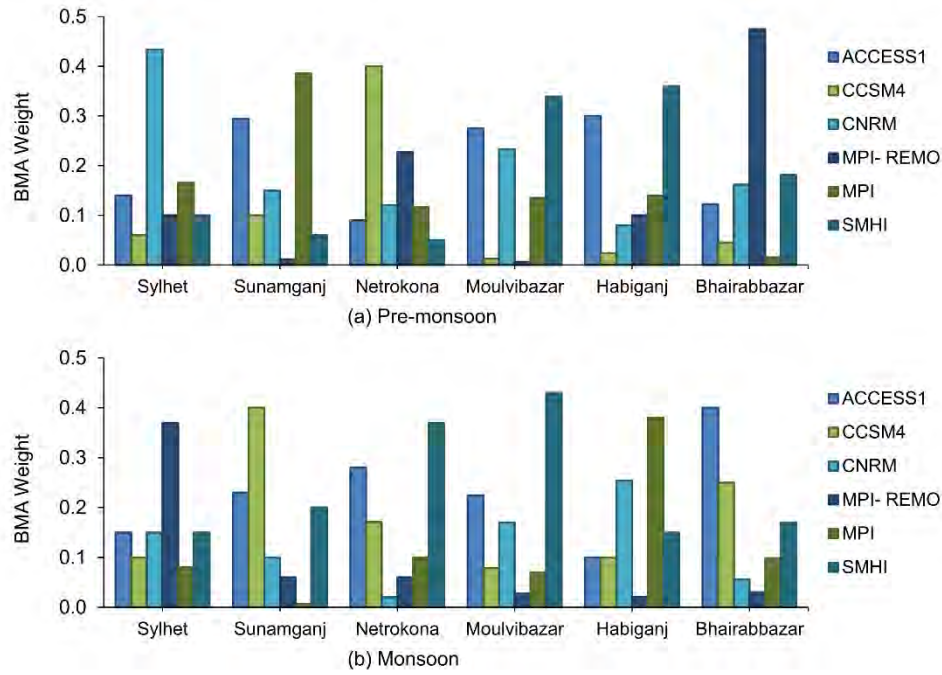


Fig 6.7 BMA weights of each RCM for monthly rainfall totals of different stations during the historical period (1976-2005): (a) Pre-monsoon and (b) Monsoon.

The optimal BMA weights for rainfall of six rainfall stations were presented in Fig 6.7. As noted previously, the BMA weights were calculated on monthly rainfall for the pre-monsoon and monsoon seasons separately. The BMA weight reflects the overall performance of the RCMs in capturing monthly rainfall for the study area. It reflects the overall performance of the RCMs in capturing monthly rainfall. The RCMs showed better performance at one station while worse performance in another station. No particular RCM was consistent for capturing higher BMA weights for all stations (Fig 6.7). Similarly, the RCMs performance varied in different seasons. Therefore, it can be inferred that there is no single best or worst model in simulating rainfall variation over the region, according to the concept of a multi-model approach.

The multi-model ensemble mean of rainfall was calculated using BMA weights, and by the simple arithmetic ensemble mean (AEM). The Normalized Root Mean Square Error (NRMSE) (RMSE was normalized by the standard deviation of the observed data), BMA and AEM for each RCMs were estimated to evaluate the performance of BMA (Table 6.2). It is noteworthy that the NRMSE of the commonly used AEM is always smaller than the corresponding statistic from each participating RCM for both seasons. This phenomenon is consistent with the general notion that the ensemble means usually outperforms all or most of the individual ensemble members [152]. Relative to the

simple AEM, the NRMSE of the BMA is even smaller. The NRMSE of BMA weights is lesser than all participating RCMs for all stations and seasons. For all six stations, the average percentage of the decrease in NRMSE from the AEM to BMA varies from 3% during the pre-monsoon to 22% during the monsoon season.

Table 6.2 Normalized Root Mean Square Error (NRMSE) for seasonal rainfall of different RCMs, Arithmetic Ensemble Mean (AEM) and BMA during the historical period (1976-2005).

Station	ACCESS	CCSM4	CNRM	MPI-REMO	MPI	SMHI	AEM	BMA
Pre-monsoon								
Sylhet	1.15	1.35	0.94	1.12	1.14	1.15	0.88	0.86
Sunamganj	1.04	1.32	1.12	1.06	1.02	1.22	0.80	0.78
Netrokona	1.17	1.01	1.10	0.96	1.13	1.22	0.75	0.72
Moulvibazar	1.05	1.36	1.05	1.33	1.30	0.99	0.81	0.76
Habiganj	1.14	1.58	1.20	1.34	1.40	1.02	0.82	0.78
Bhiarabbazar	1.37	1.53	1.39	0.97	1.66	1.19	0.92	0.78
Monsoon								
Sylhet	1.82	2.33	1.89	1.58	2.42	1.79	1.18	1.03
Sunamganj	1.89	1.98	1.89	1.58	2.37	1.84	1.39	1.01
Netrokona	2.25	1.95	1.95	1.72	2.34	1.76	1.22	1.07
Moulvibazar	1.82	2.00	1.97	1.60	1.99	1.57	1.19	1.13
Habiganj	2.01	2.32	2.48	1.76	1.94	1.85	1.65	1.24
Bhiarab Bazar	1.81	2.22	2.29	1.62	1.98	1.86	1.43	1.26

It was assumed that the BMA weights should reflect relevant model skill in the multi-model ensemble approach. In another way, it was anticipated that the RCMs having higher BMA weights should produce lower NRMSE. Sometimes, the weights of the RCMs were contradicted with NRMSE. For example, the model MPI received the second-highest BMA weight at Sylhet station during the pre-monsoon (Fig 6.7) but ranked the third lowest NRMSE among the six RCMs (Table 6.2). The paired correlations could explain this inconsistent nature between individual simulations in the ensemble. Sometimes, the RCMs with the higher BMA weight may have a lesser correlation with the observed data and vice versa. A substantial amount of redundancy caused this, and therefore results in de-weighting of the best single simulation and overweighting of the worse single simulation. Other authors [203,209,222] also found this kind of inconsistency in their studies.

6.5. The trend of future rainfall extremes

A number of plots as per the Fig 6.8 and Fig 6.9 showed Mann–Kendall based trends of the extreme rainfall indices in an intra-decadal time series (2041–2070 and 2071–2099) domain for RCP4.5 as well as RCP8.5 during the pre-monsoon and monsoon season, respectively. Sen's slopes were measured to determine the magnitude of changes of extreme indices during the projected time scale (2041–2070 and 2071–2099). The results of Sen's slope estimation are shown in Table 6.3 and Table 6.4 during the pre-monsoon and monsoon season, respectively.

Pre-monsoon

In RCP4.5, most of the extremes indices showed an increasing trend for the time series 2041–2070 while in time series 2071 to 2099, some indices showed an increasing trend and others showed a decreasing trend (Fig 6.8a and Fig 6.8b). A few of the stations, PRCPTOT, and R25 for 2041–2070 time series and R25 for 2071–2099 times series showed a significantly increasing trend. However, R99P and RX1 showed a significant decreasing trend for the 2071–2099 time series. In RCP8.5, most of the extremes indices showed an increasing trend for both 2041–2070 and 2071–2099 time series (Fig 6.8c and Fig 6.8d). Among them, R25, R95P, and R99P for 2041–2070 time series and PRCPTOT, R25, R95P and R99P for 2071–2099 showed a significantly increasing trend. The CDD showed a decreasing trend for RCP4.5 as well as RCP8.5 during both time series in some stations. It decreased significantly during the 2071–2099 for RCP8.5. The corresponding Sen's slopes of the extreme indices, which were significantly increased or decreased in Fig 6.8 were made bold and underlined in Table 6.3.

During the pre-monsoon, most of the extreme indices except CDD showed a decreasing trend for the period 1796-2005 (see Fig 5.4a) while most of the extreme indices showed an increasing trend for the scenario period except 2071-2099 for RCP4.5 (Fig 6.8). This increasing trend could be understood by analyzing the mechanisms of the pre-monsoon rainfall over northeast Bangladesh. Among different mechanisms, (discussed in Section 2.1), the heat low over India is one of the major causes. A heat low over central India adjacent to the western border of Bangladesh resulting from intense heating of the landmass triggers the southwesterly moisture flow from the Bay of Bengal towards the Meghalaya Plateau [159,195]. Due to global warming, the heat low over central India

is likely to increase [132,162]. This happening will cause more moisture flow toward the Meghalaya mountain region in India and will result in a more extreme rainfall event in northeast Bangladesh. Another cause can be explained by the Clausius–Clapeyron (C-C) relationship. The atmospheric moisture-holding capacity is likely to increase with the surface temperature through the C-C equation [144]. Several studies [5,12,31,166,177] also argued that this increase of rainfall might be attributed to the increase of low level (850 hPa) moisture content resulting from increased temperature due to global warming. In the case of RCP4.5, the emission of CO₂ peaking from 2040 to 2050, and it declines afterward while for RCP 8.5 it attains its peak in 2100 (Fig 2.4). Therefore, between 2071 and 2099 for RCP4.5, the extreme indices were decreased in most of the cases due to less moisture flow from the Bay of Bangle resulting from the slowing down of rising the sea surface temperature.

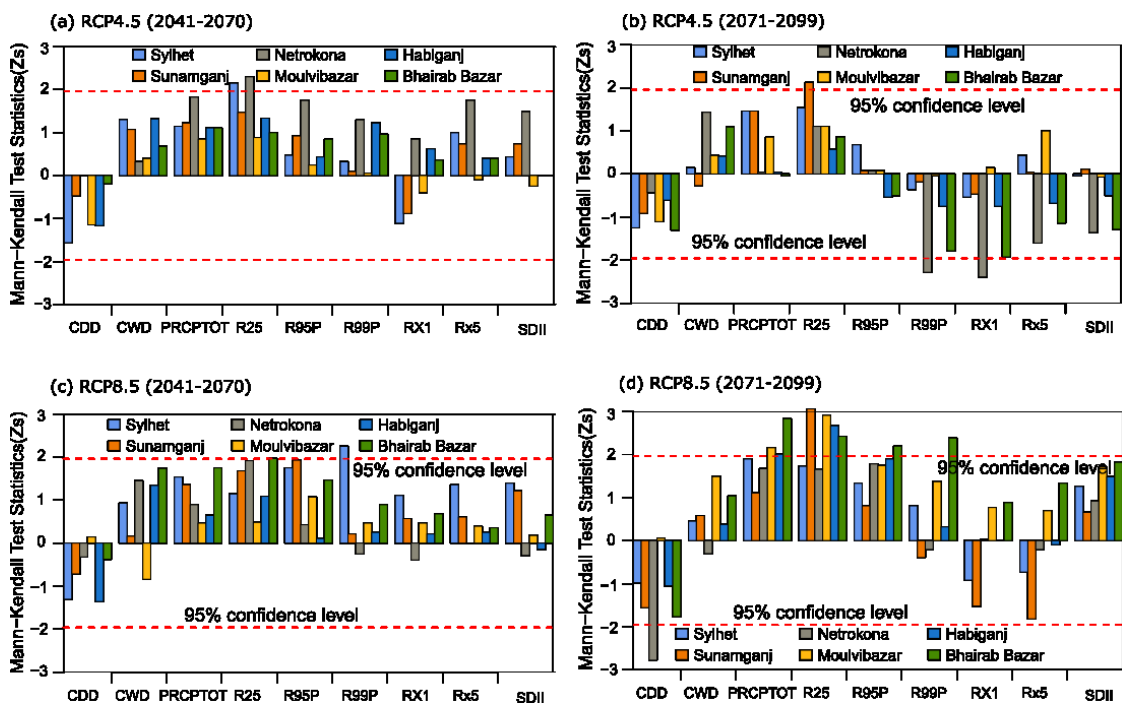


Fig 6.8 The normalized test statistic (Z_s) of the Mann-Kendall test of the indices of rainfall extremes considering all model ensemble mean derived by BMA for pre-monsoon: (a) RCP 4.5(2041-2070),(b)RCP4.5(2071-2099),(c)RCP8.5(2041-2070),(d) RCP8.5(2071-2099). (The absolute Z_s value which is higher than the critical value ($Z_c=1.96$) are considered as statistically significant at 95% confidence level.

Table 6.3 Sens's slope estimator of rainfall extremes considering all model ensemble mean derived by BMA for two future time slices (2041-2070 and 2071-2099 under RCP 4.5 and RCP 8.5 scenarios for Pre-monsoon. The corresponding Sen's slopes of the extreme indices which were significantly increased or decreased in Fig 6.8 were made bold and underlined.

Station	RCP	Period	CDD	CWD	PRCPTOT	R25	R95P	R99P	RX1	RX5	SDII
Sylhet	4.5	2041-2070	-0.05	0.02	5.17	<u>0.10</u>	0.13	0.12	-0.55	0.40	0.00
		2071-2099	-0.09	0.07	4.23	0.10	0.09	-0.08	-0.72	0.87	0.02
	8.5	2041-2070	-0.08	0.07	8.40	0.10	0.42	<u>1.00</u>	0.97	2.00	0.11
		2071-2099	-0.03	0.03	9.24	0.15	0.37	0.21	-0.52	-1.50	0.11
Sunamganj	4.5	2041-2070	-0.06	-0.01	5.60	0.15	0.01	0.05	-0.38	0.04	0.01
		2071-2099	-0.03	0.04	5.58	<u>0.07</u>	0.23	-0.14	-0.46	0.68	0.06
	8.5	2041-2070	-0.03	0.01	7.09	0.11	0.41	0.23	0.59	0.74	0.09
		2071-2099	-0.09	0.03	6.49	<u>0.17</u>	0.22	-0.24	-1.17	-3.44	0.07
Netrokona	4.5	2041-2070	-0.04	0.05	0.22	<u>0.07</u>	0.03	0.52	-1.02	-1.91	-0.12
		2071-2099	0.00	0.01	6.69	0.12	0.32	<u>-0.71</u>	0.49	2.73	0.14
	8.5	2041-2070	-0.03	0.05	3.72	<u>0.09</u>	0.12	-0.07	-0.22	0.02	-0.04
		2071-2099	-0.22	-0.01	6.58	0.09	0.30	-0.08	0.05	-0.31	0.09
Moulvibazar	4.5	2041-2070	-0.07	0.02	4.30	0.07	0.02	0.03	0.10	0.91	0.00
		2071-2099	-0.08	0.02	3.52	0.05	0.06	-0.03	-0.25	-0.16	-0.03
	8.5	2041-2070	0.01	-0.03	2.18	0.03	0.18	0.19	0.23	0.71	0.02
		2071-2099	0.00	0.05	<u>8.79</u>	<u>0.17</u>	0.45	0.58	0.49	0.70	0.20
Habiganj	4.5	2041-2070	-0.05	0.02	0.16	0.04	-0.10	0.44	-0.54	-1.11	-0.04
		2071-2099	-0.08	0.05	4.99	0.08	0.07	-0.36	0.37	0.89	0.00
	8.5	2041-2070	-0.08	0.06	3.20	0.06	0.02	0.11	0.23	0.17	-0.01
		2071-2099	-0.09	0.01	<u>7.40</u>	<u>0.13</u>	0.42	0.14	0.02	-0.10	0.11
Bhairabazar	4.5	2041-2070	-0.08	0.03	-0.07	0.04	-0.17	0.33	-0.76	-1.50	-0.12
		2071-2099	-0.01	0.04	3.65	0.04	0.17	-0.62	0.12	0.77	0.00
	8.5	2041-2070	-0.03	0.06	4.94	0.09	0.31	0.25	0.16	0.42	0.05
		2071-2099	-0.14	0.02	<u>10.71</u>	<u>0.13</u>	0.49	0.96	0.58	2.35	0.17

Monsoon:

Most of the extremes indices showed an increasing trend for the time series 2041–2070 while it showed a decreasing trend in most of the cases for the time series 2071 to 2099 for RCP4.5 (Fig 6.9a and Fig 6.9a). CDD, CWD, RX1, and SDII for the 2041–2070 time series showed a significantly increasing trend in a few stations. However, all the extreme indices except CDD and CWD showed a significant decreasing trend for 2071–

2099 time series in almost all stations. In RCP8.5, most of the extremes indices showed a decreasing trend for both 2041–2070 and 2071–2099 time series (Fig 6.9c and Fig 6.9d). Among them, almost all indices in most of the stations for 2041–2070 time series in addition to CWD, PRCPTOT, R50, RX1 and SDII for 2071–2099 at some stations showed a significant decreasing trend. The corresponding Sen's slopes of the extreme indices, which were significantly increased or decreased in Fig 6.9 were made bold and underlined in Table 6.4.

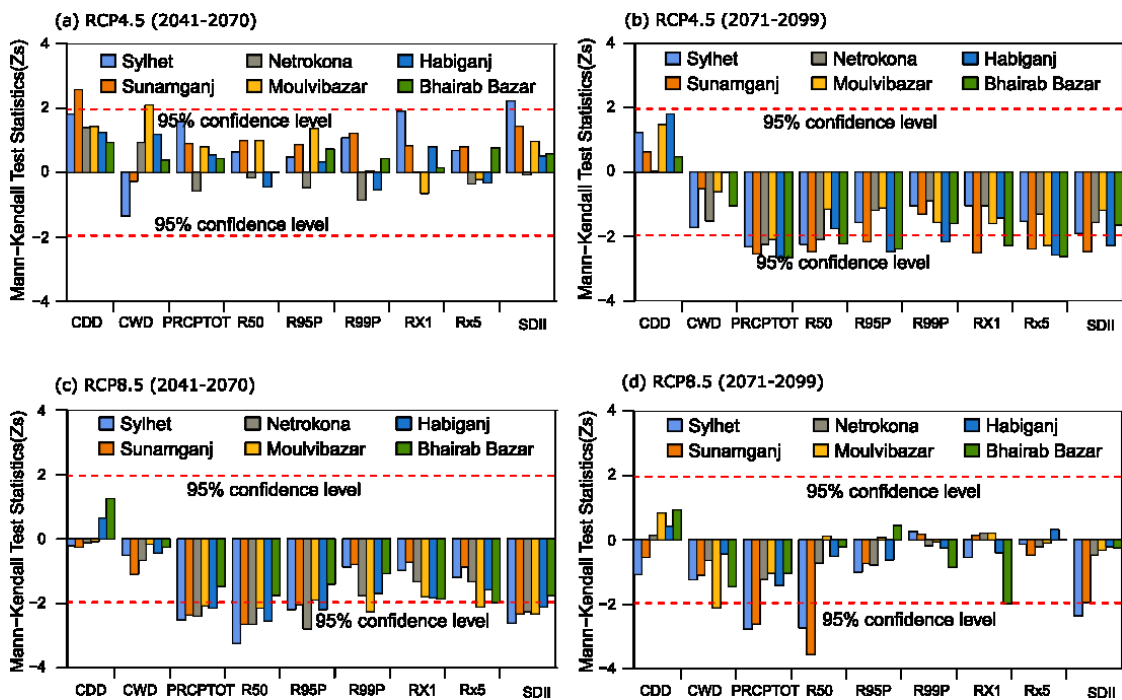


Fig 6.9 The normalized test statistic (Z_s) of the Mann-Kendall test of the indices of rainfall extremes considering all model ensemble mean derived by BMA for monsoon: (a) RCP 4.5(2041-2070),(b)RCP4.5(2071-2099),(c)RCP8.5(2041-2070),(d) RCP8.5(2071-2099). (The absolute Z_s value which is higher than the critical value ($Z_c=1.96$) are considered as statistically significant at 95% confidence level.

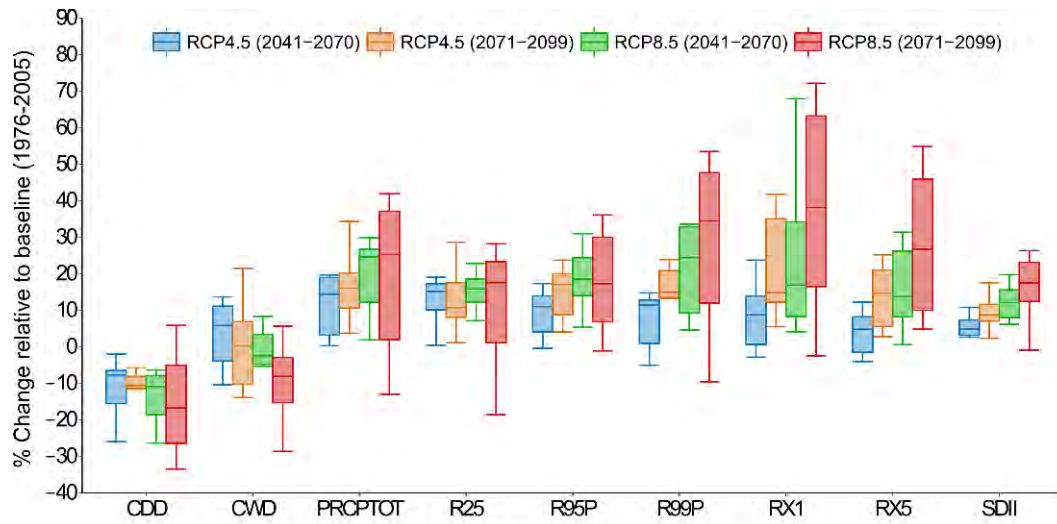
During the monsoon, the extreme indices showed a decreasing trend in most of the cases except less increase during 2041 to2070 in RCP4.5 (Fig 6.9), which is like the historical trend (Fig 5.4b). Several studies suggest that due to global warming under the increasing greenhouse, the temperature of the landmass of the subcontinent will increase slowly compared to the Indian Ocean, which will reduce the land-sea thermal gradient over the Indian subcontinent [162]. Therefore, extreme indices showed a decreasing trend during monsoon under almost emission scenarios.

Table 6.4 Sense slope estimator of rainfall extremes considering all model ensemble mean derived by BMA for two future time slices (2041-2070 and 2071-2099 under RCP 4.5 and RCP 8.5 scenarios for monsoon. The corresponding Sen's slopes of the extreme indices which were significantly increased or decreased in Fig 6.9 were made bold and underlined.

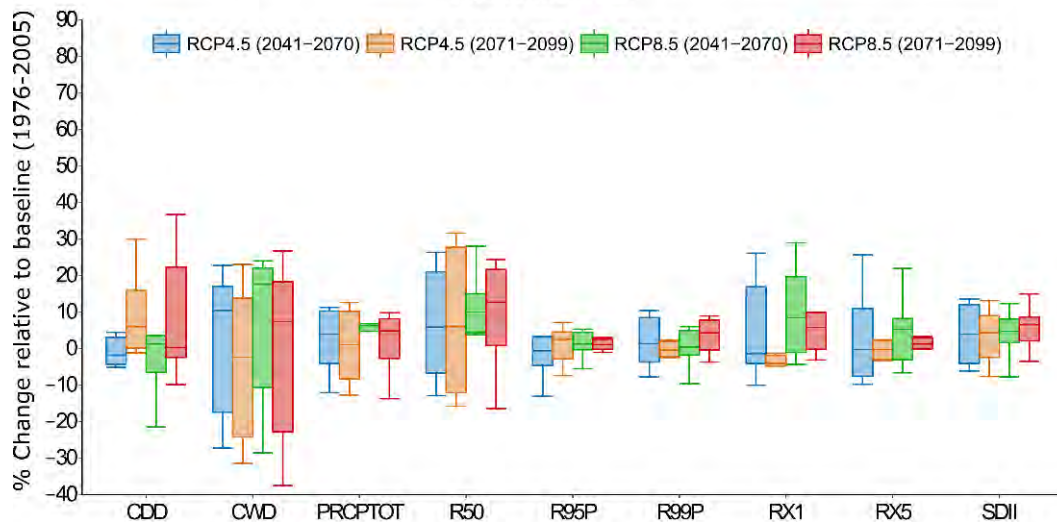
Station	RCP	Period	CDD	CWD	PRCPTOT	R50	R95P	R99P	RX1	RX5	SDII
Sylhet	4.5	2041-2070	0.06	-0.17	10.88	0.04	0.11	0.37	<u>1.15</u>	1.37	<u>0.14</u>
		2071-2099	0.04	-0.19	<u>-14.29</u>	<u>-0.11</u>	-0.27	-0.40	-0.61	-2.23	-0.10
	8.5	2041-2070	0.00	-0.06	<u>-19.58</u>	<u>-0.27</u>	<u>-0.48</u>	-0.45	-0.86	-2.01	-0.16
		2071-2099	-0.03	-0.20	<u>-19.18</u>	-0.17	-0.23	0.11	-0.38	-0.21	<u>-0.21</u>
Sunamganj	4.5	2041-2070	<u>0.05</u>	-0.04	8.67	0.08	0.18	0.54	0.43	1.57	0.16
		2071-2099	0.02	-0.05	<u>-30.30</u>	<u>-0.24</u>	<u>-0.66</u>	-0.48	<u>-1.34</u>	<u>-3.43</u>	<u>-0.23</u>
	8.5	2041-2070	0.00	-0.14	-34.22	<u>-0.23</u>	<u>-0.61</u>	-0.32	-0.55	-2.19	-0.27
		2071-2099	-0.02	-0.16	<u>-31.14</u>	-0.28	-0.22	0.14	0.05	-0.73	<u>-0.15</u>
Netrokona	4.5	2041-2070	0.03	0.06	-4.01	-0.01	-0.08	-0.22	-0.01	-0.43	0.00
		2071-2099	0.00	-0.11	<u>-14.70</u>	<u>-0.14</u>	-0.22	-0.32	-0.58	-1.23	-0.10
	8.5	2041-2070	0.00	-0.05	-17.55	<u>-0.23</u>	<u>-0.67</u>	-0.53	-0.89	-2.19	-0.14
		2071-2099	0.00	-0.04	-7.37	-0.03	-0.15	-0.08	0.12	-0.56	-0.02
Moulvibazar	4.5	2041-2070	0.03	<u>0.14</u>	3.96	0.05	0.24	0.01	-0.51	-0.23	0.07
		2071-2099	0.06	-0.04	<u>-11.50</u>	-0.05	-0.16	-0.59	-1.45	<u>-4.32</u>	-0.07
	8.5	2041-2070	0.00	-0.01	-11.39	<u>-0.10</u>	<u>-0.41</u>	<u>-0.92</u>	-1.34	-3.62	-0.11
		2071-2099	0.02	<u>-0.11</u>	-6.92	0.00	0.01	-0.02	0.32	-0.22	-0.01
Habiganj	4.5	2041-2070	0.03	0.12	2.34	-0.02	0.09	-0.17	0.37	-0.54	0.02
		2071-2099	0.06	0.00	<u>-14.67</u>	<u>-0.08</u>	<u>-0.40</u>	<u>-0.79</u>	-0.91	<u>-3.56</u>	<u>-0.12</u>
	8.5	2041-2070	0.02	-0.02	-11.18	<u>-0.13</u>	<u>-0.47</u>	-0.66	-0.87	-1.75	-0.11
		2071-2099	0.01	-0.04	-5.37	-0.02	-0.09	-0.06	-0.21	0.40	-0.01
Bhairabazar	4.5	2041-2070	0.04	0.02	3.27	0.00	0.19	0.20	0.09	1.40	0.05
		2071-2099	0.02	-0.04	<u>-11.03</u>	<u>-0.09</u>	<u>-0.35</u>	-0.62	<u>-1.07</u>	<u>-2.77</u>	-0.12
	8.5	2041-2070	0.04	-0.01	-8.02	-0.07	-0.33	-0.46	-1.47	-3.77	-0.11
		2071-2099	0.05	-0.05	-3.01	0.00	0.10	-0.29	<u>-1.02</u>	0.03	-0.01

6.6. Changes of Future Rainfall Extremes

The changes of future rainfall extremes were estimated for all RCMs, and for their ensemble mean generated by BMA weight (see Fig 6.7). Fig 6.10 shows the variability of the mean changes of extreme indices with respect to the baseline for Sylhet station. The variability of the extreme indices for other stations is presented in Fig B.16 to Fig B.20 in Appendix B.



(a) Pre-monsoon



(b) Monsoon

Fig 6.10 Box and whisker plots for changes of rainfall extremes of Sylhet station considering all RCMs for two future time slices (2041-2070 and 2071-2099) relative to the baseline period (1976-2005) under RCP 4.5 and RCP 8.5 scenarios: (a) Pre-monsoon and (b) Monsoon.

During pre-monsoon, among all extreme indices, the variability of the relative changes was more significant for the one-day maximum rainfall (RX1) and lesser for the Simple Daily Intensity Index (SDII), implying more uncertainty associated in RX1 and lesser for SDII (Fig 6.10a). This result was not unexpected because the seasonal maximum daily rainfall is the single most significant value in a season and this value has the large excursion from year to year, while the rainfall intensity index is a quantity averaged over many days in a season. The uncertainty for all extremes indices was more significant for far future (2071-2099) and for higher RCP (RCP8.5) compare to lower RCPs in the near future. Considering all RCMs, the mean relative changes were positive

for all extreme indices except for consecutive dry day (CDD) and consecutive wet day (CWD) during pre-monsoon at Sylhet station. Therefore, the consecutive dry days become shorter over time. Similar to pre-monsoon, the uncertainty in relative changes was lesser for SDII during monsoon (Fig 6.10b). Also, the significant variability was found for CWD, CDD, and R50. The range of variability for changes in rainfall extremes was more significant during the pre-monsoon than the monsoon season. The variability of the extreme indices for other stations exhibit almost similar pattern like Sylhet (see Fig B.16 to Fig B.20 in Appendix B).

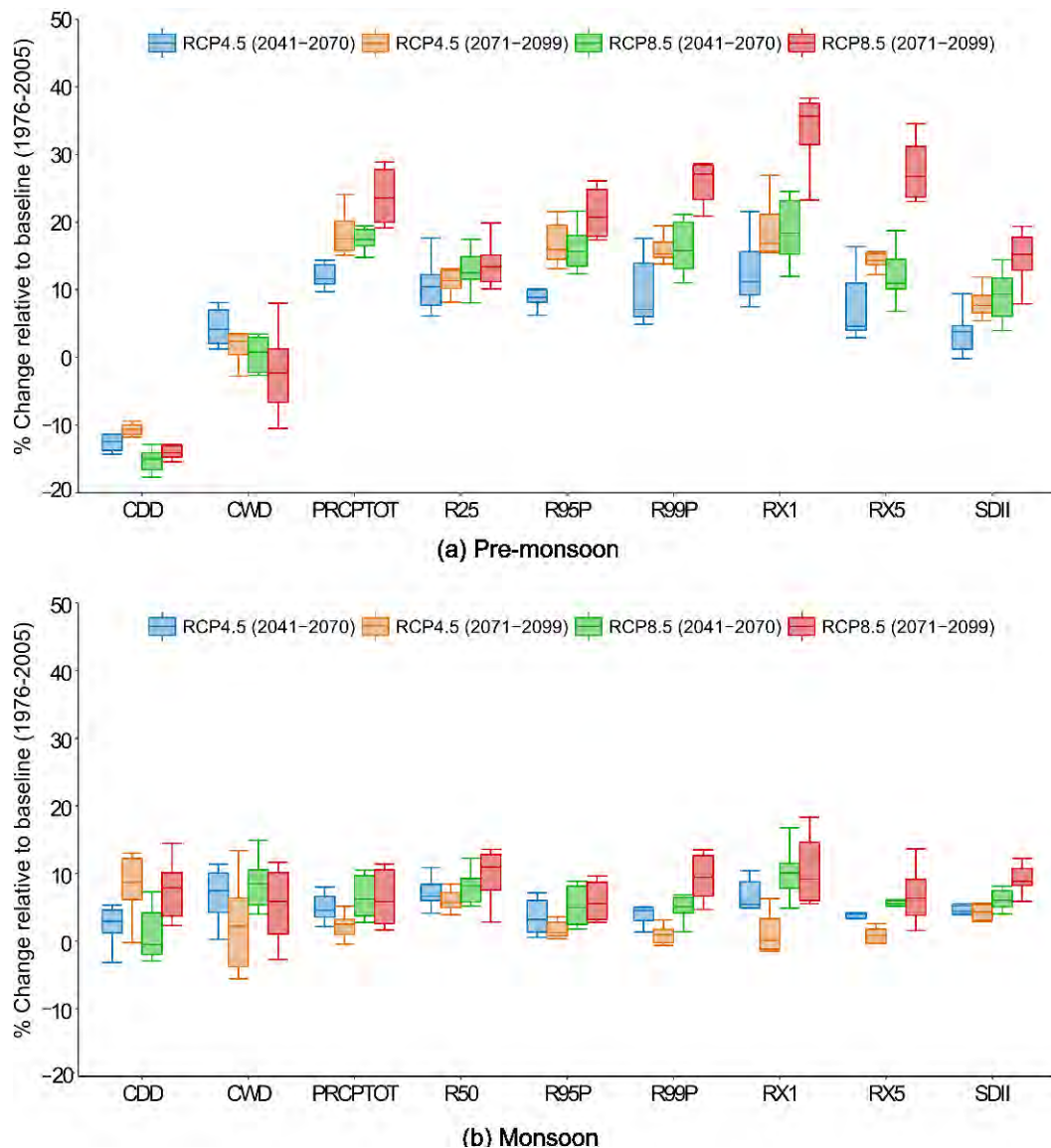


Fig 6.11 Box and whisker plots for changes of rainfall extremes over the study area considering all model ensemble mean derived by BMA for two future time slices (2041-2070 and 2071-2099) relative to the baseline period (1976-2005) under RCP 4.5 and RCP 8.5 scenarios: (a) Pre-monsoon and (b) Monsoon.

The mean changes of extreme indices for all stations were generated to get an overview of the likely changes over the whole region (Fig 6.11). In the pre-monsoon season (Fig 6.11a), the interquartile ranges of the box plot were negative for CDD while positive for RX1, RX5, PRCPTOT, R25, SDII, R95P, and R99P in future time slices under the RCP4.5 as well as RCP8.5 over the study area. This indicates an increasing level of changes for those indices with a positive range in the future.

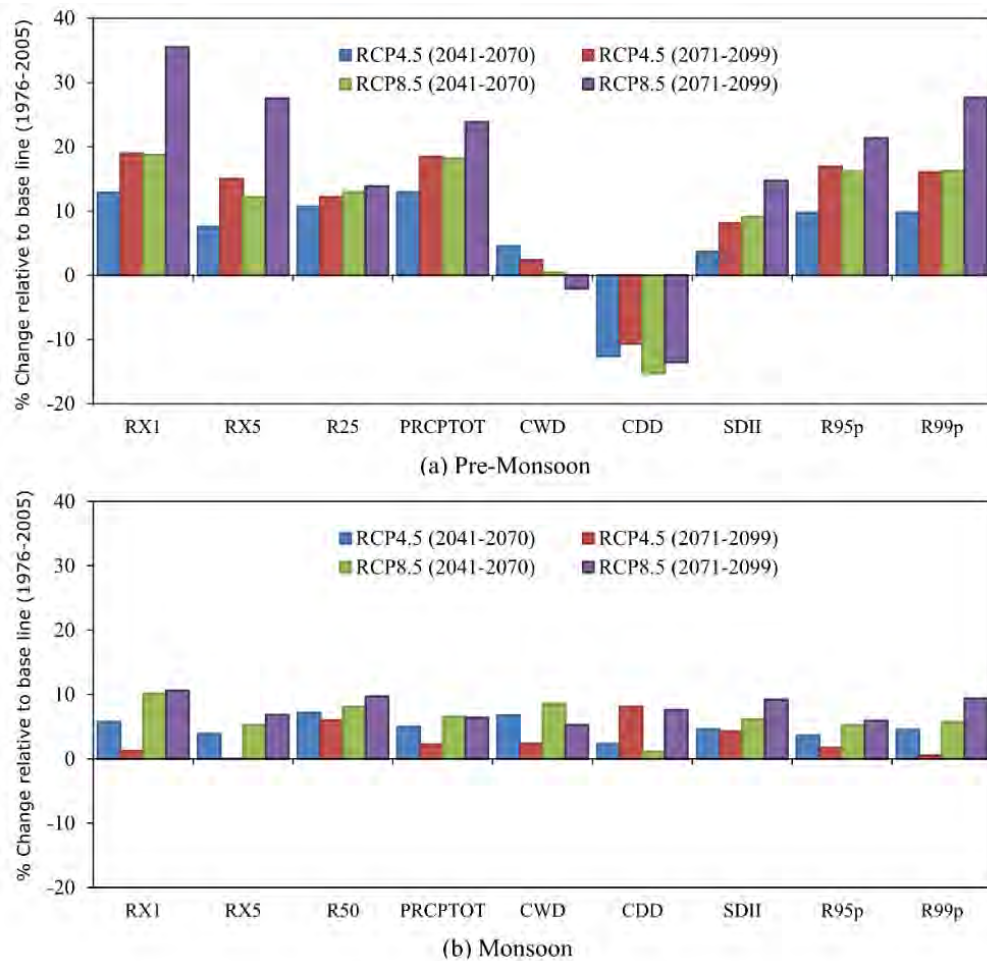


Fig 6.12 Average changes of rainfall extremes over the study area considering all model ensemble mean derived by BMA for two future time slices (2041-2070 and 2071-2099) relative to the baseline period (1976-2005) under RCP 4.5 and RCP 8.5 scenarios: (a) Pre-monsoon and (b) Monsoon.

During the monsoon season (Fig 6.11a), the interquartile ranges of the box plot were relatively smaller at lower RCP (RCP4.5) during the near future (2041-2070). However, it was more significant for higher RCP (RCP8.5) during the far future (2071-2099). The variability of all extreme indices was more significant for the period 2071-2099 under the RCP8.5 for both seasons, which indicate that there was a more considerable uncertainty associated with RCMs in projecting rainfall extremes as the RCP increases

and time slice progresses from mid-century to the late century. Another most important thing was that the interquartile ranges of all extreme indices except CDD and CWD in both seasons were positive, meaning that all RCMs projected positive change. These positive changes made us more confident that these extreme indices were expected to increase in the future. The interquartile ranges of CDD in the monsoon and CWD in both seasons vary between positive and negative values; however, their median values were positive. Therefore, it could not be inferred with confidence that the CDD and CWD are likely to increase in the future.

Average changes of rainfall extremes over the study area considering all stations, the multi-model ensemble mean derived by BMA was presented in Fig 6.12. All the extreme indices were projected to increase in the future, but a decrease of CDD and CWD under RCP8.5 for the period 2071-2099 during the pre-monsoon season (Fig 6.12a).

Table 6.5 p-values of average changes of rainfall extremes over the study area considering all model ensemble mean in different RCP scenarios using Mann–Whitney U test. The extreme indices which changed significantly at 95 % confidence level (p-value ≤ 0.05) are bold and underlined.

Index	RCP4.5		RCP8.5		
	2041-2070	2071-2099	2041-2070	2071-2099	
Pre-monsoon	RX1	<u>0.013</u>	<u>0.000</u>	<u>0.000</u>	<u>0.000</u>
	RX5	0.100	<u>0.003</u>	<u>0.012</u>	<u>0.000</u>
	CDD	<u>0.003</u>	<u>0.020</u>	<u>0.001</u>	<u>0.002</u>
	CWD	0.234	0.581	0.919	0.323
	SDII	0.221	<u>0.038</u>	<u>0.011</u>	<u>0.000</u>
	PRCPTOT	<u>0.008</u>	<u>0.001</u>	<u>0.002</u>	<u>0.000</u>
	R99P	<u>0.023</u>	<u>0.001</u>	<u>0.001</u>	<u>0.000</u>
	R95P	<u>0.025</u>	<u>0.001</u>	<u>0.001</u>	<u>0.000</u>
	R25	<u>0.038</u>	<u>0.019</u>	<u>0.025</u>	<u>0.019</u>
Monsoon	RX1	0.149	0.963	<u>0.041</u>	<u>0.007</u>
	RX5	0.621	0.853	0.239	0.120
	CDD	0.756	0.090	0.797	0.075
	CWD	0.058	0.846	<u>0.034</u>	0.273
	SDII	0.193	0.233	<u>0.079</u>	<u>0.000</u>
	PRCPTOT	0.362	0.700	0.182	0.093
	R99P	0.286	0.877	0.145	<u>0.006</u>
	R95P	0.677	0.805	0.322	0.057
R50	0.240	0.301	0.213	0.086	

During the monsoon, all the extreme rainfall indices were likely to increase in the future under all scenarios (Fig 6.12b). However, the increasing rate of extreme indices was more significant in the pre-monsoon season than monsoon season. Moreover, all the extreme indices except CWD likely to change significantly at the 95% confidence level during the pre-monsoon season (see Table 6.5). The average pre-monsoon rainfall of the study area was projected to increase by 12.93% for the near future and 18.42% in the far future under RCP4.5. Under the RCP8.5, it was projected to increase by 18.18% in the near future and 23.85% in the far future (Fig 6.12a). During the monsoon, it was projected to increase by 4.96% in the near future and 2.27% in the far future under the RCP4.5. However, it was projected to increase by 6.56% in the near future and 6.40% in the far future under the RCP8.5. Therefore, the study area is expected to experience more frequent floods in both the pre-monsoon and monsoon seasons when climate changes. Notably, the intensity and the magnitude of the flash flood in pre-monsoon is likely to increase more in the future as a result of the high increasing rate of most extreme indices related to the occurrence of the flash flood (e.g., PRCPTOT, RX1, SDII, R95p, R99p) with a high decrease rate of CDD. This situation is projected to be more intense as the century progresses.

6.7. Summary

The impact of climate change on extreme rainfall in northeast Bangladesh using six RCMs over CORDEX South Asia domain under the RCP4.5 and RCP8.5 was summarized here. Generally, the RCMs are affected by biases inherited from driving GCMs. It was found that the RCMs overestimate the heavy rainfall events and underestimate low rainfall events during the pre-monsoon season while underestimating as a whole during the monsoon season. Therefore, the quantile mapping method was applied to correct the bias associated with RCMs. After that, the BMA approach was used to generate the multi-model ensemble mean. The BMA mean is a weighted average related to each RCM's predictive skill. A closer look at each RCM showed that no single model was best or worst in simulating rainfall variations over northeast Bangladesh. However, the BMA produced more reliable results since NRMSE of it was lower than all six individual models and the arithmetic multi-model ensemble mean.

The result of the trend analysis showed that most of the extreme indices showed an increasing trend for the scenario period, except 2071-2099 for RCP4.5 while it showed a decreasing trend for the baseline period during pre-monsoon season. The extreme indices decreased in most cases, similar to the historical trend during monsoon season.

The seasonal rainfall, together with other extreme indices, is expected to increase with respect to baseline except for a decrease of CDD during both the pre-monsoon and monsoon seasons. However, the increasing rate of extreme indices is generally more significant in the pre-monsoon season than monsoon season. The average pre-monsoon rainfall of the study area is projected to increase by 12.93% in the near future and 18.42% in the far future under RCP4.5. Under the RCP8.5, it is projected to increase by 18.18% in the near future and 23.85%. During the monsoon, it is projected to increase by 4.96% in the near future and 2.27% in the far future under the RCP4.5 while 6.56% in the near future and 6.40% in the far future under the RCP8.5. Therefore, the study area is likely to experience more frequent floods in the pre-monsoon season under the warming climate. Notably, the intensity and the magnitude of the flash flood in pre-monsoon is expected to increase more in future because of the high, increasing rate of all extreme indices related to the occurrence of the flash flood (e.g., PRCPTOT, RX1, SDII, R95p, R99p). This situation is projected to be more intense in 2071-2099 than in 2041-2070.

These results show that the pre-monsoon season, in particular, may witness the most significant changes in rainfall in northeast Bangladesh. Seasonal rainfall together with other extreme indices expected to increase, causing the occurrence of the more frequent high magnitude of flash floods putting the harvest of Boro rice, as well as infrastructure and lives at risk. This situation may intensify further as the century progresses. In the next chapter, the linkage of pre-monsoon rainfall with ENSO and its response under climate change is discussed.

CHAPTER 7

RELATIONSHIP BETWEEN EI NINO SOUTHERN OSCILLATION (ENSO) AND PRE-MONSOON RAINFALL AND ITS RESPONSE UNDER THE WARMING WORLD

7.1. Introduction

The historical and future trends of extreme rainfall indices were discussed in Chapter 5 and Chapter 6, respectively. The changes in rainfall extreme indices with respect to baseline due to climate change was also described in Chapter 6. As it was discussed earlier that Boro rice is the main crop of northeast Bangladesh and the pre-monsoon rainfall is the primary concern of the community of the region since the pre-monsoon heavy rainfall destroys this Boro rice. Therefore, it is essential to know the behavior of the next pre-monsoon rainfall in one or two months in advance so that the communities can have enough time to search for advance measures to manage the risks. ENSO can have a high potential value in this aspect if it is possible to establish its relationship with the variability of the pre-monsoon rainfall of the region. In this context, this chapter describes the relationship between El Niño Southern Oscillation (ENSO) and pre-monsoon rainfall, particularly in April over the Meghna basin and its response under the warming world.

The relationships between large-scale process and a pre-monsoon rainfall in the Meghna basin was performed in three steps. Firstly, the relationship between pre-monsoon rainfall and heat low in central India during the pre-monsoon, particularly in April was determined. Because the southwesterly moisture flows from the Bay of Bengal is triggered by the low-pressure system in central India adjacent to the northwest border of Bangladesh which brings moist air towards the foothills of the Meghalaya Mountain which feeds deep convection over the Meghna basin. Before determining the relationship between heat low over India and ENSO, it is essential to know the answer of two questions: firstly, does there exist any significant relationship between pre-monsoon rainfall and ENSO? Secondly, if there is a significant relationship between pre-monsoon rainfall and ENSO then among different ENSO index (e.g., ESOI, SOI, ONI, and MEI) which is the best suited ENSO index for the study area? Therefore, the relationship between the pre-monsoon rainfall and different ENSO indexes (e.g., ESOI, SOI, ONI, MEI) with different monthly lags was determined in the second step. Since

heat wave produces heat low, the relationship between heat low in central India during April and best suited ENSO index (identified in the second step) was determined in the third step. The impact of climate change on ENSO was determined in terms of changes of ENSO frequency and intensity at different RCP scenarios with respect to the baseline. The detail description of the data and the methodology can be found in Chapter 3 and Chapter 4, respectively.

In this chapter, the relationship between the rainfall of April and different ENSO indices was discussed first to show how April rainfall was connected with ENSO. After that, the possible changes in the intensity and magnitude of the ENSO index under different RCP scenarios in future time slices were discussed.

7.2. Relationship between ENSO and pre-monsoon rainfall

The southwesterly moisture flows from the Bay of Bengal towards the Meghalaya Mountain region driven by the heat low over central India adjacent to the north-western border of Bangladesh resulting from strong heating of the landmass causes heavy pre-monsoon rainfall over the Meghna basin [159]. To investigate this mechanism, the wind map was plotted for some flooding events (e.g., 2004, 2010, 2016 and 2017) and some non-flooding events (e.g., 2008 and 2014) during April in Fig 7.1 and Fig 7.2, respectively. It was observed that there was a low-pressure system (Cyclonic) in central India and the high-pressure system (Anticyclonic) in the Bay of Bengal during the flooding event (Fig 7.1). However, there was no such situation during the non-flooding event (Fig 7.2).

In the next steps, the relationship between pre-monsoon rainfall of Cherrapungi and heat low over central India during the pre-monsoon particularly, in April was established (Fig 7.3). Since the intense heating of the earth's surface creates low pressure in the surrounding area, this relationship was determined with MSL instead of heat low. It was found that there is a high inverse correlation ($\rho \leq -0.55$) between April rainfall over the Cherrapungi and heat low over central India during April. Therefore, the mechanism of heavy pre-monsoon rainfall discussed in the previous section was justified by this relationship.

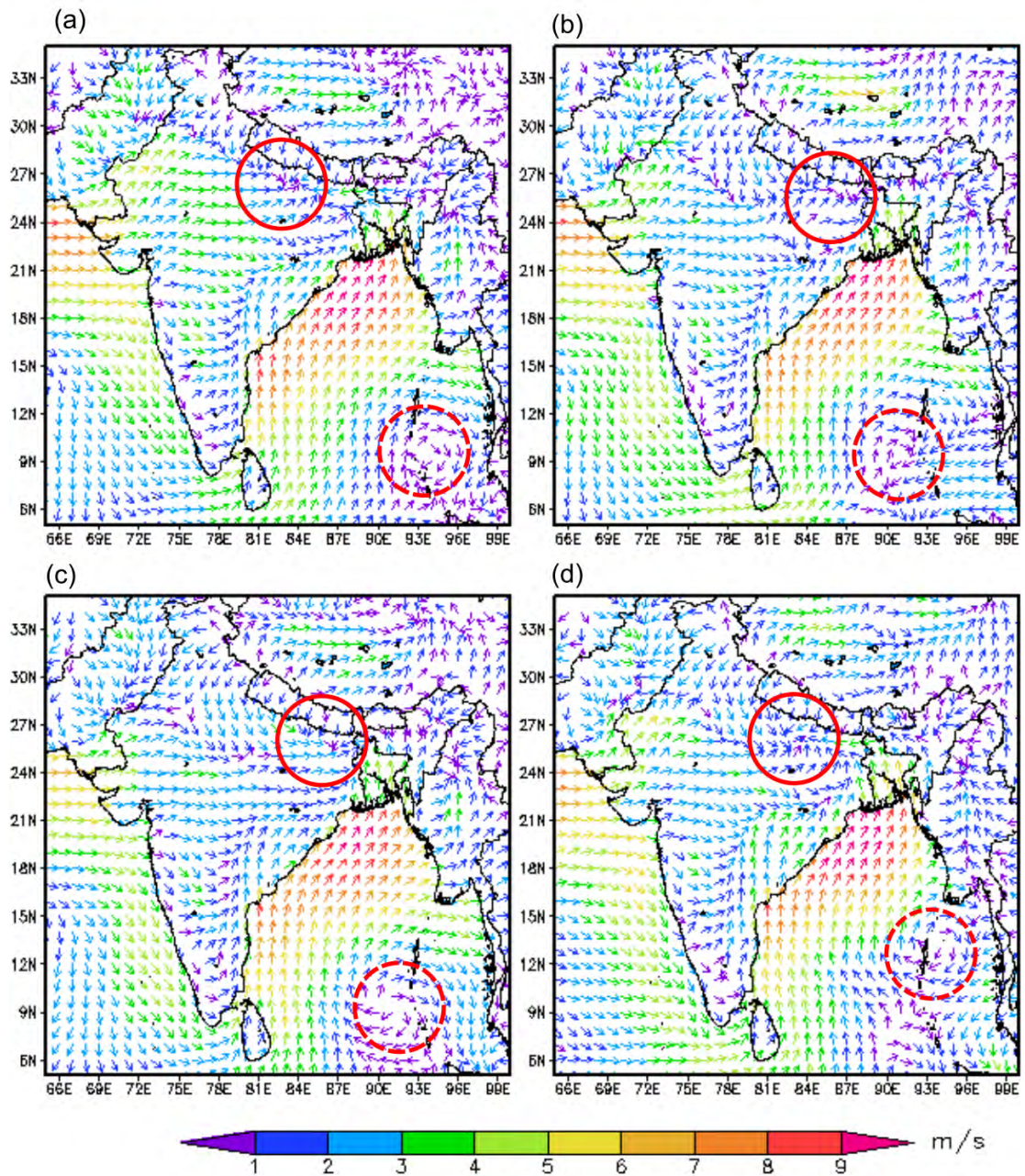


Fig 7.1 Average Wind flow direction during some flooding event in April: (a) April 9 to April 19, 2004; (b) April 1 to April 4, 2010; (c) April 20 to April 30, 2016, and (d) April 1 to April 4, 2017. The low-pressure zone is marked with a solid red circle, and the high-pressure zone is marked with a dashed red circle.

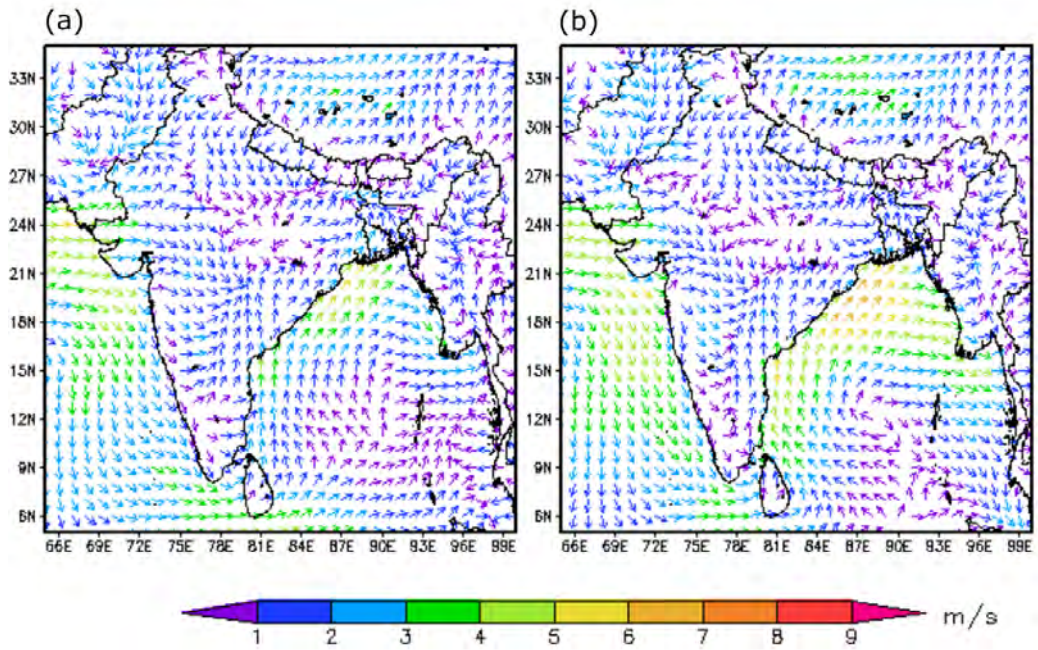


Fig 7.2 Average Wind flow direction during some non-flooding event in April: (a) April 1 to April 30, 2008, and (b) April 1 to April 30, 2014.

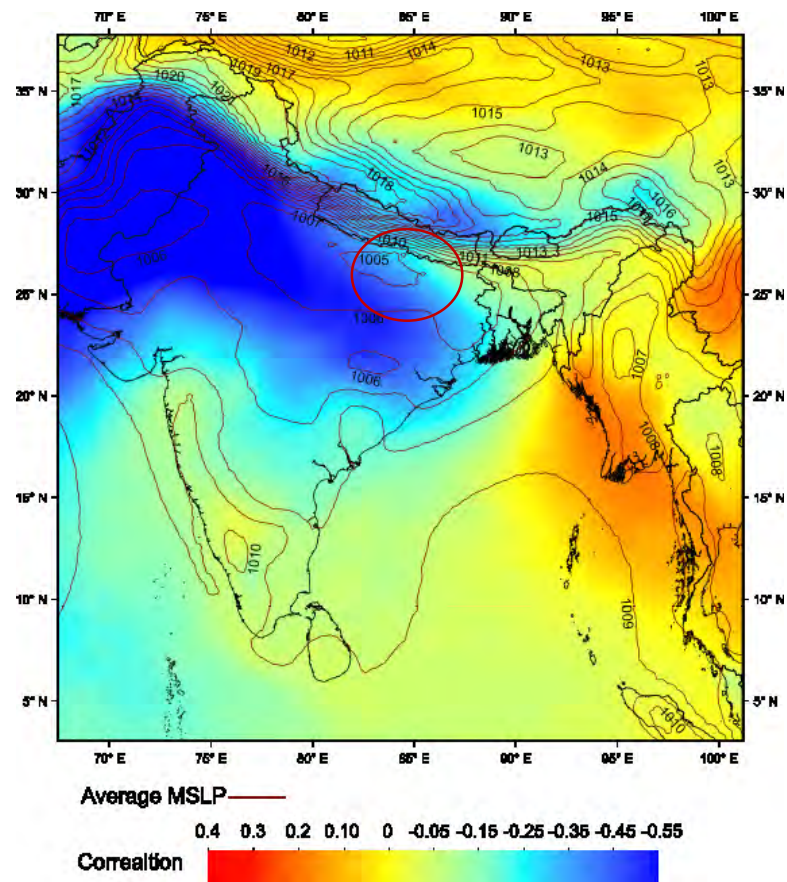


Fig 7.3 Correlation between MSL pressure and April rainfall over Cherrapunji during the year 1979 to 2017.

Before determining the relationship between heat low over India and ENSO, the relationship between the rainfall of April for the study area and different ENSO index with different monthly lags (e.g., December, January, and February) were identified the most significant ENSO index for the study area. The relationship between rainfalls of April in the study area with different ENSO index was presented in Fig 7.4. In this study, 38 years (1979 to 2017) data were used, and for this data period, the correlation value for a 95% confidence level is 0.32 [156]. The part of the study area in which the correlation value is statistically significant (p -value ≤ 0.05) is shaded with red color, as shown in Fig 7.4. In this figure, it is observed that the ONI index during January (Fig 7.4h) has the utmost correlation value ($\rho=0.52$) and SOI index during January (Fig 7.4b) has the uppermost spatial coverage of the correlation value for which it is statistically significant. However, the Cherrapunji, the rainfall of which station plays a vital role in flooding of the study area is outside of the statistically significant area for the SOI index during January. Therefore, it can be stated that the ONI index during January is important for forecasting of flooding during April for the study area.

The normalized rainfall of Cherrapunji during April against ONI the index during January was also plotted to see how it influences the flooding of the study area (Fig 7.5). The year in which the ONI index higher than 0.5°C (less than 0.5°C) are classified as El Niño (La Niña) year and any year not meeting the El Niño or La Niña phase criteria is defined as a neutral year [110]. In most of the cases, the normalized rainfall anomaly is positive (negative) for El Niño (La Niña) years, and there is a mixture of rainfall trend during the neutral year (Fig 7.5). The year in which there was a flood in April was also leveled in Fig 7.1 and found that all the flooding event occurred during El Niño or Neutral year except only 1985. From this figure, it can be concluded that most of the positive rainfall anomaly and the flooding events occurred when the ONI index during January is positive.

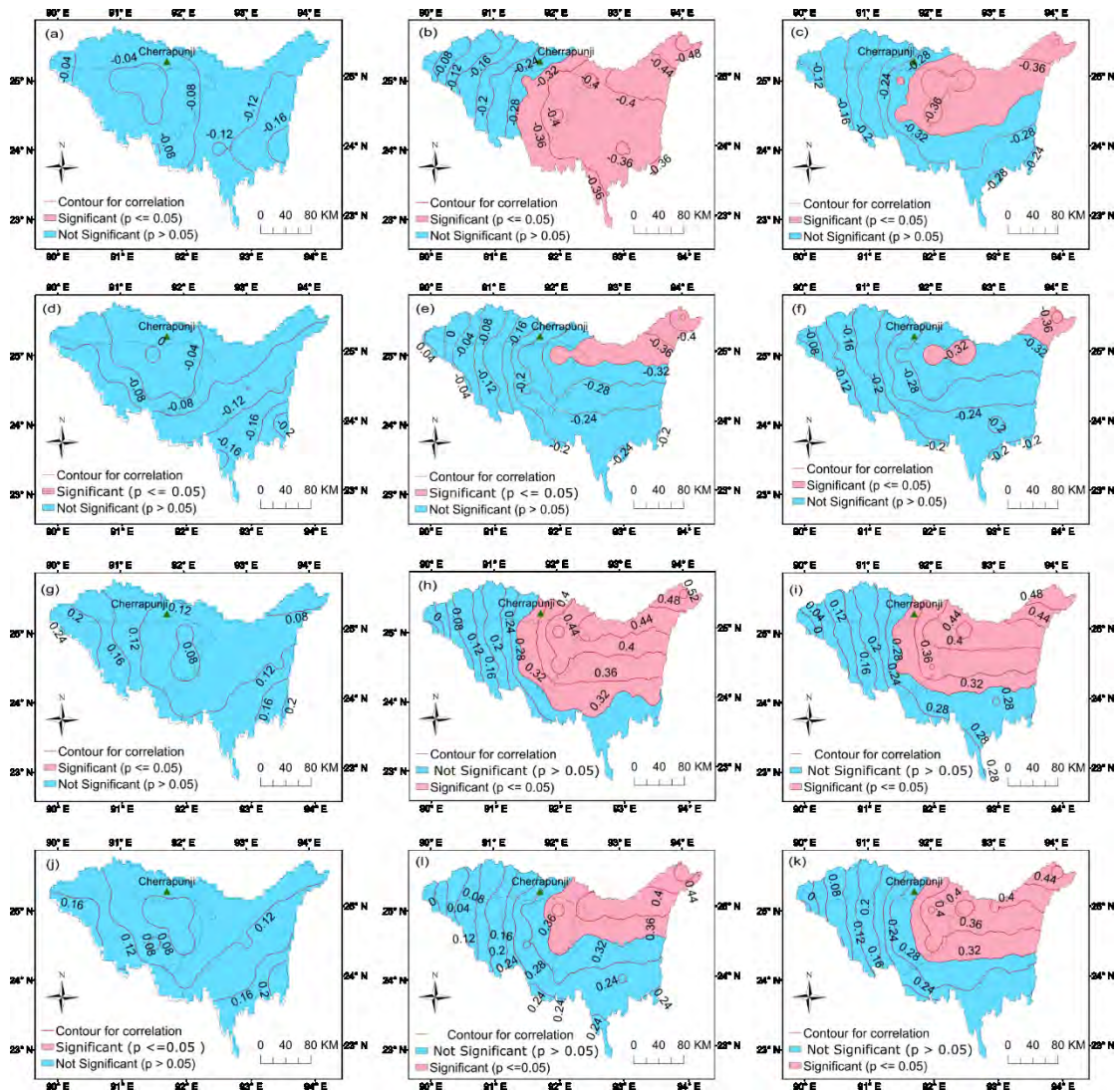


Fig 7.4 Correlation between April rainfall and different ENSO index for the period 1979 to 2017: (a) SOI for December; (b) SOI for January; (c) SOI for February; (d) ESOI for December; (e) ESOI for January; (f) ESOI for February; (g) ONI for December; (h) ONI for January; (i) ONI for February; (j) MEI for December; (k) MEI for January and (l) MEI for February. The study area in which the correlation value is statistically significant (p -value ≤ 0.05) is shaded with red color.

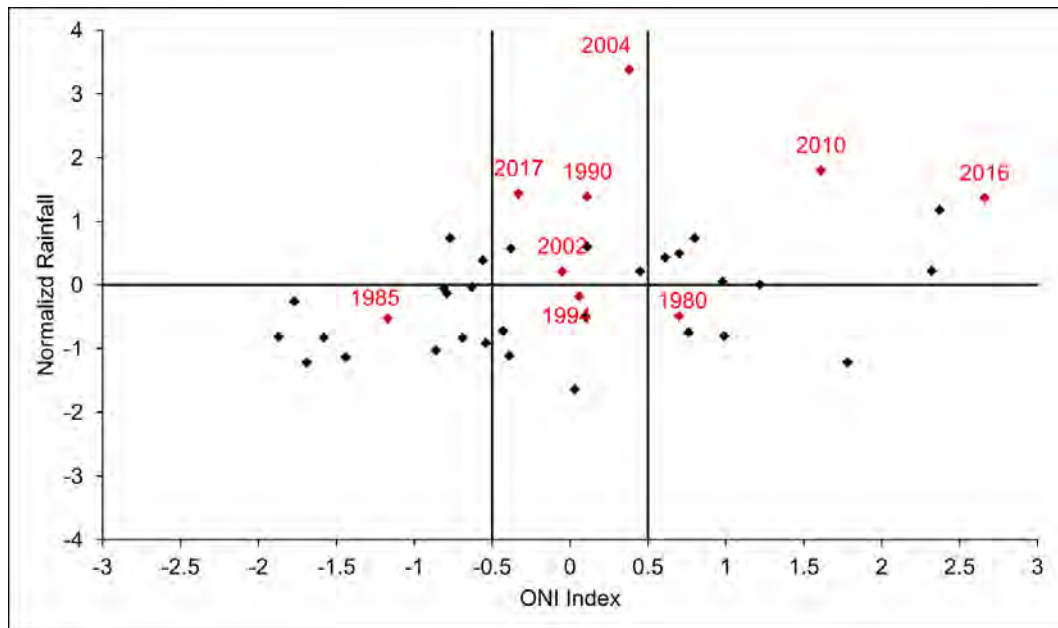


Fig 7.5 Normalized rainfall anomaly for Cherrapunji during April and ONI Index for January during the year 1979 to 2017. The red level of the points indicates the flooding year in April.

Finally, the relationship between the heat low over central India and the best suited ENSO index identified in the previous step was examined. This relationship was determined in terms of a heatwave since the heatwave generates heat low over central India. In this study, Excessive Heat Factor (EHF) was used to define heatwave, which is based on Excess Heat and Heat Stress. Therefore, the correlation between EHF over central India during April and previously identified best suited ENSO Index (ONI during January) was determined for the study area (Fig 7.6). Here, it was found that there is a high inverse correlation of heatwave over central India with the ONI index during January ($\rho=-0.55$). This infers that if the ENSO index during January is positive, then there is a possibility of heat low over central India during April. In the previous step, it was shown that the heat low over central India impacts over heavy rainfall during April over the Meghna basin. Therefore, it is proven that the El Niño during January is related to heavy rainfall during April over the Meghna basin, which was already shown in Fig 7.4 and Fig 7.5. This means that there is a high chance of a flood in April over the study area during the El Niño event.

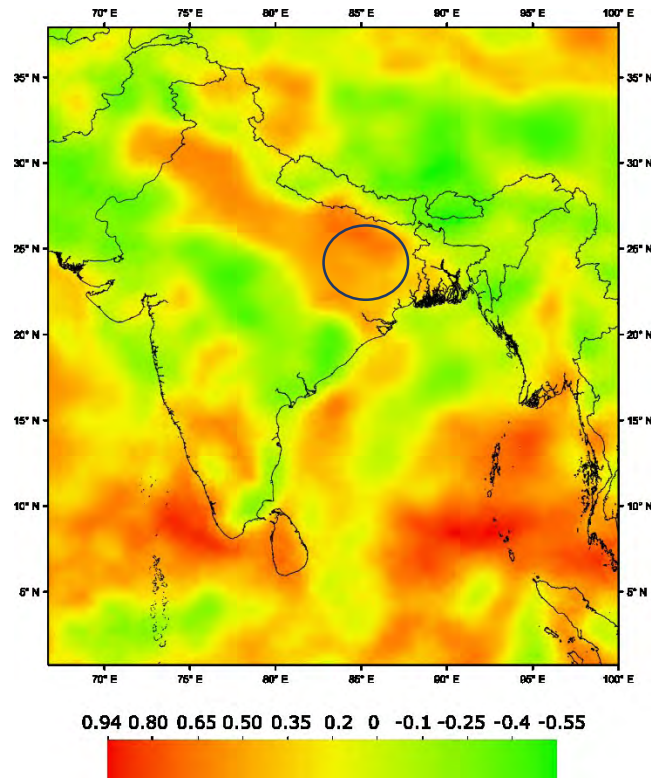


Fig 7.6 Correlation between ONI during January and EHF over central India during April.

7.3. Impact of global warming on ENSO

In the previous section, it was identified that the ONI index during January is more sensitive to April rainfall for this study area. Therefore, it is imperative to examine the response of ENSO (i.e., ONI index) intensity and amplitude to the global warming scenario. Hence, the change of intensity and amplitude of ENSO in terms of ONI index was studied for all months as well as for January under the warming world using the output of 10 GCMs from CMIP5. The ENSO intensity is defined as the number El Niño event (SST anomaly higher than 0.5° C) and La Niña Event (SST anomaly less than 0.5° C) for a particular time while the ENSO amplitude is defined as the standard deviation of the SST anomaly of that period. The percentage change of ENSO (i.e., ONI index) intensity for all month as well as for January and amplitude under RCP4.5 and RCP8.5 for the period of 2041-2070 and 2071-2100 with respect to the baseline (1976-2005) were presented in Fig 7.7, Fig 7.8 and Fig 7.9, respectively. The result shows that the intensity of El Niño event increases as the day progresses under extreme scenario while it is opposite in the case of La Niña event (Fig 7.7 and Fig 7.8). Therefore, under the warming world, the study area is subjected to more frequent

flooding in April since it was found that a positive correlation of flooding in April and ENSO. On the other hand, the amplitude of the ENSO index shows a different projection in the future under the warming world (Fig 7.9).

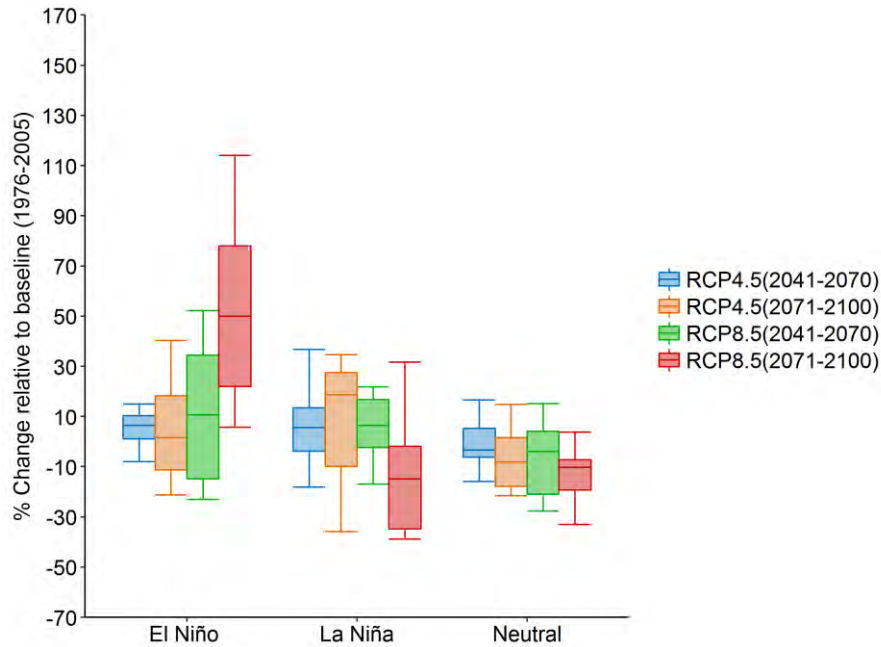


Fig 7.7 Relative change of ENSO intensity for all month under warming world with respect to the baseline.

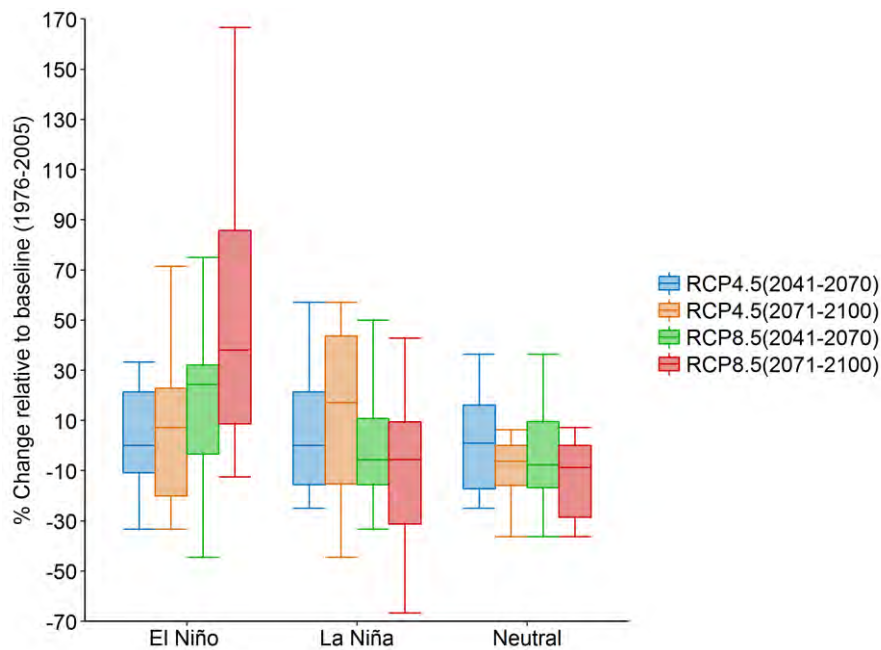


Fig 7.8 Relative change of ENSO intensity for January under the warming world with respect to the baseline.

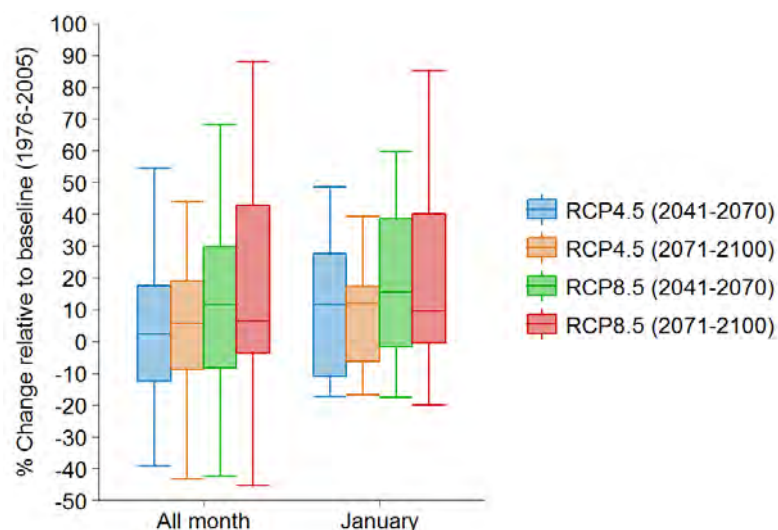


Fig 7.9 Relative change of ENSO amplitude under warming world with respect to the baseline.

Some models showed a marked increase in ENSO amplitude, whereas others showed a decrease or nearly no change. Several studies have also drawn a similar conclusion regarding future scenarios of ENSO amplitude [29,30,49,90,95]. These uncertainties of ENSO amplitude are likely due to the biases of GCMs in projecting the mean climatic state of the equatorial Pacific and the physical process that control ENSO [2015].

7.4. Summary

In this chapter, the relationship between the ENSO index and pre-monsoon rainfall, particularly in April over the Meghna basin and how ENSO is likely to be impacted under warming world was discussed. The correlation between different ENSO indices (such as SOI, ESOI, ONI, and MEI) during December, January, and February to April rainfall over the Meghna basin were determined to establish the relationship between ENSO index and April rainfall over the Meghna basin. It was found that the correlation varies (high to low) from East to West of the study area. Among the different set of combinations, the result showed that ONI index during January has the highest correlation value ($\rho=0.52$) with April rainfall and maximum spatial coverage of the correlation value for which it is statistically significant (0.32 for the 95 % confidence level). The Cherrapunji, the rainfall of which station plays a vital role in flooding of the study area, has fallen in the statistically significant area for the ONI index during January. Therefore, the ONI index during January was selected as the best-suited index among the different indices that were considered for this study area.

The normalized monthly rainfall anomaly during April of the Cherrapunji against ONI index during January was plotted to show how the ENSO influences the early flooding (floods in April when the principal crop of the study area is about to harvest) for the period 1979 to 2017. The plot showed that in most of the cases, early flooding occurs when the ENSO index is positive or even neutral in the NINO 3.4 region over the eastern equatorial Pacific. Therefore, we have to more careful about early flooding when there is El Niño or even Neutral during January.

A heatwave over central India during the month of April-May- June is one of the primary concern for not only central India but also the whole Indian sub-continent. It occurs on average every 3 to 4 years and affects different parts of the continent differently. In this study, it was found that there is a high correlation ($\rho \geq 0.55$) between April rainfall over the Meghna basin and heat low over central India during April. The mechanism of this relationship is that heatwave creates a low-pressure system (Cyclonic) in central India and the high-pressure system (Anticyclonic) in the Bay of Bengal. This two-systems trigger the south-westerly moisture flow from the Bay of Bengal towards the Meghalaya Mountain region and causes heavy rainfall over the Meghna basin. It was also found that this heatwave is again related to the ENSO index (the correlation between the ONI index during January and heatwave over central India over 0.65).

As it was found that El Niño influences early flooding over the Meghna basin, the impact of global warming on ENSO was also studied. The response to ENSO under warming world was studied in terms of ENSO frequency (number of ENSO events) as well as ENSO amplitude (standard deviation of the SST anomaly). It was done by using the output (monthly SST data) of the latest available GCMs under CMIP5 for RCP4.5 and RCP8.5 during 2041-2070 and 2071-2100. The result showed that the intensity of El Niño event increases as the day progresses under extreme scenario while it is opposite in the case of a La Niña event. However, there is no significant change in ENSO amplitude under a warming climate. However, though, the study area is subjected to more frequent flooding in April as it found a remarkable increase of El Niño event in the future. In the next chapter, a brief discussion of the findings of the study and its implication was presented.

CHAPTER 8

DISCUSSIONS AND IMPLICATION OF THE RESULTS

8.1. Introduction

This study is about to understand how rainfall extremes in northeast Bangladesh may change in the future and how this rainfall is connected to large-scale processes like ENSO. It was undertaken as part of the broader Norwegian Research Council-funded TRACKS project (TRAnSforming Climate Knowledge with and for Society), which attempts to ‘co-produce’ an improved understanding of climate variability in northeast Bangladesh through active collaboration between scientific and local. In the framing phase, the project completed 234 qualitative interviews with people from communities in Jamalganj, Sunamganj, Hakaluki haor, and Barlekha, in November 2014; with these interviews, helping to identify the weather phenomena that have the most critical impact on communities and the information they need to adapt to these phenomena. The interviews voiced the communities’ need for information on rainfall, storms and associated flooding as a priority, particularly in the pre-monsoon season.

This work covered the assessing the trend of extreme rainfall indices in past using daily rainfall data from seven rainfall stations, evaluation of the performance of RCMs in CORDEX south domain in simulating the present-day climate of the study area, bias correction of RCMS using quantile mapping method, trend analysis of rainfall extreme indices for future, projecting the extreme rainfall indices under the warming world using BMA approach. This work also covered investigating the teleconnection between large-scale process like ENSO and pre-monsoon rainfall and how it is likely to be influenced by climate change.

8.2. Implication of the results

This study found that most of the extremes rainfall indices showed a decreasing trend in the past (1984-216) for both seasons with most of them decreased significantly during the monsoon. This reduction of monsoon rainfall may be because of more significant warming of the Indian Ocean compared to the landmass of Indian sub-continent. Since 1950, the Indian Ocean is warming rapidly compare to the landmass of Indian sub-continent. These results decrease in moisture flow from the Bay of Bengal

because of the reduction of land-sea thermal contrast, which decreases the monsoon rainfall over the Indian subcontinent [163].

Most of the extreme indices showed an increasing trend during the pre-monsoon season in the future (1941-2070 & 2071-2099) except 2071-2099 for RCP4.5. One of the causes of the increasing trend of extreme rainfall in the future during the pre-monsoon may be the increase of heat low over central India adjacent to the western border of Bangladesh because of global warming. This will result in more moisture flow toward the Meghalaya mountain region in India and causes in more extreme rainfall event in northeast Bangladesh. Another cause can be explained by the Clausius–Clapeyron (C-C) relationship. The atmospheric moisture-holding capacity is likely to increase with surface temperature through the C-C equation [144]. Several studies [5,12,31,166,177] also argued that this increase of rainfall might be attributed to the increase of low level (850 hPa) moisture content resulting from increased temperature due to global warming.

The future, the extreme indices are expected to decrease in most cases similar to the historical trend during monsoon season. Several studies suggest that due to global warming under the increasing greenhouse, the temperature of the landmass of the subcontinent will increase slowly compared to the Indian Ocean, which will reduce the land-sea thermal gradient over the Indian subcontinent [166]. Therefore, extreme indices showed a decreasing trend during the monsoon under almost all emission scenarios. However, compared to baseline (1976-2005), the seasonal rainfall together with other extreme indices are expected to increase in the future (1941-2070 & 2071-2099) expect a decrease of CDD during both the pre-monsoon and monsoon season. Though, the increasing rate of extreme indices is more significant in the pre-monsoon season than monsoon season.

In this study, it was found that the pre-monsoon rainfall, particularly in April, is significantly influenced by the ONI index during January and in most of the cases, floods in April occur during the El Niño event or even Neutral event during January. It was also found that there is a high correlation ($\rho \geq 0.55$) between April rainfall over the Meghna basin and heat low over central India during April. This heatwave is again related to the El Niño event during January. The intensity of El Niño events is likely to increase because of climate change.

These findings of the study show that the pre-monsoon season may witness the most significant changes in rainfall extremes in northeast Bangladesh. Seasonal rainfall together with other extreme indices likely to increase, causing the occurrence of the more frequent high magnitude of flash floods putting the harvest of Boro rice, infrastructure, fisheries, livelihood together with bio-diversity and ecological balance at risk. This situation may intensify further as the century progresses.

CHAPTER 9

CONCLUSIONS AND RECOMMENDATIONS

9.1. Conclusions

This study is about to understand how rainfall extremes in northeast Bangladesh may change in the future and how this rainfall is connected to large-scale processes like ENSO. The key findings that can be drawn based on the research described in this thesis are as follows:

- Among the seven stations, only Sunamganj was found inhomogeneous and was not considered for trend analysis. All indices of rainfall extremes showed a decreasing trend in both seasons, with the most significant decrease during the monsoon. Importantly, it was found that a decreasing trend in the seasonal total rainfall and consecutive wet days, whereas there was an increasing trend in consecutive dry days. A decreasing trend in one-day maximum rainfall, five-day maximum rainfall, the intensity of the daily rainfall over 25 mm during the pre-monsoon and 50 mm was observed during the monsoon.
- RCMs underestimate in simulating present-day average rainfall of the study area during pre-monsoon as well as the monsoon season. However, the normalized bias and RMSE were higher for the monsoon than pre-monsoon.
- The RCMs underestimated the low-intensity rainfall and overestimated the high-intensity rainfall during pre-monsoon while they always underestimated the observed rainfall during the monsoon.
- The BMA weight showed that there was no single model that was best or worst in simulating rainfall variations over northeast Bangladesh. However, the BMA produced more reliable results compared to AEM as it has the lowest NRMSE for all six individual models.
- The result of the trend analysis showed that most of the extreme indices exhibited an increasing trend for the scenario period, except far future (2071-2099) for RCP4.5 while it showed a decreasing trend for the baseline period (1976-2005) during pre-monsoon season. The trend of the extreme indices

decreased in most of the cases which are similar to the historical trend during the monsoon season.

- The seasonal rainfall, together with other extreme indices, is expected to increase both in pre-monsoon and monsoon season, expect a decrease of CDD during pre-monsoon with respect to the baseline period. However, the increasing rate of extreme indices is generally more significant in pre-monsoon season than monsoon season.
- The average pre-monsoon rainfall of the study area is projected to increase by 12.93% in the near future (2041-2070) and 18.42% in the far future (2071-2099) under RCP4.5. Under the RC8.5, it is projected to increase by 18.18% in the near future and 23.85% in the far future. During the monsoon, it is projected to increase by 4.96% in the near future and 2.27% in the far future under the RCP4.5 while 6.56% in the near future and 6.40% in the far future under the RCP8.5.
- All extreme indices related to the occurrence of the flash flood (e.g., PRCPTOT, RX1, SDII, R95p, R99p) is expected to increase. This situation is projected to be more intense in 2071-2099 than in 2041-2070.
- These results indicate that the pre-monsoon season, in particular, may witness the most significant changes in rainfall in northeast Bangladesh. Seasonal rainfall together with other extreme indices expected to increase, causing the occurrence of the more frequent high magnitude of flash floods putting the harvest of Boro rice, as well as infrastructure and lives at risk. This situation may intensify further as the century progresses.
- The correlation between different ENSO indices (such as SOI, ESOI, ONI, and MEI) during December, January, and February with April rainfall over the Meghna basin showed that it varies (from high to low) from East to West of the study area.
- Among the different set of combinations, the ONI index during January has the highest correlation value ($\rho=0.52$) and maximum spatial coverage of the

correlation value for which it is statistically significant ($\rho=0.32$ for the 95% confidence level) with April rainfall.

- This study found that in most of the cases, early flooding occurs when the ONI index during January is positive or even neutral in the NINO 3.4 region over the eastern equatorial Pacific. Therefore, we have to be more careful about early flooding when there is El Niño or even Neutral during January.
- In this study, it was found that there is a high correlation ($\rho \geq 0.55$) between April rainfall over the Meghna basin and heat low over central India during April.
- The mechanism of this relationship is that heatwave creates a low-pressure system (Cyclonic) in central India and the high-pressure system (Anticyclonic) in the Bay of Bengal. This two-system triggers the south-westerly moisture flow from the Bay of Bengal towards the Meghalaya Mountain region and causes heavy rainfall over the Meghna basin. It was also found that this heatwave is again related to the ENSO index (the correlation between the ONI index during January and heatwave over central India is over 0.65).
- It was observed that the intensity of El Niño event is expected to increase as the day progresses under extreme scenario while it is opposite for the case of La Niña event. However, there is no significant change of ENSO amplitude under a warming climate. However, though, the study area is subjected to more frequent flooding in April as it was shown a remarkable increase of El Niño event in the future.

9.2. Limitations of the study

- The major limitation of this study was the lack of availability of observed rainfall data over the catchment areas of the Meghna basin located inside India.
- Lack of continuous observed daily rainfall data from BMD and BWDB limits the study.
- Challenges exist in comparing grid-based climate model data with a point-based observed data.

- The prediction of climate change has uncertainties arises from the social and economic aspects as well as earth system modeling. Therefore, the results of this study would also contain uncertainty.
- Application of the bias correction method is another limitation of this study since there are many debates among the scientific community regarding better bias correction method.

9.3. Recommendations

- Impact of climate change on rainfall extremes was performed in the downstream part of the Meghna basin using observed rainfall data from Bangladesh part only. Therefore, further studies are needed to perform over the whole Meghna basin incorporating the observed rainfall data from India for the upstream part of the basin.
- In this study, the impact of climate change on rainfall extremes due to anthropogenic causes was studied. However, more research is needed to investigate the combined effects of anthropogenic influences and the variability of the climate system especially, regarding changes in rainfall extremes.
- In this case, as the rainfall extremes are likely to increase in future, it is necessary to examine the impact of changes of rainfall extremes on water resources and the extent of the flood at various urban and rural catchments of the study area. This study will provide some insights into the rainfall-runoff relationship and for a better understanding of its implication on different catchments.
- In this study, RCMs under CMIP5 was used, which are much more improved from GCMs under CMIP3. However, there exists a considerable bias and uncertainty in RCMs under CMIP5. Therefore, further studies are needed using the upcoming regional climate model under CMIP6.
- Based on the result of this study, a detailed study of policy guidelines and adaptation strategies is recommended in future studies.

REFERENCES

- [1] Ahmadalipour, A., Moradkhani, H., & Rana, A. (2018). Accounting for downscaling and model uncertainty in fine-resolution seasonal climate projections over the Columbia River Basin. *Climate Dynamics*, 50(1-2), 717-733.
- [2] Ahmed, K., Shahid, S., Ismail, T., Nawaz, N., & Wang, X. J. (2018). Absolute homogeneity assessment of precipitation time series in an arid region of Pakistan. *Atmósfera*, 31(3), 301-316.
- [3] Ahmed, R., & Karmakar, S. (1993). Arrival and withdrawal dates of the summer monsoon in Bangladesh. *International Journal of Climatology*, 13(7), 727-740.
- [4] Ajami, N. K., Duan, Q., & Sorooshian, S. (2007). An integrated hydrologic Bayesian multimodel combination framework: Confronting input, parameter, and model structural uncertainty in hydrologic prediction. *Water Resources Research*, 43(1).
- [5] Akhter, J., Das, L., & Deb, A. (2017). CMIP5 ensemble-based spatial rainfall projection over homogeneous zones of India. *Climate Dynamics*, 49(5-6), 1885-1916.
- [6] Alam, M. S., Quayum, M. A., & Islam, M. A. (2010). Crop production in the Haor areas of Bangladesh: insights from farm level survey. *The Agriculturists*, 8(2), 88-97.
- [7] Alexandersson, H. (1986). A homogeneity test applied to precipitation data. *Journal of Climatology*, 6(6), 661-675.
- [8] Annamalai, H., Hamilton, K., & Sperber, K. R. (2007). The South Asian summer monsoon and its relationship with ENSO in the IPCC AR4 simulations. *Journal of Climate*, 20(6), 1071-1092.
- [9] Arjasakusuma, S., Yamaguchi, Y., Hirano, Y., & Zhou, X. (2018). ENSO-and Rainfall-Sensitive Vegetation Regions in Indonesia as Identified from Multi-Sensor Remote Sensing Data. *ISPRS International Journal of Geo-Information*, 7(3), 103.
- [10] Asadieh, B., & Krakauer, N. Y. (2015). Global trends in extreme precipitation: climate models versus observations. *Hydrology and Earth System Sciences*, 19(2), 877-891.
- [11] Ashfaq, M., Bowling, L. C., Cherkauer, K., Pal, J. S., & Diffenbaugh, N. S. (2010). Influence of climate model biases and daily- scale temperature and precipitation events on hydrological impacts assessment: A case study of the United States. *Journal of Geophysical Research: Atmospheres*, 115(D14).

- [12] Asharaf, S., & Ahrens, B. (2015). Indian summer monsoon rainfall processes in climate change scenarios. *Journal of Climate*, 28(13), 5414-5429.
- [13] Akinsanola, A. A., Ajayi, V. O., Adejare, A. T., Adeyeri, O. E., Gbode, I. E., Ogunjobi, K. O., Grigory, N. & Abolude, A. T. (2018). Evaluation of rainfall simulations over West Africa in dynamically downscaled CMIP5 global circulation models. *Theoretical and applied climatology*, 132(1-2), 437-450.
- [14] Basistha, A., Arya, D. S., & Goel, N. K. (2009). Analysis of historical changes in rainfall in the Indian Himalayas. *International Journal of Climatology*, 29(4), 555-572.
- [15] Begum, S., & Alam, M. S. (2013). Climate Change Impact on Rainfall over Bangladesh for Last Decades. *International Journal of Open Scientific Research IJOSR*, 1(4), 1-8.
- [16] Bennett, N. D., Newham, L. T. H., Croke, B. F. W., & Jakeman, A. J. (2007, December). Patching and disaccumulation of rainfall data for hydrological modelling. In *Int. Congress on Modelling and Simulation (MODSIM 2007), Modelling and Simulation Society of Australia and New Zealand Inc., New Zealand* (pp. 2520-2526).
- [17] Blanchet, J., Molinié, G., & Touati, J. (2018). Spatial analysis of trend in extreme daily rainfall in southern France. *Climate Dynamics*, 51(3), 799-812.
- [18] Block, P. J., Souza Filho, F. A., Sun, L., & Kwon, H. H. (2009). A streamflow forecasting framework using multiple climate and hydrological models 1. *JAWRA Journal of the American Water Resources Association*, 45(4), 828-843.
- [19] Boe, J., Terray, L., Habets, F., & Martin, E. (2007). Statistical and dynamical downscaling of the Seine basin climate for hydro- meteorological studies. *International Journal of Climatology: A Journal of the Royal Meteorological Society*, 27(12), 1643-1655.
- [20] Bremer, S. (2017). Have we given up too much? On yielding climate representation to experts. *Futures*, 91, 72-75.
- [21] Birsan, M. V., Zaharia, L. I. L. I. A. N. A., Chendes, V. I. O. R. E. L., & Branescu, E. M. I. L. I. A. (2012). Recent trends in streamflow in Romania (1976–2005). *Romanian Reports in Physics*, 64(1), 275-280.
- [22] Cannon, A. J. (2018). Multivariate quantile mapping bias correction: an N-dimensional probability density function transform for climate model simulations of multiple variables. *Climate dynamics*, 50(1-2), 31-49.
- [23] Casanueva, A., Bedia, J., Herrera, S., Fernández, J., & Gutiérrez, J. M. (2018). Direct and component-wise bias correction of multi-variate climate indices: the percentile adjustment function diagnostic tool. *Climatic Change*, 147(3-4), 411-425.

- [24] Chakraborty, A. (2018). Preceding winter La Niña reduces Indian summer monsoon rainfall. *Environmental Research Letters*, 13(5), 054030.
- [25] Chaturvedi, R. K., Joshi, J., Jayaraman, M., Bala, G., & Ravindranath, N. H. (2012). Multi-model climate change projections for India under representative concentration pathways. *Current Science*, 103(7), 791-802.
- [26] Chen, H., & Sun, J. (2013). Projected change in East Asian summer monsoon precipitation under RCP scenario. *Meteorology and Atmospheric Physics*, 121(1-2), 55-77.
- [27] Chen, J., Brissette, F. P., & Leconte, R. (2011). Uncertainty of downscaling method in quantifying the impact of climate change on hydrology. *Journal of Hydrology*, 401(3-4), 190-202.
- [28] Chen, Z., Du, Y., Wen, Z., Wu, R., & Wang, C. (2018). Indo-Pacific climate during the decaying phase of the 2015/16 El Niño: role of southeast tropical Indian Ocean warming. *Climate Dynamics*, 50(11-12), 4707-4719.
- [29] Chen, L., Li, T., & Yu, Y. (2015). Causes of strengthening and weakening of ENSO amplitude under global warming in four CMIP5 models. *Journal of Climate*, 28(8), 3250-3274.
- [30] Chen, L., Li, T., Yu, Y., & Behera, S. K. (2017). A possible explanation for the divergent projection of ENSO amplitude change under global warming. *Climate dynamics*, 49(11-12), 3799-3811.
- [31] Cherchi, A., Alessandri, A., Masina, S., & Navarra, A. (2011). Effects of increased CO₂ levels on monsoons. *Climate Dynamics*, 37(1-2), 83-101.
- [32] Choudhary, A., Dimri, A. P., & Maharana, P. (2018). Assessment of CORDEX-SA experiments in representing precipitation climatology of summer monsoon over India. *Theoretical and Applied Climatology*, 134(1-2), 283-307.
- [33] Chow, W. T. (2018). The impact of weather extremes on urban resilience to hydro-climate hazards: a Singapore case study. *International Journal of Water Resources Development*, 34(4), 510-524.
- [34] Chowdhury, M. R. (2003). The El Niño-southern oscillation (ENSO) and seasonal flooding–Bangladesh. *Theoretical and applied climatology*, 76(1-2), 105-124.
- [35] Christensen, J. H., Boberg, F., Christensen, O. B., & Lucas-Picher, P. (2008). On the need for bias correction of regional climate change projections of temperature and precipitation. *Geophysical Research Letters*, 35(20).
- [36] Chu, P. S., & Zhao, X. (2011). Bayesian analysis for extreme climatic events: A review. *Atmospheric research*, 102(3), 243-262.

- [37] Chu, P.S., Zhao, X., Karamperidou, C. & Zhang, H. (2016). Bayesian model averaging and its application to an El Niño index in CMIP5 models. *International Meetings on Statistical Climatology, 6-10 June, Canmore, Canada.*
- [38] Collins, M., An, S. I., Cai, W., Ganachaud, A., Guilyardi, E., Jin, F. F., Jochum, M., Lengaigne, M., Power, S., Timmermann, A. & Vecchi, G. (2010). The impact of global warming on the tropical Pacific Ocean and El Niño. *Nature Geoscience*, 3(6), 391.
- [39] Crost, B., Duquennois, C., Felter, J. H., & Rees, D. I. (2018). Climate change, agricultural production and civil conflict: Evidence from the Philippines. *Journal of Environmental Economics and Management*, 88, 379-395.
- [40] Dankers, R., & Feyen, L. (2009). Flood hazard in Europe in an ensemble of regional climate scenarios. *Journal of Geophysical Research: Atmospheres*, 114(D16).
- [41] Das, S., Tomar, C. S., Saha, D., Shaw, S. O., & Singh, C. (2015). Trends in Rainfall Patterns over North-East India during 1961–2010. *Int. J. of Earth and Atmospheric Science*, 2(2), 37-48.
- [42] Deka, R. L., Mahanta, C., Pathak, H., Nath, K. K., & Das, S. (2013). Trends and fluctuations of rainfall regime in the Brahmaputra and Barak basins of Assam, India. *Theoretical and applied climatology*, 114(1-2), 61-71.
- [43] Déqué, M., Rowell, D.P., Lüthi, D., Giorgi, F., Christensen, J.H., Rockel, B., Jacob, D., Kjellström, E., De Castro, M. and van den Hurk, B.J.J.M. (2007). An intercomparison of regional climate simulations for Europe: assessing uncertainties in model projections. *Climatic Change*, 81(1), pp.53-70.
- [44] Déqué, M., Somot, S., Sanchez-Gomez, E., Goodess, C. M., Jacob, D., Lenderink, G., & Christensen, O. B. (2012). The spread amongst ENSEMBLES regional scenarios: regional climate models, driving general circulation models and interannual variability. *Climate Dynamics*, 38(5-6), 951-964.
- [45] Dobler, A., & Ahrens, B. (2008). Precipitation by a regional climate model and bias correction in Europe and South Asia. *Meteorologische Zeitschrift*, 17(4), 499-509.
- [46] Dong, G., Zhang, H., Moise, A., Hanson, L., Liang, P., & Ye, H. (2016). CMIP5 model-simulated onset, duration and intensity of the Asian summer monsoon in current and future climate. *Climate dynamics*, 46(1-2), 355-382.
- [47] Dosio, A., & Paruolo, P. (2011). Bias correction of the ENSEMBLES high-resolution climate change projections for use by impact models: evaluation on the present climate. *Journal of Geophysical Research: Atmospheres*, 116(D16).

- [48] Fahad, M. G. R., Saiful Islam, A. K. M., Nazari, R., Alfi Hasan, M., Tarekul Islam, G. M., & Bala, S. K. (2018). Regional changes of precipitation and temperature over Bangladesh using bias- corrected multi- model ensemble projections considering high- emission pathways. *International Journal of Climatology*, 38(4), 1634-1648.
- [49] Fasullo, J. T., Otto- Bliesner, B. L., & Stevenson, S. (2018). ENSO's Changing Influence on Temperature, Precipitation, and Wildfire in a Warming Climate. *Geophysical Research Letters*, 45(17), 9216-9225.
- [50] Fan, F., Mann, M. E., Lee, S., & Evans, J. L. (2010). Observed and modeled changes in the South Asian summer monsoon over the historical period. *Journal of Climate*, 23(19), 5193-5205.
- [51] Fantini, A., Raffaele, F., Torma, C., Bacer, S., Coppola, E., Giorgi, F., Ahrens, B., Dubois, D., Sanchez, E., & Verdecchia, M. (2018). Assessment of multiple daily precipitation statistics in ERA-Interim driven Med-CORDEX and EURO-CORDEX experiments against high resolution observations. *Climate dynamics*, 51(3), 877-900.
- [52] FFWC, 2016. Annual flood report, Flood *Forecasting and Warning Centre*, Bangladesh Water Development Board.
- [53] Field, C. B. (Ed.). (2014). Climate change 2014–Impacts, adaptation and vulnerability: Regional aspects. *Cambridge University Press*.
- [54] Firat, M., Dikbas, F., Koç, A. C., & Gungor, M. (2010). Missing data analysis and homogeneity test for Turkish precipitation series. *Sadhana*, 35(6), 707.
- [55] Frich, P., Alexander, L. V., Della-Marta, P. M., Gleason, B., Haylock, M., Tank, A. K., & Peterson, T. (2002). Observed coherent changes in climatic extremes during the second half of the twentieth century. *Climate Research*, 19(3), 193-212.
- [56] Fu, G., Yu, J., Yu, X., Ouyang, R., Zhang, Y., Wang, P., Liu, W. and Min, L. (2013). Temporal variation of extreme rainfall events in China, 1961–2009. *Journal of Hydrology*, 487, pp.48-59.
- [57] Fujinami, H., Yasunari, T., & Morimoto, A. (2014). Dynamics of distinct intraseasonal oscillation in summer monsoon rainfall over the Meghalaya–Bangladesh–western Myanmar region: covariability between the tropics and mid-latitudes. *Climate Dynamics*, 43(7-8), 2147-2166.
- [58] Giorgi, F., Diffenbaugh, N.S., Gao, X.J., Coppola, E., Dash, S.K., Frumento, O., Rauscher, S.A., Remedio, A., Sanda, I.S., Steiner, A. and Sylla, B. (2008). The regional climate change hyper- matrix framework. *Eos, Transactions American Geophysical Union*, 89(45), pp.445-446.

- [59] Giorgi, F., Jones, C., & Asrar, G. R. (2009). Addressing climate information needs at the regional level: the CORDEX framework. *World Meteorological Organization (WMO) Bulletin*, 58(3), 175.
- [60] Glantz, M. H., Naranjo, L., Baudoin, M. A., & Ramírez, I. J. (2018). What Does It Mean to Be El Niño Ready?. *Atmosphere*, 9(3), 94.
- [61] Ghosh, A., Lohar, D., & Das, J. (2008). Initiation of Nor'wester in relation to mid-upper and low-level water vapor patterns on METEOSAT-5 images. *Atmospheric Research*, 87(2), 116-135.
- [62] Government of Bangladesh (2012). Master Plan of Haor Areas 2012. Government of Bangladesh, Ministry of Water Resources, *Bangladesh Haor and Wetland Development Board, Dhaka*.
- [63] Hanley, D. E., Bourassa, M. A., O'Brien, J. J., Smith, S. R., & Spade, E. R. (2003). A quantitative evaluation of ENSO indices. *Journal of Climate*, 16(8), 1249-1258.
- [64] Hasan, G.M.J.; Alam, R.; Islam, Q.N.; Hossain, M.S. (2012). Frequency structure of major rainfall events in the north-east part of Bangladesh. *J Eng Sci Techno* 16(2012):690–700
- [65] Hay, L. E., & Clark, M. P. (2003). Use of statistically and dynamically downscaled atmospheric model output for hydrologic simulations in three mountainous basins in the western United States. *Journal of Hydrology*, 282(1-4), 56-75.
- [66] Hatsuzuka, D., Yasunari, T., & Fujinami, H. (2014). Characteristics of low pressure systems associated with intraseasonal oscillation of rainfall over Bangladesh during boreal summer. *Monthly Weather Review*, 142(12), 4758-4774.
- [67] Herold, N., & Santoso, A. (2018). Indian Ocean warming during peak El Niño cools surrounding land masses. *Climate Dynamics*, 51(5-6), 2097-2112.
- [68] Hirabayashi, Y., Kanae, S., Emori, S., Oki, T., & Kimoto, M. (2008). Global projections of changing risks of floods and droughts in a changing climate. *Hydrological Sciences Journal*, 53(4), 754-772.
- [69] Hoeting, J. A., Madigan, D., Raftery, A. E., & Volinsky, C. T. (1999). Bayesian model averaging: a tutorial. *Statistical science*, 382-401.
- [70] Horton, P., Schaefli, B., Mezghani, A., Hingray, B., & Musy, A. (2006). Assessment of climate- change impacts on alpine discharge regimes with climate model uncertainty. *Hydrological Processes: An International Journal*, 20(10), 2091-2109.

- [71] Hsu, P. C., Li, T., Luo, J. J., Murakami, H., Kitoh, A., & Zhao, M. (2012). Increase of global monsoon area and precipitation under global warming: A robust signal?. *Geophysical Research Letters*, 39(6).
- [72] Huber, M., & Knutti, R. (2011). Anthropogenic and natural warming inferred from changes in Earth's energy balance. *Nature Geoscience*, 5(1), 31–36. doi:10.1038/ngeo1327.
- [73] Ihara, C., Kushnir, Y., Cane, M. A., & Victor, H. (2007). Indian summer monsoon rainfall and its link with ENSO and Indian Ocean climate indices. *International Journal of Climatology*, 27(2), 179-187.
- [74] Ines, A. V., & Hansen, J. W. (2006). Bias correction of daily GCM rainfall for crop simulation studies. *Agricultural and forest meteorology*, 138(1-4), 44-53.
- [75] IPCC, (2007). Climate Change 2007: The Physical Science Basis. Contribution of Working Group I to the Fourth Assessment Report of the Intergovernmental Panel on Climate Change [Solomon, S., D. Qin, M. Manning, Z. Chen, M. Marquis, K.B. Averyt, M. Tignor and H.L. Miller (eds.)]. *Cambridge University Press, Cambridge, United Kingdom and New York, NY, USA*, 996 pp.
- [76] IPCC, (2012). Managing the Risks of Extreme Events and Disasters to Advance Climate Change Adaptation. A Special Report of Working Groups I and II of the Intergovernmental Panel on Climate Change [Field, C.B., V. Barros, T.F. Stocker, D. Qin, D.J. Dokken, K.L. Ebi, M.D. Mastrandrea, K.J. Mach, G.-K. Plattner, S.K. Allen, M. Tignor, and P.M. Midgley (eds.)]. *Cambridge University Press, Cambridge, UK, and New York, NY, USA*, 582 pp.
- [77] IPCC, (2013). Climate Change 2013: The Physical Science Basis. Contribution of Working Group I to the Fifth Assessment Report of the Intergovernmental Panel on Climate Change [Stocker, T.F., D. Qin, G.-K. Plattner, M. Tignor, S.K. Allen, J. Boschung, A. Nauels, Y. Xia, V. Bex and P.M. Midgley (eds.)]. *Cambridge University Press, Cambridge, United Kingdom and New York, NY, USA*, 1535 pp.
- [78] IPCC, (2014) Climate Change 2014: Synthesis Report. Contribution of Working Groups I, II and III to the Fifth Assessment Report of the Intergovernmental Panel on Climate Change [Core Writing Team, R.K. Pachauri and L.A. Meyer (eds.)]. *IPCC, Geneva, Switzerland*, 151 pp.
- [79] Izumo, T., Vialard, J., Lengaigne, M., de Boyer Montegut, C., Behera, S. K., Luo, J. J., Sophie, C., Sébastien, M., & Yamagata, T. (2010). Influence of the state of the Indian Ocean Dipole on the following year's El Niño. *Nature Geoscience*, 3(3), 168.
- [80] Jain, S. K., Kumar, V., & Saharia, M. (2013). Analysis of rainfall and temperature trends in northeast India. *International Journal of Climatology*, 33(4), 968-978.

- [81] Janis, M. J., & Robeson, S. M. (2004). Determining the spatial representativeness of air-temperature records using variogram-nugget time series. *Physical Geography*, 25(6), 513-530.
- [82] Johnson, F., & Sharma, A. (2011). Accounting for interannual variability: A comparison of options for water resources climate change impact assessments. *Water Resources Research*, 47(4).
- [83] Kane, R. P. (1998). Extremes of the ENSO phenomenon and Indian summer monsoon rainfall. *International Journal of Climatology: A Journal of the Royal Meteorological Society*, 18(7), 775-791.
- [84] Kang, H. M., & Yusof, F. (2012). Homogeneity tests on daily rainfall series. *Int. J. Contemp. Math. Sciences*, 7(1), 9-22.
- [85] Karmaker, S. (1995). Variability and probabilistic estimates of rainfall extremes in Bangladesh during the southwest monsoon season. *Mausam*, 46, 47-56.
- [86] Kato, H., Nishizawa, K., Hirakuchi, H., Kadokura, S., Oshima, N., & Giorgi, F. (2001). Performance of RegCM2. 5/NCAR-CSM nested system for the simulation of climate change in East Asia caused by global warming. *Journal of the Meteorological Society of Japan. Ser. II*, 79(1), 99-121.
- [87] Katz, R. W. (1999). Extreme value theory for precipitation: sensitivity analysis for climate change. *Advances in Water Resources*, 23(2), 133-139.
- [88] Kendall, M. G. (1975). Rank Correlation Methods, Charles Griffin, London (1975). *Google Scholar*.
- [89] Khaliq, M. N., & Ouarda, T. B. M. J. (2007). On the critical values of the standard normal homogeneity test (SNHT). *International Journal of Climatology: A Journal of the Royal Meteorological Society*, 27(5), 681-687.
- [90] Kim, S. T., & Yu, J. Y. (2012). The two types of ENSO in CMIP5 models. *Geophysical Research Letters*, 39(11).
- [91] Kim, K. B., Kwon, H. H., & Han, D. (2015). Bias correction methods for regional climate model simulations considering the distributional parametric uncertainty underlying the observations. *Journal of Hydrology*, 530, 568-579.
- [92] Kripalani, R. H., Inamdar, S., & Sontakke, N. A. (1996). Rainfall variability over Bangladesh and Nepal: Comparison and connections with features over India. *International Journal of Climatology: A Journal of the Royal Meteorological Society*, 16(6), 689-703.
- [93] Kripalani, R. H., Oh, J. H., Kulkarni, A., Sabade, S. S., & Chaudhari, H. S. (2007). South Asian summer monsoon precipitation variability: coupled climate model simulations and projections under IPCC AR4. *Theoretical and Applied Climatology*, 90(3-4), 133-159.

- [94] Krishnamurthy, V., & Goswami, B. N. (2000). Indian monsoon–ENSO relationship on interdecadal timescale. *Journal of Climate*, 13(3), 579-595.
- [95] Kug, J. S., An, S. I., Ham, Y. G., & Kang, I. S. (2010). Changes in El Niño and La Niña teleconnections over North Pacific–America in the global warming simulations. *Theoretical and applied climatology*, 100(3-4), 275-282.
- [96] Kumar, K. R., Sahai, A. K., Kumar, K. K., Patwardhan, S. K., Mishra, P. K., Revadekar, J. V., ... & Pant, G. B. (2006). High-resolution climate change scenarios for India for the 21st century. *Current science*, 90(3), 334-345.
- [97] Kumar, K. K., Kamala, K., Rajagopalan, B., Hoerling, M. P., Eischeid, J. K., Patwardhan, S. K., ... & Nemani, R. (2011). The once and future pulse of Indian monsoonal climate. *Climate Dynamics*, 36(11-12), 2159-2170.
- [98] Kumar, V., & Jain, S. K. (2011). Trends in rainfall amount and number of rainy days in river basins of India (1951–2004). *Hydrology Research*, 42(4), 290-306.
- [99] Kumar, V., Jain, S. K., & Singh, Y. (2010). Analysis of long-term rainfall trends in India. *Hydrological Sciences Journal-Journal des Sciences Hydrologiques*, 55(4), 484-496.
- [100] Lal, M., Meehl, G. A., & Arblaster, J. M. (2000). Simulation of Indian summer monsoon rainfall and its intraseasonal variability in the NCAR climate system model. *Regional Environmental Change*, 1(3-4), 163-179.
- [101] Leander, R., & Buishand, T. A. (2007). Resampling of regional climate model output for the simulation of extreme river flows. *Journal of Hydrology*, 332(3-4), 487-496.
- [102] Leander, R., Buishand, T. A., van den Hurk, B. J., & de Wit, M. J. (2008). Estimated changes in flood quantiles of the river Meuse from resampling of regional climate model output. *Journal of Hydrology*, 351(3-4), 331-343.
- [103] Lee, J. Y., & Wang, B. (2014). Future change of global monsoon in the CMIP5. *Climate Dynamics*, 42(1-2), 101-119.
- [104] Lefort, T. (2013). Dry-line, nor'westers and tornadic storms over east India and Bangladesh: an operational perspective through synergy, the new IMD forecaster's workstation. *Mausam*, 64, 517-530.
- [105] Li, H., Feng, L., & Zhou, T. (2011). Multi-model projection of July–August climate extreme changes over China under CO2 doubling. Part I: Precipitation. *Advances in Atmospheric Sciences*, 28(2), 433-447.
- [106] Li, J., Sharma, A., Evans, J., & Johnson, F. (2018). Addressing the mischaracterization of extreme rainfall in regional climate model simulations—A synoptic pattern based bias correction approach. *Journal of Hydrology*, 556, 901-912.

- [107] Li, Z., Cai, W., & Lin, X. (2016). Dynamics of changing impacts of tropical Indo-Pacific variability on Indian and Australian rainfall. *Scientific reports*, 6, 31767.
- [108] Li, Z., Lin, X., & Cai, W. (2017). Realism of modelled Indian summer monsoon correlation with the tropical Indo-Pacific affects projected monsoon changes. *Scientific reports*, 7(1), 4929.
- [109] Lins, H. F., & Slack, J. R. (1999). Stream flow trends in the United States. *Geophysical research letters*, 26(2), 227-230.
- [110] Lindsey, R. (2013). In watching for El Nino and La Nina, NOAA adapts to global warming. Climate Watch.[Available online at <https://www.climate.gov/news-features/understanding-climate/watching-el-niño-and-la-niña-noaa-adapts-global-warming>.]
- [111] Longobardi, A., & Villani, P. (2010). Trend analysis of annual and seasonal rainfall time series in the Mediterranean area. *International journal of Climatology*, 30(10), 1538-1546.
- [112] Lu, X., & Cheng, G. (2009). Climate change effects on soil carbon dynamics and greenhouse gas emissions in *Abies fabri* forest of subalpine, southwest China. *Soil Biology and Biochemistry*, 41(5), 1015-1021.
- [113] Lupo, A., & Kininmonth, W. (2013). Global climate models and their limitations. *Climate change reconsidered II: Physical science*, 9-147.
- [114] Ma, Y., Hong, Y., Chen, Y., Yang, Y., Tang, G., Yao, Y., Long, D., Li, C., Han, Z. and Liu, R. (2018). Performance of optimally merged multi-satellite precipitation products using the dynamic Bayesian model averaging scheme over the Tibetan Plateau. *Journal of Geophysical Research: Atmospheres*, 123(2), pp.814-834.
- [115] Maier, H. R., Guillaume, J. H., van Delden, H., Riddell, G. A., Haasnoot, M., & Kwakkel, J. H. (2016). An uncertain future, deep uncertainty, scenarios, robustness and adaptation: How do they fit together?. *Environmental modelling & software*, 81, 154-164.
- [116] Mal, S., Singh, R. B., Huggel, C., & Grover, A. (2018). Introducing linkages between climate change, extreme events, and disaster risk reduction. In *Climate Change, Extreme Events and Disaster Risk Reduction* (pp. 1-14). Springer, Cham.
- [117] Makhuvha, T., Pegram, G., Sparks, R., & Zucchini, W. (1997). Patching rainfall data using regression methods. 1. Best subset selection, EM and pseudo-EM methods: theory. *Journal of Hydrology*, 198(1-4), 289-307.
- [118] Mann, H. B. (1945). Non-Parametric Tests against Trend. *Econometrica*, 13, 245-259. Mantua, NJ, SR Hare, Y. Zhang, JM Wallace, and RC Francis (1997), *A Pacific decadal*.

- [119] Maraun, D., Wetterhall, F., Ireson, A.M., Chandler, R.E., Kendon, E.J., Widmann, M., Brienen, S., Rust, H.W., Sauter, T., Themeßl, M. and Venema, V.K.C. (2010). Precipitation downscaling under climate change: Recent developments to bridge the gap between dynamical models and the end user. *Reviews of Geophysics*, 48(3).
- [120] Maraun, D. (2016). Bias correcting climate change simulations-a critical review. *Current Climate Change Reports*, 2(4), 211-220.
- [121] Markowski, P., & Richardson, Y. (2010). Organization of isolated convection. *Mesoscale meteorology in midlatitudes*, 201-244.
- [122] Masood, M., & Takeuchi, K. (2016). Climate change impacts and its implications on future water resource management in the Meghna Basin. *Futures*, 78, 1-18.
- [123] May, W. (2011). The sensitivity of the Indian summer monsoon to a global warming of 2 C with respect to pre-industrial times. *Climate Dynamics*, 37(9-10), 1843-1868.
- [124] Mearns, L.O., Arritt, R., Biner, S., Bukovsky, M.S., McGinnis, S., Sain, S., Caya, D., Correia Jr, J., Flory, D., Gutowski, W. and Takle, E.S.(2012). The North American regional climate change assessment program: overview of phase I results. *Bulletin of the American Meteorological Society*, 93(9), pp.1337-1362.
- [125] Mercure, J. F., Pollitt, H., Edwards, N. R., Holden, P. B., Chewpreecha, U., Salas, P., Lam, A., Knobloch, F & Vinuales, J. E. (2018). Environmental impact assessment for climate change policy with the simulation-based integrated assessment model E3ME-FTT-GENIE. *Energy strategy reviews*, 20, 195-208.
- [126] Minaei, M., & Irannezhad, M. (2018). Spatio-temporal trend analysis of precipitation, temperature, and river discharge in the northeast of Iran in recent decades. *Theoretical and Applied Climatology*, 131(1-2), 167-179.
- [127] Mirza, M. Q., Warrick, R. A., Ericksen, N. J., & Kenny, G. J. (1998). Trends and persistence in precipitation in the Ganges, Brahmaputra and Meghna river basins. *Hydrological Sciences Journal*, 43(6), 845-858.
- [128] Moeletsi, M. E., Shabalala, Z. P., De Nysschen, G., & Walker, S. (2016). Evaluation of an inverse distance weighting method for patching daily and dekadal rainfall over the Free State Province, South Africa. *Water SA*, 42(3), 466-474.
- [129] Mondal, A., Kundu, S., & Mukhopadhyay, A. (2012). Rainfall trend analysis by Mann-Kendall test: A case study of north-eastern part of Cuttack district, Orissa. *International Journal of Geology, Earth and Environmental Sciences*, 2(1), 70-78.

- [130] Moss, R. H., Edmonds, J. A., Hibbard, K. A., Manning, M. R., Rose, S. K., Van Vuuren, D. P., ... & Meehl, G. A. (2010). The next generation of scenarios for climate change research and assessment. *Nature*, 463(7282), 747.
- [131] Moss, R.H., Meehl, G.A., Lemos, M.C., Smith, J.B., Arnold, J.R., Arnott, J.C., Behar, D., Brasseur, G.P., Broomell, S.B., Busalacchi, A.J. and Dessai, S. (2013). Hell and high water: practice-relevant adaptation science. *Science*, 342(6159), pp.696-698.
- [132] Murari, K. K., Ghosh, S., Patwardhan, A., Daly, E., & Salvi, K. (2015). Intensification of future severe heat waves in India and their effect on heat stress and mortality. *Regional Environmental Change*, 15(4), 569-579.
- [133] Murata, F., Terao, T., Kiguchi, M., Fukushima, A., Takahashi, K., Hayashi, T., Habib, A., BHUIYAN, S.H. and Choudhury, S.A. (2011). Daytime thermodynamic and airflow structures over northeast Bangladesh during the pre-monsoon season: a case study on 25 April 2010. *Journal of the Meteorological Society of Japan. Ser. II*, 89, pp.167-179.
- [134] Naidu, C. V., Durgalakshmi, K., Krishna, K. M., Rao, S. R., Satyanarayana, G. C., Lakshminarayana, P., & Rao, L. M. (2009). Is summer monsoon rainfall decreasing over India in the global warming era?. *Journal of Geophysical Research: Atmospheres*, 114(D24).
- [135] Nashwan, M. S., Shahid, S., & Rahim, N. A. (2018). Unidirectional trends in annual and seasonal climate and extremes in Egypt. *Theoretical and Applied Climatology*, 1-17.
- [136] Nengker, T., Choudhary, A., & Dimri, A. P. (2018). Assessment of the performance of CORDEX-SA experiments in simulating seasonal mean temperature over the Himalayan region for the present climate: part I. *Climate dynamics*, 50(7-8), 2411-2441.
- [137] Neuman, S. P. (2003). Maximum likelihood Bayesian averaging of uncertain model predictions. *Stochastic Environmental Research and Risk Assessment*, 17(5), 291-305.
- [138] Nikulin, G., Jones, C., Giorgi, F., Asrar, G., Büchner, M., Cerezo-Mota, R., Christensen, O.B., Déqué, M., Fernandez, J., Hänsler, A. and van Meijgaard, E. (2012). Precipitation climatology in an ensemble of CORDEX-Africa regional climate simulations. *Journal of Climate*, 25(18), pp.6057-6078.
- [139] North, G. R., Pyle, J. A., & Zhang, F. (Eds.). (2014). *Encyclopedia of atmospheric sciences* (Vol. 1). Elsevier.
- [140] Nourani, V., Mehr, A. D., & Azad, N. (2018). Trend analysis of hydroclimatological variables in Urmia lake basin using hybrid wavelet Mann-Kendall and Şen tests. *Environmental Earth Sciences*, 77(5), 207.

- [141] Nowreen, S., Murshed, S. B., Islam, A. S., Bhaskaran, B., & Hasan, M. A. (2015). Changes of rainfall extremes around the haor basin areas of Bangladesh using multi-member ensemble RCM. *Theoretical and applied climatology*, 119(1-2), 363-377.
- [142] Önöz, B., & Bayazit, M. (2003). The power of statistical tests for trend detection. *Turkish Journal of Engineering and Environmental Sciences*, 27(4), 247-251.
- [143] Oza, M., & Kishtawal, C. M. (2014). Trends in Rainfall and Temperature Patterns over North East India. *Earth Science India*, 7(4).
- [144] Panthou, G., Mailhot, A., Laurence, E., & Talbot, G. (2014). Relationship between surface temperature and extreme rainfalls: A multi-time-scale and event-based analysis. *Journal of hydrometeorology*, 15(5), 1999-2011.
- [145] Pettitt, A. N. (1979). A non-parametric approach to the change-point problem. *Applied statistics*, 126-135.
- [146] Piani, C., Haerter, J. O., & Coppola, E. (2010). Statistical bias correction for daily precipitation in regional climate models over Europe. *Theoretical and Applied Climatology*, 99(1-2), 187-192.
- [147] Pierce, D. W., Barnett, T. P., Santer, B. D., & Gleckler, P. J. (2009). Selecting global climate models for regional climate change studies. *Proceedings of the National Academy of Sciences*, pnas-0900094106.
- [148] Pirnia, A., Golshan, M., Darabi, H., Adamowski, J., & Rozbeh, S. (2018). Using the Mann–Kendall test and double mass curve method to explore stream flow changes in response to climate and human activities. *Journal of Water and Climate Change*.
- [149] Power, S., Delage, F., Chung, C., Kociuba, G., & Keay, K. (2013). Robust twenty-first-century projections of El Niño and related precipitation variability. *Nature*, 502(7472), 541.
- [150] Prokop, P., & Walanus, A. (2015). Variation in the orographic extreme rain events over the Meghalaya Hills in northeast India in the two halves of the twentieth century. *Theoretical and Applied Climatology*, 121(1-2), 389-399.
- [151] Rafiuddin, M., Uyeda, H., & Islam, M. N. (2010). Characteristics of monsoon precipitation systems in and around Bangladesh. *International Journal of Climatology: A Journal of the Royal Meteorological Society*, 30(7), 1042-1
- [152] Raftery, A. E., Gneiting, T., Balabdaoui, F., & Polakowski, M. (2005). Using Bayesian model averaging to calibrate forecast ensembles. *Monthly Weather Review*, 133(5), 1155-1174.
- [153] Raftery, A. E., Madigan, D., & Hoeting, J. A. (1997). Bayesian model averaging for linear regression models. *Journal of the American Statistical Association*, 92(437), 179-191.

- [154] Rahman, M. R., Salehin, M., & Matsumoto, J. (1997). Trends of monsoon rainfall pattern in Bangladesh. *Bangladesh Journal of Water Resources*, 14(18), 121-138.
- [155] Räisänen, J., & Räty, O. (2013). Projections of daily mean temperature variability in the future: cross-validation tests with ENSEMBLES regional climate simulations. *Climate Dynamics*, 41(5-6), 1553-1568.
- [156] Ramsey, P. H. (1989). Critical values for Spearman's rank order correlation. *Journal of educational statistics*, 14(3), 245-253.
- [157] Ratnam, J. V., Behera, S. K., Ratna, S. B., Rajeevan, M., & Yamagata, T. (2016). Anatomy of Indian heatwaves. *Scientific reports*, 6, 24395.
- [158] Revadekar, J. V., Patwardhan, S. K., & Rupa Kumar, K. (2011). Characteristic features of precipitation extremes over India in the warming scenarios. *Advances in Meteorology*, 2011.
- [159] Reeve, M., A. (2015). Monsoon onset in Bangladesh: reconciling scientific and societal perspectives.
- [160] Rohini, P., Rajeevan, M., & Srivastava, A. K. (2016). On the variability and increasing trends of heat waves over India. *Scientific reports*, 6, 26153.
- [161] Rojas, R., Feyen, L., Dosio, A., & Bavera, D. (2011). Improving pan-European hydrological simulation of extreme events through statistical bias correction of RCM-driven climate simulations. *Hydrology & Earth System Sciences*, 15(8).
- [162] Roxy, M. K., Ritika, K., Terray, P., Murtugudde, R., Ashok, K., & Goswami, B. N. (2015). Drying of Indian subcontinent by rapid Indian Ocean warming and a weakening land-sea thermal gradient. *Nature Communications*, 6, 7423.
- [163] Roxy, M. K. (2017). Climate dynamics: Land warming revives monsoon. *Nature Climate Change*, 7(8), 549.
- [164] Roy, B., Islam, A. S., Islam, G. T., Khan, M. J. U., Bhattacharya, B., Ali, M. H., Khan, A. S., Hossain, M. S., Sarker, G. C., & Pieu, N. M. (2019). Frequency Analysis of Flash Floods for Establishing New Danger Levels for the Rivers in the Northeast Haor Region of Bangladesh. *Journal of Hydrologic Engineering*, 24(4), 05019004.
- [165] Sabade, S.S., Kulkarni, A., Kripalani, R.H., 2011. Projected changes in South Asian summer monsoon by multi-model global warming experiments. *Theor. Appl. Climatol.*, 103(3-4): 543-565.
- [166] Sabeerali, C. T., Rao, S. A., Dhakate, A. R., Salunke, K., & Goswami, B. N. (2015). Why ensemble mean projection of south Asian monsoon rainfall by CMIP5 models is not reliable?. *Climate Dynamics*, 45(1-2), 161-174.

- [167] Salman, S. A., Shahid, S., Ismail, T., Rahman, N. B. A., Wang, X., & Chung, E. S. (2018). Unidirectional trends in daily rainfall extremes of Iraq. *Theoretical and applied climatology*, 134(3-4), 1165-1177.
- [168] Sangelantoni, L., Russo, A., & Gennaretti, F. (2019). Impact of bias correction and downscaling through quantile mapping on simulated climate change signal: a case study over Central Italy. *Theoretical and Applied Climatology*, 135(1-2), 725-740.
- [169] Sato, T. (2013). Mechanism of orographic precipitation around the Meghalaya Plateau associated with intraseasonal oscillation and the diurnal cycle. *Monthly Weather Review*, 141(7), 2451-2466.
- [170] Schmidli J., Frei C. 2005. Trends of heavy precipitation and wet and dry spells in Switzerland during the 20th century. *International Journal of Climatology* 25(6): 753–771.
- [171] Schmidli, J., Frei, C., & Vidale, P. L. (2006). Downscaling from GCM precipitation: a benchmark for dynamical and statistical downscaling methods. *International Journal of Climatology: A Journal of the Royal Meteorological Society*, 26(5), 679-689.
- [172] Schmidli, J., Goodess, C. M., Frei, C., Haylock, M. R., Hurrell, J. W., Ribalaygua, J., & Schmuth, T. (2007). Statistical and dynamical downscaling of precipitation: An evaluation and comparison of scenarios for the European Alps. *Journal of Geophysical Research: Atmospheres*, 112(D4).
- [173] Sen, P. K. (1968). Estimates of the regression coefficient based on Kendall's tau. *Journal of the American statistical association*, 63(324), 1379-1389.
- [174] Sennikovs, J., & Bethers, U. (2009, July). Statistical downscaling method of regional climate model results for hydrological modelling. *In Proc. 18 th World IMACS/MODSIM Congress, Cairns, Australia*.
- [175] Shahid, S. (2008). Spatial and temporal characteristics of droughts in the western part of Bangladesh. *Hydrological Processes: An International Journal*, 22(13), 2235-2247.
- [176] Shahid, S. (2011). Trends in extreme rainfall events of Bangladesh. *Theoretical and Applied Climatology* 104(3-4): 489-499.
- [177] Sharmila, S., Joseph, S., Sahai, A. K., Abhilash, S., & Chattopadhyay, R. (2015). Future projection of Indian summer monsoon variability under climate change scenario: *An assessment from CMIP5 climate models. Global and Planetary Change*, 124, 62-78.
- [178] Singh, O. P. (2001). Multivariate ENSO index and Indian monsoon rainfall: relationships on monthly and subdivisional scales. *Meteorology and Atmospheric physics*, 78(1-2), 1-9.

- [179] Sinha, A., Kathayat, G., Cheng, H., Breitenbach, S. F., Berkelhammer, M., Mudelsee, M., ... & Edwards, R. L. (2015). Trends and oscillations in the Indian summer monsoon rainfall over the last two millennia. *Nature Communications*, 6, ncomms7309.
- [180] Stenseth, N.C., Ottersen, G., Hurrell, J.W., Mysterud, A., Lima, M., Chan, K.S., Yoccoz, N.G. and Ådlandsvik, B. (2003). Studying climate effects on ecology through the use of climate indices: the North Atlantic Oscillation, El Nino Southern Oscillation and beyond. *Proceedings of the Royal Society of London. Series B: Biological Sciences*, 270(1529), pp.2087-2096.
- [181] Stoffel, M., Tiranti, D., and Huggel, C. (2014). Climate change impacts on mass movements — Case studies from the European Alps. *Science of The Total Environment*, 493: 1255-1266.
- [182] Sun, F., Roderick, M. L., Lim, W. H., & Farquhar, G. D. (2011). Hydroclimatic projections for the Murray- Darling Basin based on an ensemble derived from Intergovernmental Panel on Climate Change AR4 climate models. *Water Resources Research*, 47(12).
- [183] Taxak, A. K., Murumkar, A. R., & Arya, D. S. (2014). Long term spatial and temporal rainfall trends and homogeneity analysis in Wainganga basin, Central India. *Weather and Climate Extremes*, 4, 50-61.
- [184] Taylor, K. E. (2009). A summary of the CMIP5 experiment design. http://cmip-pcmdi.llnl.gov/cmip5/docs/Taylor_CMIP5_design.pdf.
- [185] Terao, T., Murata, F., Habib, A., Bhuiyan, M. S. H., Choudhury, S. A., & Hayashi, T. (2013). Impacts of rapid warm-to-cold ENSO transitions on summer monsoon rainfall over the northeastern Indian subcontinent. *Journal of the Meteorological Society of Japan. Ser. II*, 91(1), 1-21.
- [186] Terao, T., Islam, M. N., Hayashi, T., & Oka, T. (2006). Nocturnal jet and its effects on early morning rainfall peak over northeastern Bangladesh during the summer monsoon season. *Geophysical research letters*, 33(18).
- [187] Teutschbein, C., & Seibert, J. (2010). Regional climate models for hydrological impact studies at the catchment scale: a review of recent modeling strategies. *Geography Compass*, 4(7), 834-860.
- [188] Teutschbein, C., & Seibert, J. (2012). Bias correction of regional climate model simulations for hydrological climate-change impact studies: Review and evaluation of different methods. *Journal of Hydrology*, 456, 12-29.
- [189] Teutschbein, C., & Seibert, J. (2013). Is bias correction of regional climate model (RCM) simulations possible for non-stationary conditions?. *Hydrology and Earth System Sciences*, 17(12), 5061-5077.

- [190] Themeßl, M. J., Gobiet, A., & Heinrich, G. (2012). Empirical-statistical downscaling and error correction of regional climate models and its impact on the climate change signal. *Climatic Change*, 112(2), 449-468.
- [191] Themeßl, M. J., Gobiet, A., & Leuprecht, A. (2011). Empirical- statistical downscaling and error correction of daily precipitation from regional climate models. *International Journal of Climatology*, 31(10), 1530-1544.
- [192] Torrence, C., & Webster, P. J. (1999). Interdecadal changes in the ENSO– monsoon system. *Journal of Climate*, 12(8), 2679-2690.
- [193] Tozer, C. R., Kiem, A. S., & Verdon- Kidd, D. C. (2017). Large- scale ocean- atmospheric processes and seasonal rainfall variability in South Australia: potential for improving seasonal hydroclimatic forecasts. *International Journal of Climatology*, 37(S1), 861-877.
- [194] Turco, M., Quintana- Seguí, P., Llasat, M. C., Herrera, S., & Gutiérrez, J. M. (2011). Testing MOS precipitation downscaling for ENSEMBLES regional climate models over Spain. *Journal of Geophysical Research: Atmospheres*, 116(D18).
- [195] Turner, A. G., & Annamalai, H. (2012). Climate change and the South Asian summer monsoon. *Nature Climate Change*, 2(8), 587.
- [196] UK Met. Office. (2014). *What is climate change?* 3 February. Accessed: September 5, 2014. <http://www.metoffice.gov.uk/climate-guide/climate-change>.
- [197] Villani, V., Rianna, G., Mercogliano, P., & Zollo, A. L. (2015). Statistical approaches versus weather generator to downscale RCM outputs to slope scale for stability assessment: a comparison of performances. *Electron J Geotech Eng*, 20(4), 1495-1515.
- [198] Visbeck, M. (2007). From climate assessment to climate services. *Nature Geoscience*, 1(1), 2.
- [199] Volosciuk, C., Maraun, D., Semenov, V. A., & Park, W. (2015). Extreme precipitation in an atmosphere general circulation model: Impact of horizontal and vertical model resolutions. *Journal of Climate*, 28(3), 1184-1205.
- [200] Vrugt, J. A. (2015). Multi-criteria optimization using the AMALGAM software package: Theory, concepts, and MATLAB implementation. *Manual, Version, 1*, 1-53.
- [201] Vrugt, J. A. (2016). Markov chain Monte Carlo simulation using the DREAM software package: Theory, concepts, and MATLAB implementation. *Environmental Modelling & Software*, 75, 273-316.
- [202] Vrugt, J. A., & Robinson, B. A. (2007). Treatment of uncertainty using ensemble methods: Comparison of sequential data assimilation and Bayesian model averaging. *Water Resources Research*, 43(1).

- [203] Vrugt, J. A., Diks, C. G., & Clark, M. P. (2008). Ensemble Bayesian model averaging using Markov chain Monte Carlo sampling. *Environmental fluid mechanics*, 8(5-6), 579-595.
- [204] Wang, H.J., Zhang, Y. (2010). Model projections of East Asia summer climate under the “free Arctic” scenario. *Atmos Ocean Sci Lett* 3(3):176–180.
- [205] Wang, X., Tan, W., & Wang, C. (2018). A new index for identifying different types of El Niño Modoki events. *Climate Dynamics*, 1-13.
- [206] Weyant, J., Azar, C., Kainuma, M., Kejun, J., Nakicenovic, N., Shukla, P. R., Emilio La Rovere, E., L. & Yohe, G. (2009). Report of 2.6 versus 2.9 Watts/m² RCPP evaluation panel. *Integrated Assessment Modeling Consortium*.
- [207] Willems, P. (2009). A time series tool to support the multi-criteria performance evaluation of rainfall-runoff models. *Environmental Modelling & Software*, 24(3), 311-321.
- [208] Winkler, J.A., Guentchev, G.S., Liszewska, M. and Tan, P.N. (2011). Climate Scenario Development and Applications for Local/Regional Climate Change Impact Assessments: An Overview for the Non- Climate Scientist: Part II: Considerations When Using Climate Change Scenarios. *Geography Compass*, 5(6), pp.301-328.
- [209] Woehling, T., & Vrugt, J. A. (2008). Combining multi-objective optimization and Bayesian model averaging to calibrate forecast ensembles of soil hydraulic models. *Water Resources Research*, 44(12).
- [210] Wolter, K. (1993). Monitoring ENSO in COADS with a seasonally adjusted principal component index. In *Proc. of the 17th Climate Diagnostics Workshop, 1993*.
- [211] Worqlul, A. W., Ayana, E. K., Maathuis, B. H., MacAlister, C., Philpot, W. D., Leyton, J. M. O., & Steenhuis, T. S. (2018). Performance of bias corrected MPEG rainfall estimate for rainfall-runoff simulation in the upper Blue Nile Basin, Ethiopia. *Journal of Hydrology*, 556, 1182-1191.
- [212] Wu, X., Wang, Z., Zhou, X., Lai, C., Lin, W., & Chen, X. (2016). Observed changes in precipitation extremes across 11 basins in China during 1961–2013. *International Journal of Climatology*, 36(8), 2866-2885.
- [213] Xia, Y., Fabian, P., Winterhalter, M., & Zhao, M. (2001). Forest climatology: estimation and use of daily climatological data for Bavaria, Germany. *Agricultural and Forest Meteorology*, 106(2), 87-103.
- [214] Yamane, Y., Hayashi, T., Dewan, A. M., & Akter, F. (2010). Severe local convective storms in Bangladesh: Part II.: Environmental conditions. *Atmospheric Research*, 95(4), 407-418.

- [215] Yamazaki, K., & Watanabe, M. (2015). Effects of extratropical warming on ENSO amplitudes in an ensemble of a coupled GCM. *Climate Dynamics*, 44(3-4), 679-693.
- [216] Yang, L., Villarini, G., Smith, J. A., Tian, F., & Hu, H. (2013). Changes in seasonal maximum daily precipitation in China over the period 1961–2006. *International Journal of Climatology*, 33(7), 1646-1657.
- [217] Zarenistanak, M., Dhorde, A. G., & Kripalani, R. H. (2014). Trend analysis and change point detection of annual and seasonal precipitation and temperature series over southwest Iran. *Journal of earth system science*, 123(2), 281-295.
- [218] Zhang, Q., Xu, C. Y., Zhang, Z., Ren, G., & Chen, Y. D. (2008). Climate change or variability? The case of Yellow river as indicated by extreme maximum and minimum air temperature during 1960–2004. *Theoretical and Applied Climatology*, 93(1-2), 35-43.
- [219] Zhang, X., Xiong, Z., Zhang, X., Shi, Y., Liu, J., Shao, Q., & Yan, X. (2016). Using multi-model ensembles to improve the simulated effects of land use/cover change on temperature: A case study over northeast China. *Climate Dynamics*, 46(3-4), 765-778.
- [220] Zhang, Y. Sun, J.Q. (2012). Model projection of precipitation minus evaporation over China. *Acta Meteor Sinica* 26(3):376–388
- [221] Zeleňáková, M., Purcz, P., Blišťan, P., Vranayová, Z., Hlavatá, H., Diaconu, D., & Portela, M. (2018). Trends in Precipitation and Temperatures in Eastern Slovakia (1962–2014). *Water*, 10(6), 727.
- [222] Zhu, R., Zheng, H., Wang, E., & Zhao, W. (2013). Multi-model ensemble simulation of flood events using Bayesian model averaging. In MODSIM2013, 20th Int. Congress on Modelling and Simulation (pp. 455-461). Modelling and Simulation Society of Australia and New Zealand.
- [223] Zobel, Z., Wang, J., Wuebbles, D. J., & Kotamarthi, V. R. (2018). Evaluations of high-resolution dynamically downscaled ensembles over the contiguous United States. *Climate Dynamics*, 50(3-4), 863-884.

APPENDICES

Appendix A: Theory

A.1 Standard Normal Homogeneity Test

The SNHT is sensitive in detecting the breaks near the beginning and the end of the series, and it assumes testing variables is normally distributed. In this test, a statistic $T(y)$ is used to compare the mean of the first y years with the last of $(n-y)$ years and can be written as below:

$$T_y = y\bar{z}_1^2 + (n - y)\bar{z}_2^2, y=1,2,\dots,n \quad (1)$$

$$\text{Where, } \bar{z}_1 = \frac{1}{y} \sum_{i=1}^n \frac{(Y_i - \bar{Y})}{s} \text{ and } \bar{z}_2 = \frac{1}{n-y} \sum_{i=y+1}^n \frac{(Y_i - \bar{Y})}{s} \quad (2)$$

Where Y_i is the i^{th} observation, \bar{Y} is the mean of the observations and s is the standard deviation. The year y consisted of a break if the value of T is maximum. To reject the null hypothesis, the test statistic, T_0 needs to be greater than the critical value, which is defined by [89].

$$T_0 = \underbrace{\max}_{1 \leq y \leq n} T_y \quad (3)$$

A.2 Pettit Test

The Pettit test (Pettit 1979) is sensitive in detecting the breaks in the middle of the series, and it is a non-parametric rank test. This test is based on ranked data and ignore the normality of the series. The test statistic P_y is computed by the following equation.

$$P_y = 2 \sum_{i=0}^n r_i - y(n + 1) \quad (4)$$

Where r_i is the rank of the i^{th} observation arranged in ascending order and $y= 1, 2, \dots, n$. The break occurs where in year K when

$$P_k = \underbrace{\max}_{1 \leq y \leq n} |P_y| \quad (5)$$

The value is then compared with the critical value by Pettit (1979).

A.3 Auto Correlation with One Day Lag

Let the time series of length n be $Y_i, i = 1, \dots, n$. The lagged scatter plot for lag 1 is a scatter plot of the last observations against the first $n-1$ observations. The observations Y_2, Y_3, \dots, Y_n are plotted against observations Y_1, Y_2, \dots, Y_{n-1} . The correlation coefficient is then given by

$$r = \frac{\sum_{n=1}^{n-1} (y_n - \bar{y}_{(1)})(y_{n+1} - \bar{y}_{(2)})}{[\sum_{n=1}^{n-1} (y_n - \bar{y}_{(1)})^2]^{1/2} [\sum_{n=2}^n (y_n - \bar{y}_{(2)})^2]^{1/2}} \quad (6)$$

Where, $\bar{y}_{(1)}$ is the mean of the first $n - 1$ observations and $\bar{y}_{(2)}$ is the mean of the last $n - 1$ observations. At 95% confidence level, the sample is a random event if r is within the band of $\frac{-1 \pm 1.96\sqrt{N-2}}{N-1}$. Where, N is the sample size.

A.4 Mann–Kendall Trend Test

The Mann Kendall test is performed in an ordered time series. Each data are compared to all succeeding data. Initially, the value of S is anticipated to 0. If a latter data point is higher than an earlier data point, S is increased by 1. On the contrary, a latter data point is lesser than an earlier data point, S is decreased by 1. The net result of all such increments and decrements yields the final value of S .

If $Y_1, Y_2, Y_3, \dots, Y_n$ represent n data points then S is given by

$$S = \sum_{K=1}^{n-1} \sum_{j=k+1}^n \text{sign}(Y_j - Y_k) \quad (7)$$

Where, Y_j and Y_k represents the data point at time j and $k, j > k$ and

$$\text{sign}(Y_j - Y_k) = \begin{cases} 1 & \text{if } (Y_j - Y_k) > 0 \\ 0 & \text{if } (Y_j - Y_k) = 0 \\ -1 & \text{if } (Y_j - Y_k) < 0 \end{cases} \quad (8)$$

The probability, associated with S and the sample size, n is then computed to quantify the significance of the trend statistically. If sample size, $n < 10$, the value of $|S|$ is compared directly to the theoretical distribution of S derived by Mann and Kendall. If $|S| \geq S_{\alpha/2}$, where $S_{\alpha/2}$ is the smallest S which has the probability less than $\alpha/2$, the null hypothesis H_0 is rejected in favor of H_1 at a certain probability. A positive value of S indicates an upward trend, and a negative value of S indicates a downward trend.

If sample size, $n \geq 10$, the statistic S is approximately normally distributed with the mean and variance as follows.

$$E(S) = 0 \quad (9)$$

$$Var(s) = [n(n - 1)(2n + 5) - \sum_t t(t - 1)(2t + 5)]/18 \quad (10)$$

Where t refers to the extent of any given tie and \sum_t state the summation over all tie. The Normalized test statistic Z is computed as follows:

$$Z = \begin{cases} \frac{S-1}{\sqrt{VAR(S)}} & \text{if } S > 0 \\ 0 & \text{if } S = 0 \\ \frac{S+1}{\sqrt{VAR(S)}} & \text{if } S < 0 \end{cases} \quad (11)$$

Therefore, in case $|Z| \leq Z_{1-\alpha/2}$ in a two-sided test for trend, the null hypothesis H_0 should be accepted at the level of significance. A positive value of S indicates an upward trend, and the negative value of S indicates a downward trend.

A.5 Sen's Slope Estimator

In the case of linear trend analysis, the Sen's Slope method (Sen, 1968) is applied to estimate the magnitude of the trend. A time series of equally spaced data is required for this method and is not affected by missing values or gap in data. The slope estimates Q of N pairs of data are calculated as

$$Q = \frac{Y_j - Y_k}{j - k} \quad (12)$$

Where Q is the slope between data points Y_j and Y_k ,

If there are n values Y_j in the time series, then there will be as many as $N = n(n - 1)/2$ slope estimates Q_i . The Sen's estimator of the slope is the median of these N values of Q_i . The N values of Q_i are ranked from the smallest to the largest, and the Sen's estimator is

$$Q = Q_{[(N+1)/2]}, \text{ if } N \text{ is odd} \quad (13)$$

$$Q = \frac{1}{2} \left(Q_{\left[\frac{N}{2}\right]} + Q_{\left[\frac{N+2}{2}\right]} \right), \text{ if } N \text{ is even} \quad (14)$$

A6. Bias and RMSE

The bias and RMSE were calculated over average pre-monsoon and monsoon rainfall over the period of 1976-2005 which are given below.

$$\text{Bias} = \frac{1}{N} \sum_{t=1}^N (P_{m,t} - P_{o,t}) \quad (15)$$

$$\text{RMSE} = \sqrt{\left[\frac{1}{N} \sum_{t=1}^N (P_{m,t} - P_{o,t})^2 \right]} \quad (16)$$

Where, $P_{o,t}$ and $P_{m,t}$ is the observed and RCM rainfall, respectively at a time t for a particular grid point. The bias and the RMSE were normalized by the mean and standard deviation of the observed data, respectively.

A.7 Quantile Mapping Bias Correction

A brief procedure of the quantile mapping bias correction is as follows:

Step 1: In order to adjust the wet-day frequency of RCM simulated rainfall according to observed rainfall, a cut-off threshold corresponding to the wet day ($\geq 1\text{mm}$) is selected before applying quantile mapping method.

Step 2: The gamma Cumulative Distribution Function (CDF) of the observed and RCM reference rainfall is determined for each month separately.

Step 3: The CDF of RCM reference simulation is mapped with CDF of observations for generating the transfer function. The schematic representation is presented in Fig A.1.

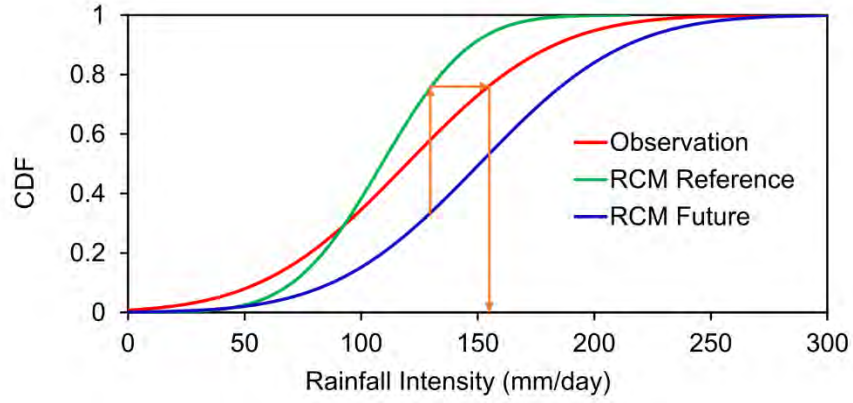


Fig A-1 A schematic representation of quantile mapping bias-correction approach. A transfer function is used to correct rainfall intensity for RCMs simulation during the reference and scenario period.

Step 4: Then, this correction function is finally used to correct the RCM scenario period.

The equation of the transfer function can be expressed as:

$$P_{ref}^*(d) = F_{\gamma}^{-1}(F_{\gamma}(P_{ref}(d)|\alpha_{ref,m},\beta_{ref,m})|\alpha_{obs,m},\beta_{obs,m}) \quad (17)$$

$$P_{scen}^*(d) = F_{\gamma}^{-1}(F_{\gamma}(P_{scen}(d)|\alpha_{ref,m},\beta_{ref,m})|\alpha_{obs,m},\beta_{obs,m}) \quad (18)$$

where, $P_{ref}(d)$ = raw daily rainfall for reference simulation,

$P_{scen}(d)$ = Raw daily rainfall for scenario simulation,

$P_{ref}^*(d)$ = Bias corrected daily rainfall for reference simulation,

$P_{scen}^*(d)$ = Bias corrected daily rainfall for scenario simulation,

F_{γ}^{-1} = Transfer function for gamma distribution,

$\alpha_{obs,m}$ = Shape parameter of gamma distribution for observed data of month m

$\alpha_{ref,m}$ = Shape parameter of gamma distribution for the reference period of month m

$\beta_{obs,m}$ = Scale parameter of gamma distribution for observed data of month m

$\beta_{ref,m}$ = Scale parameter of gamma distribution for the reference period of month m

A.8 Bayesian Model Averaging (BMA)

Bayesian Model Averaging (BMA) produces a complete PDF of the ensemble mean and quantifies the associated uncertainty of forecasts. In this approach, the predictive Probability Density Function (PDF) of the ensemble mean is the weighted average of the conditional PDF of an individual model, where the weights are posterior

probabilities of the models generating the forecasts and reflect the relative contributions of each individual model to the overall predictive skill. [69] comprehensively described the BMA theory, and Raftery et al., (2005) extended it for statistical post-processing of forecast ensembles. Given the training data Y^T and k climate models ($M_1 \dots M_k$), the forecast PDF of a variable Y is given by:

$$P(Y|Y_1, Y_2, \dots, Y_k) = \sum_{k=1}^k P(Y|M_k)P(M_k|Y^T) \quad (19)$$

where $P(Y|M_k)$ is the conditional PDF of Y on M_k , given that M_k is the best forecast in the ensemble and $P(M_k|Y^T)$ is the posterior probability of model M_k being the best one given the training data. The posterior model probabilities reflect how the model M_k performs to fit the training data and can be viewed as weights which are non-negative and added up to one, so that $\sum_{k=1}^k w_k = \sum_{k=1}^k P(M_k|Y^T) = 1$. Thus equation (19) can be written as:

$$P(Y|Y_1, Y_2, \dots, Y_k) = \sum_{k=1}^k w_k P(Y|M_k) \quad (20)$$

The BMA method assumes that the conditional PDF, $P(Y|M_k)$ of the individual model can be approximated by the normal distribution with mean $a_k + b_k M_k$ and standard deviation σ_k which is given by:

$$P(Y|M_k) \sim N(a_k + b_k M_k, \sigma_k^2) \quad (21)$$

The values for a_k and b_k are estimated by simple linear regression of $P(Y|M_k)$ on M_k for each model. Using the Kolmogorov–Smirnov test and graphical techniques (histograms and density estimate), it was found that the gamma distribution best fits the monthly rainfall data for the study area. This is the case for both pre-monsoon and monsoon seasons. Therefore, we considered the gamma distribution and modified the conditional PDF in equation 19. The conditional PDF for the gamma distribution with shape parameter α and scale parameter β can be given by:

$$P(Y|M_k) \sim \frac{1}{\beta\Gamma(\alpha)} Y^{\alpha-1} \exp(-Y/\beta) \quad (22)$$

for $Y > 0$. $P(Y|M_K) = 0$ for $Y \leq 0$. The mean of this distribution is $\mu = \alpha\beta$ and its variance is $\sigma^2 = \alpha\beta^2$. The parameters, $\alpha_k = \mu_k^2/\sigma_k^2$ and $\beta_k = \sigma_k^2/\mu_k$ of the gamma distribution for the actual forecast, Y_k of a particular ensemble member can be derived from the following relationship:

$$\mu_k = \bar{Y}_k \quad (23)$$

and

$$\sigma_k^2 = c_0 Y_k + c_1 \quad (24)$$

where, c_0 and c_1 are the coefficients of regression.

Thus BMA multi-model ensemble mean is a conditional expectation which is defined as:

$$\bar{Y} = E[Y|M_1, \dots, M_k] \quad (25)$$

The values of w_k , σ_k , c_0 and c_1 are estimated by the maximum likelihood function (ML) from simulated data set for the training period. The log-likelihood function, \mathcal{L} for the BMA multi-model ensemble mean in equation (25) can be given as:

$$\mathcal{L}(w_1, \dots, w_k, \sigma^2 | M_1, \dots, M_k, P(Y|M_K)) = \sum_{n=1}^N \log(\sum_{k=1}^k w_k P(Y_n|M_{kn})) \quad (26)$$

where N is the total number of measurement in the training dataset.

To derive the ML estimation of model parameters, a common approach is to use an expectation-maximization algorithm [36, 37]. Given an initial set of the model parameters, the expectation-maximization algorithm will converge quickly to a fixed set of parameter estimation after a few iterations. However, there are some inherent limitations of expectation-maximization: (i) it provides a local optimal solution instead of the global convergence, (ii) it does not yield the uncertainty associated with final BMA weights and the variance [203]. To overcome this limitation of the expectation-maximization approach, the ML function was optimized using the Differential Evolution Adaptive Metropolis Markov Chain Monte Carlo algorithm for estimating the BMA weights and variance [200,201,203]. The DREAM scheme is adapted from the Shuffled Complex Evolution Metropolis global optimization algorithm and is

capable of running multiple chains simultaneously for searching the global optimal solution [203].

A.9 Excessive Heat Factor (EHF)

The Excess Heat Factor (EHF) is the joined effect of Excess Heat Index and Heat Stress. It provides a comparative measure of frequency, duration, and spatial distribution of a heatwave event. Positive values of EHF signifies the heatwave condition.

The Excess Heat Index is defined as,

$$EHI_{sig} = \frac{(T_i + T_{i-1} + T_{i-2})}{3} - T_{95} \quad (27)$$

Where T_{95} is the 95th percentile of DMT (T_i) for the climate reference period of 1979-2017. The daily mean temperature was calculated by averaging the daily maximum and daily minimum temperatures which are defined as,

$$T = (T_{max} + T_{min})/2 \quad (28)$$

The heat stress results when the temperature is warmer than the recent past average temperature for a certain period of time. It is characterized by comparing the current three days average daily mean temperature with previous 30 days daily mean temperature. It is also expressed as short-term (acclimatization) temperature anomaly.

Therefore, the heat stress is defined as,

$$EHI_{accl} = \frac{T_i + T_{i-1} + T_{i-2}}{3} - (T_3 + \dots + T_{t-32})/30 \quad (29)$$

Where T_i is the DMT on day i . In effect, EHI_{accl} is an anomaly of three-day DMT with respect to the previous 30 days.

Therefore, the Excess Heat Factor (EHF) is defined as,

$$EHF = EHI_{sig} \times \max(1, EHI_{accl}) \quad (30)$$

Appendix B: Supplementary Figures

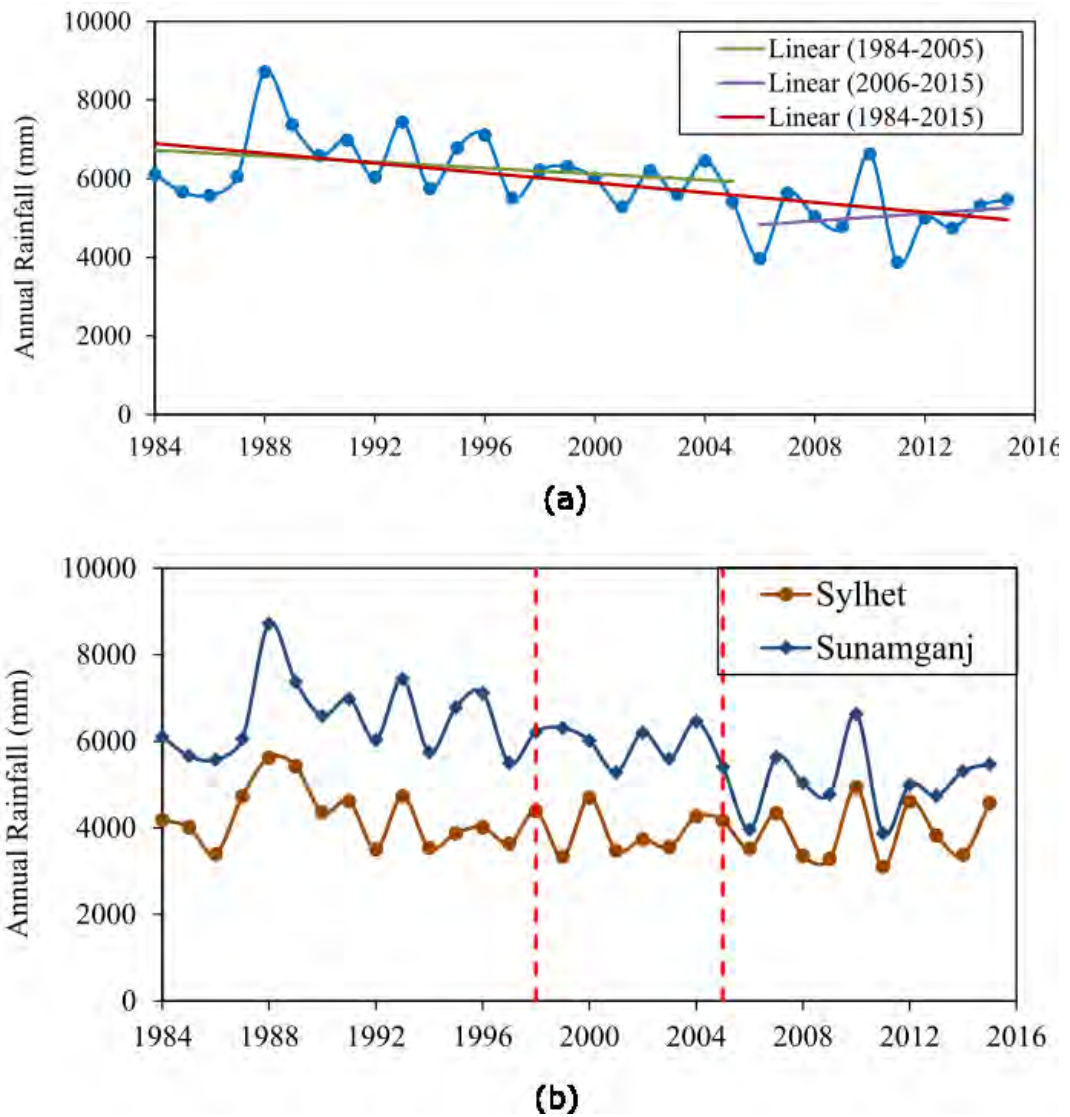


Fig B.1 (a) Trend line of annual rainfall (mm) of Sunamganj before and after change point (2005). (b) Comparison of the de-trending annual rainfall of Sunamganj with Sylhet.

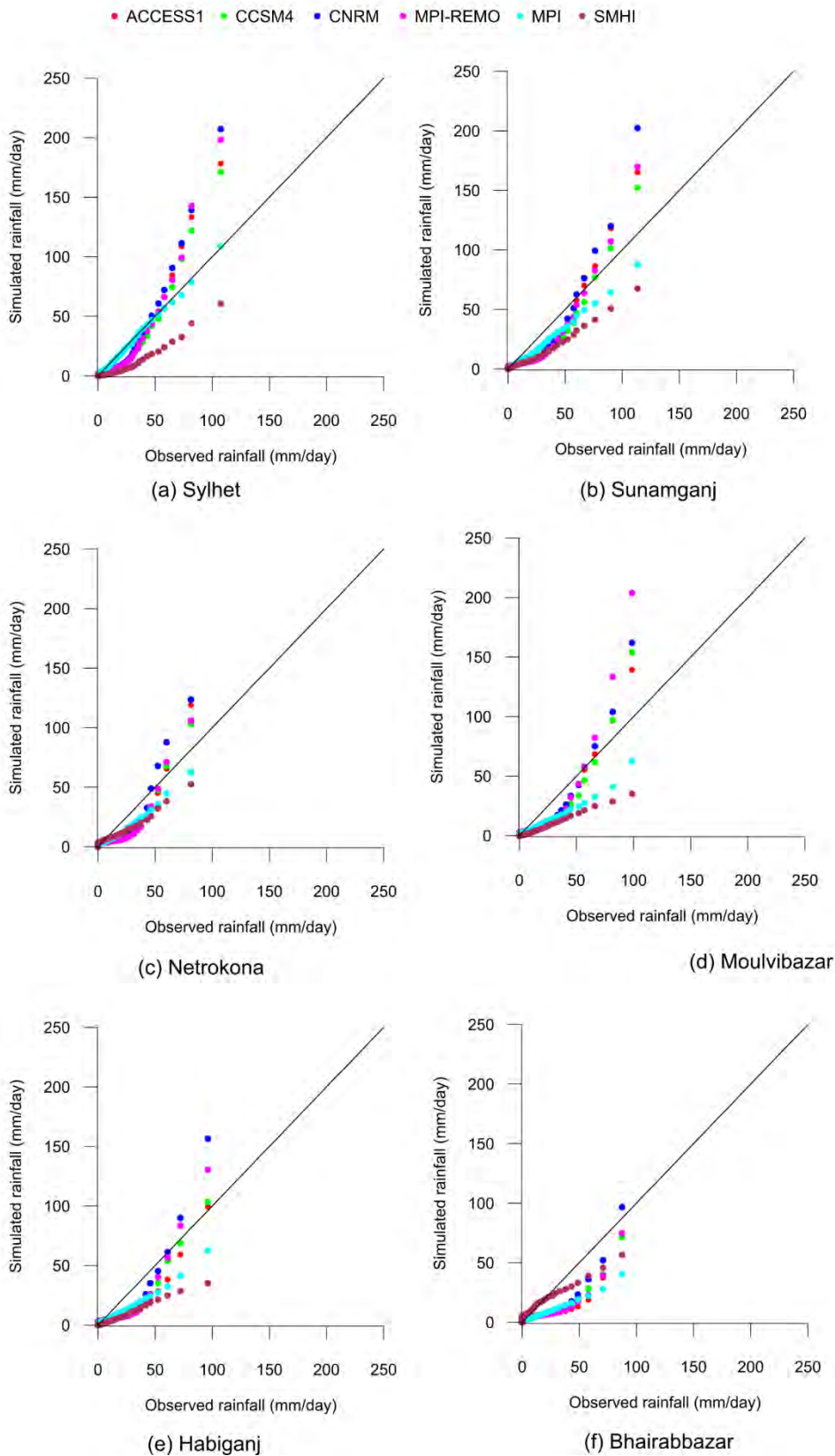


Fig B.2 Quantile-quantile plots for the uncorrected of simulated daily rainfall by RCMs against observed daily rainfall for all stations during Pre-monsoon.

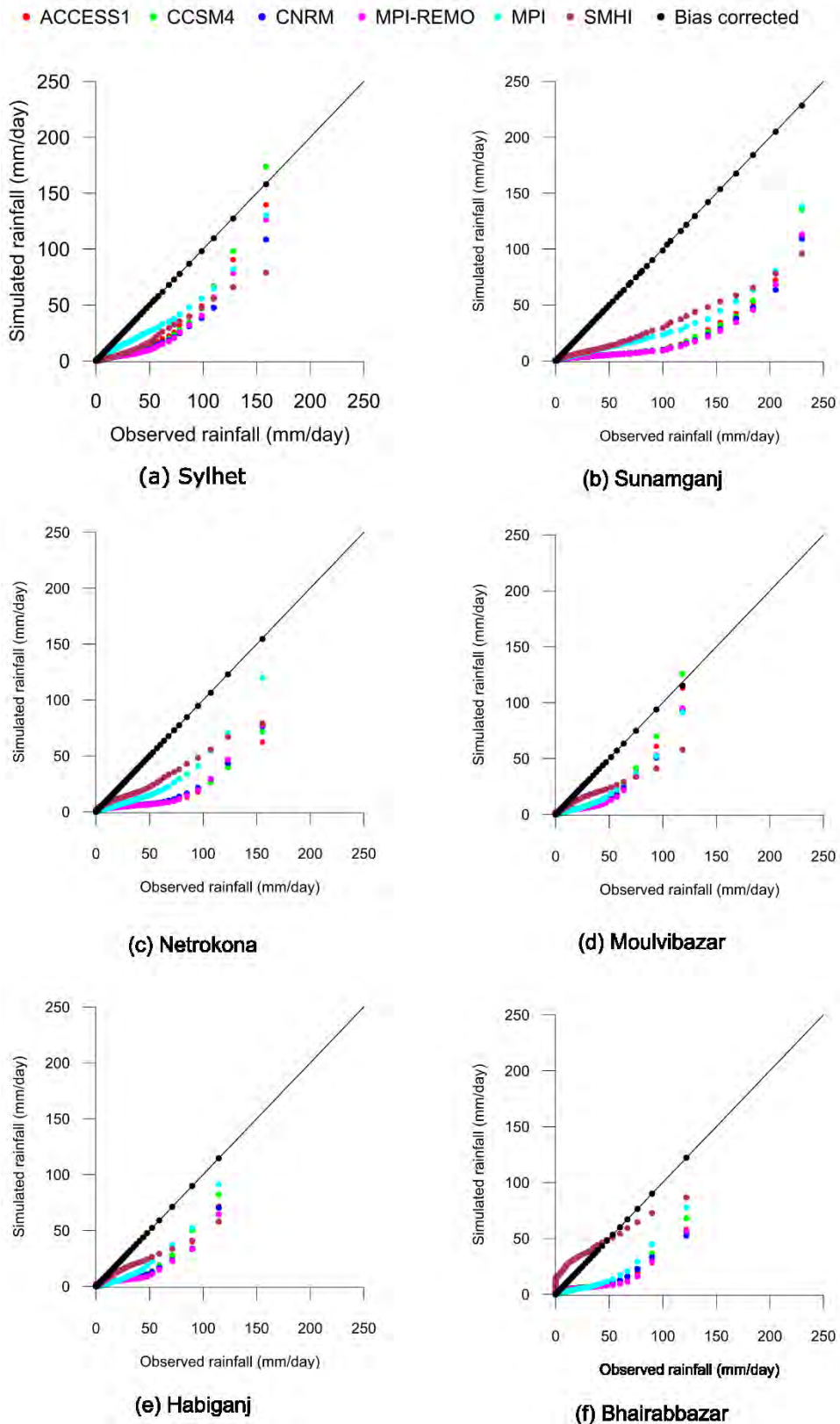


Fig B.5 Quantile-quantile plots for the uncorrected (colored marker) and corrected (black marker) of simulated daily rainfall by RCMs against observed daily rainfall for all stations during monsoon.

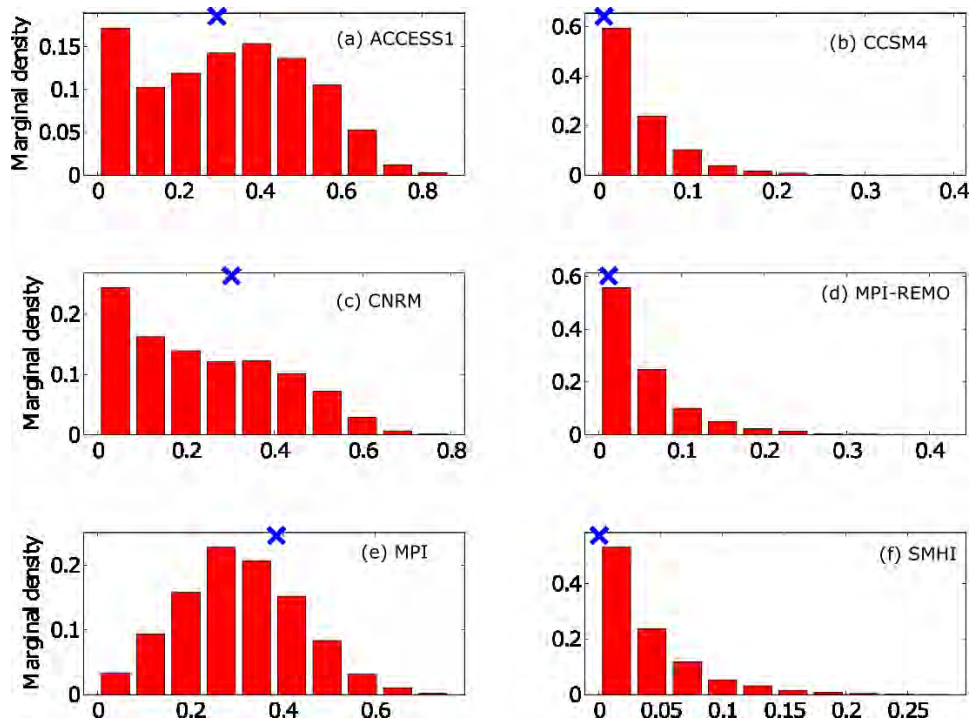


Fig B.6 Marginal posterior pdfs of the DREAM derived BMA weights of monthly rainfall totals for pre-monsoon of Sunamganj station.

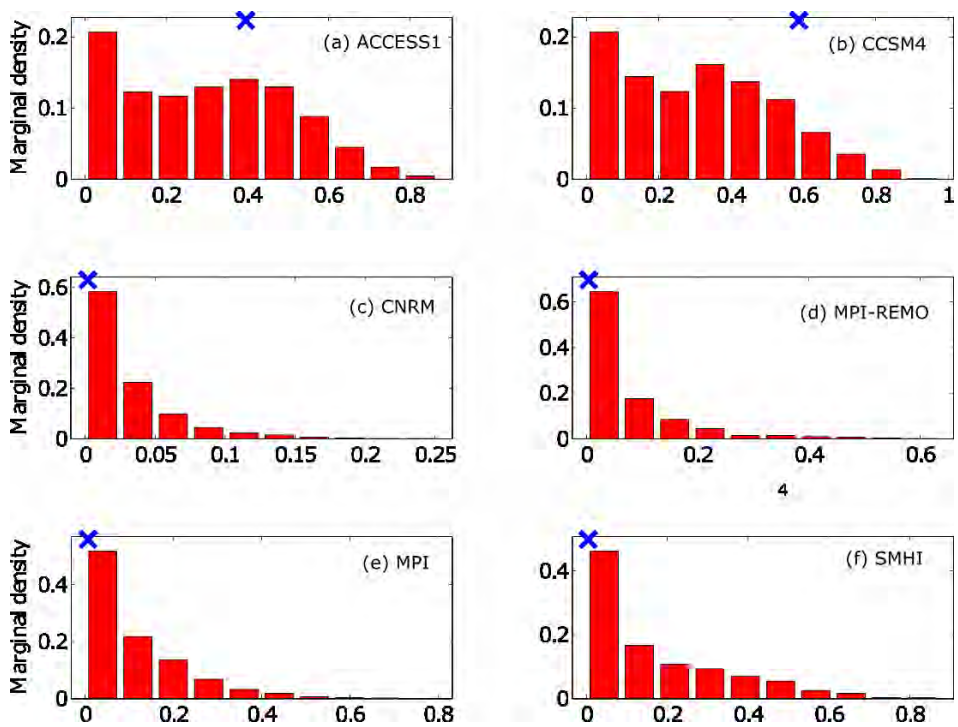


Fig B.7 Marginal posterior pdfs of the DREAM derived BMA weights of monthly rainfall totals for the monsoon of Sunamganj station.

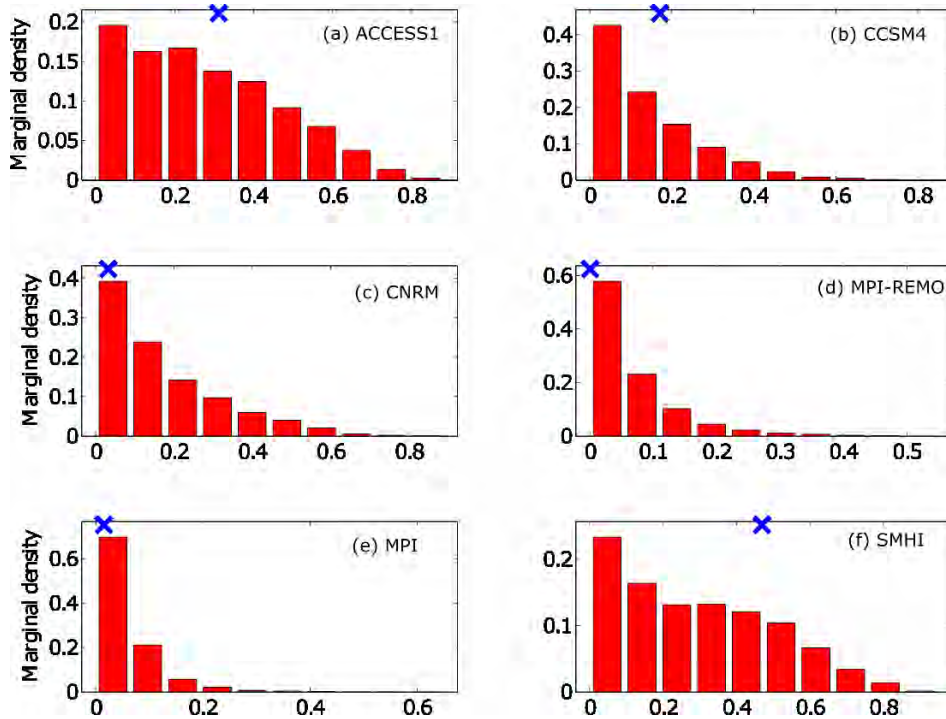


Fig B.8 Marginal posterior pdfs of the DREAM derived BMA weights of monthly rainfall totals for pre-monsoon of Netrokona station.

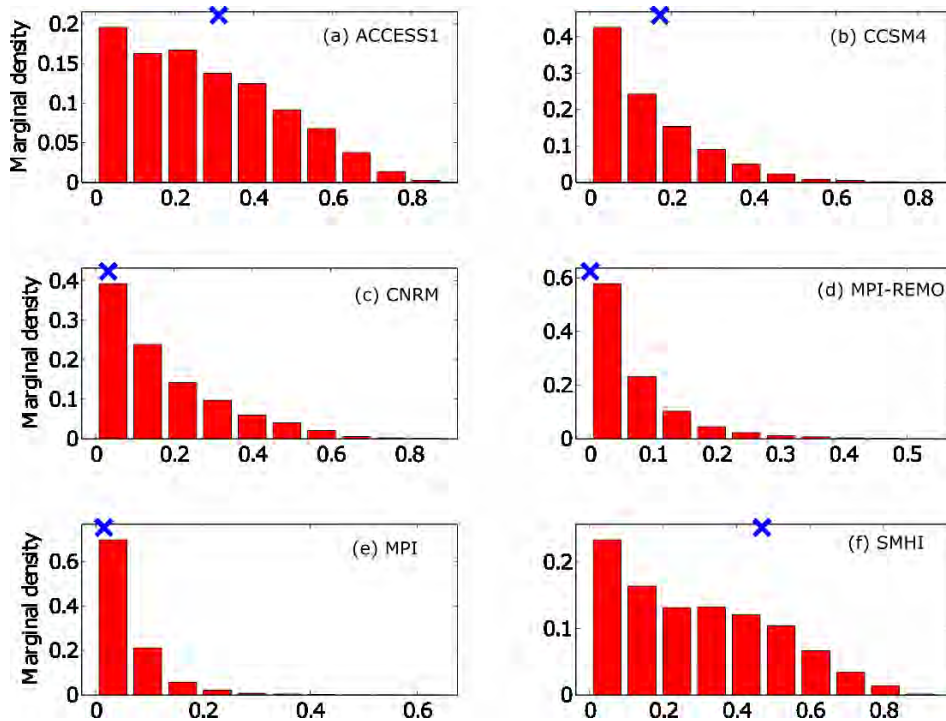


Fig B.9 Marginal posterior pdfs of the DREAM derived BMA weights of monthly rainfall totals for the monsoon of Netrokona station.

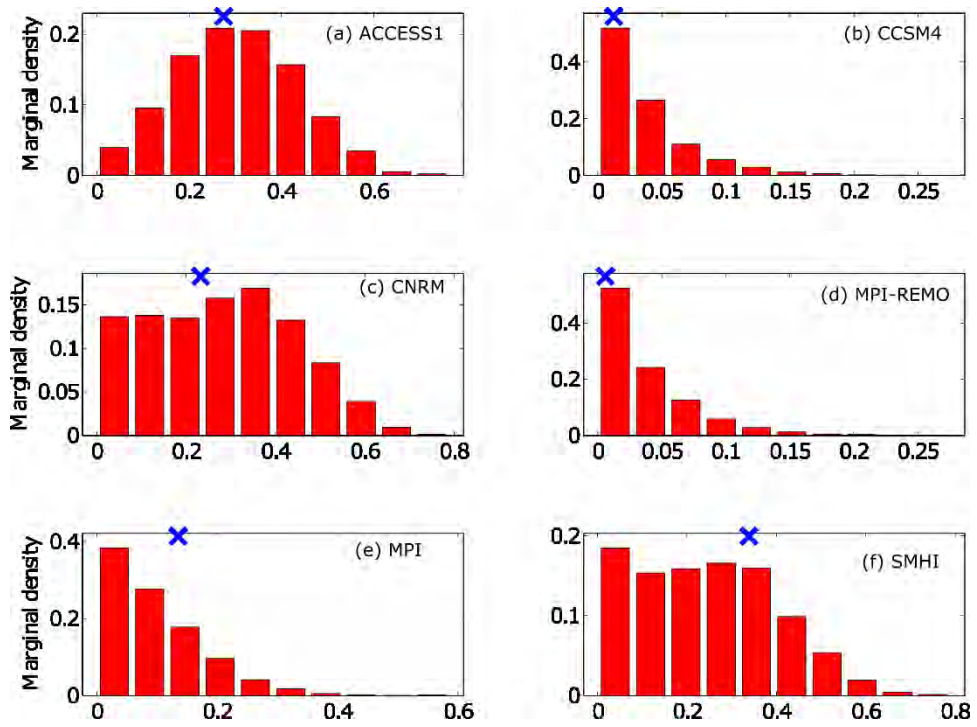


Fig B.10 Marginal posterior pdfs of the DREAM derived BMA weights of monthly rainfall totals for pre-monsoon of Moulvibazar station.

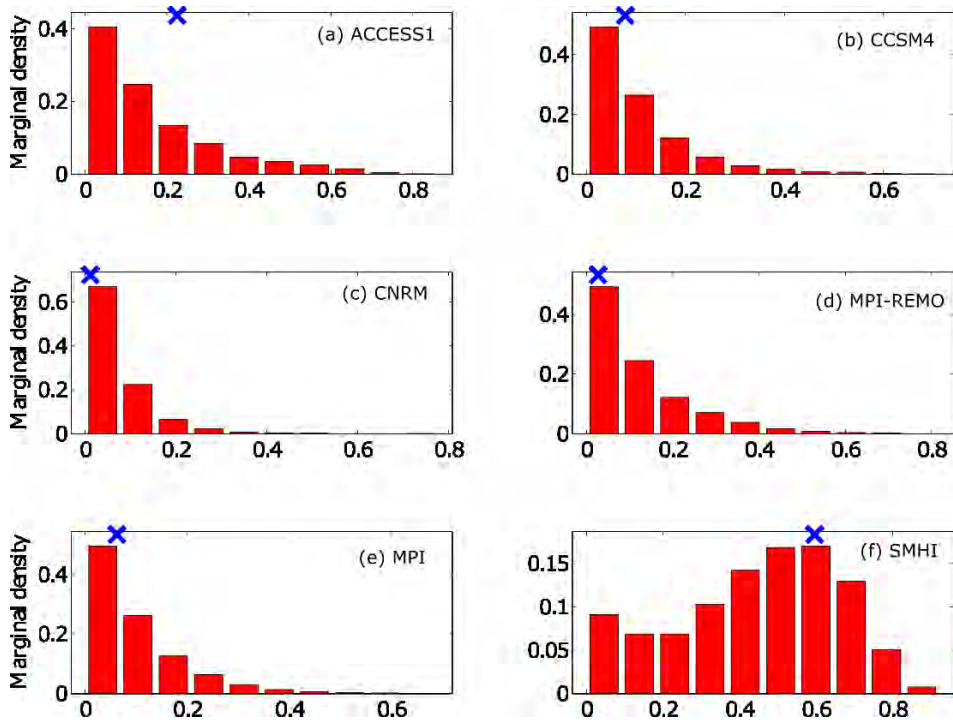


Fig B.11 Marginal posterior pdfs of the DREAM derived BMA weights of monthly rainfall totals for the monsoon of Moulvibazar station.

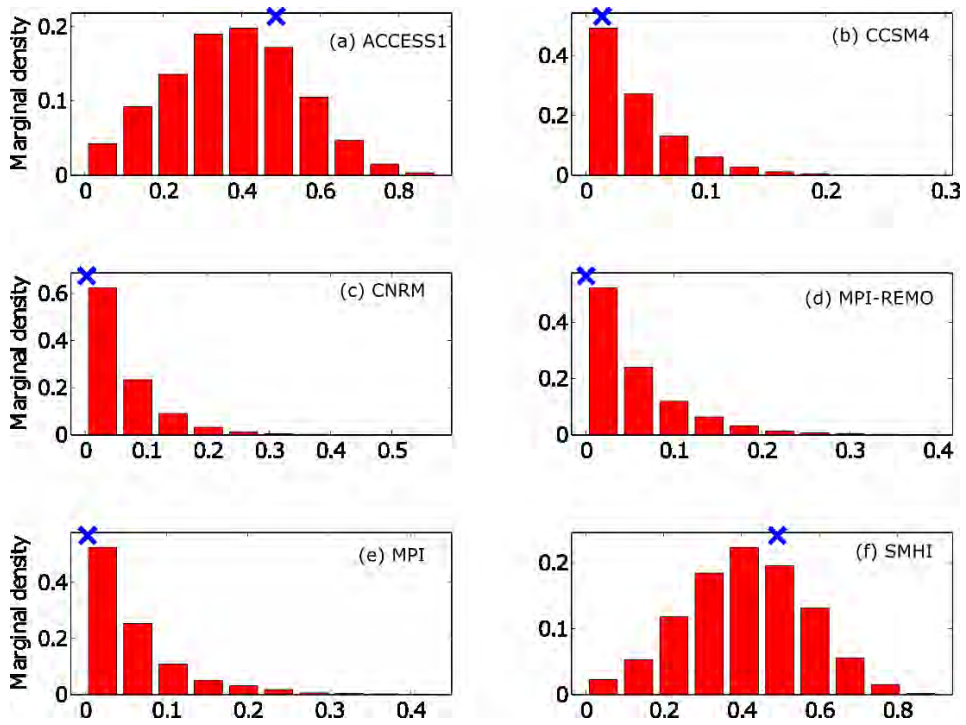


Fig B.12 Marginal posterior pdfs of the DREAM derived BMA weights of monthly rainfall totals for pre-monsoon of Habiganj station.

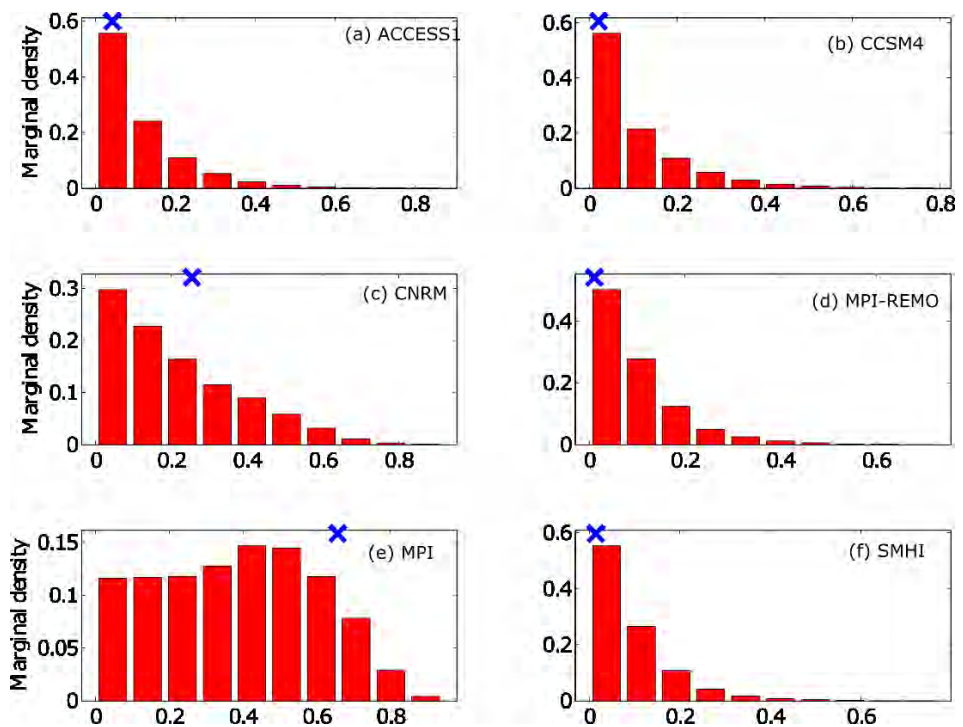


Fig B.13 Marginal posterior pdfs of the DREAM derived BMA weights of monthly rainfall totals for the monsoon of Habiganj station.

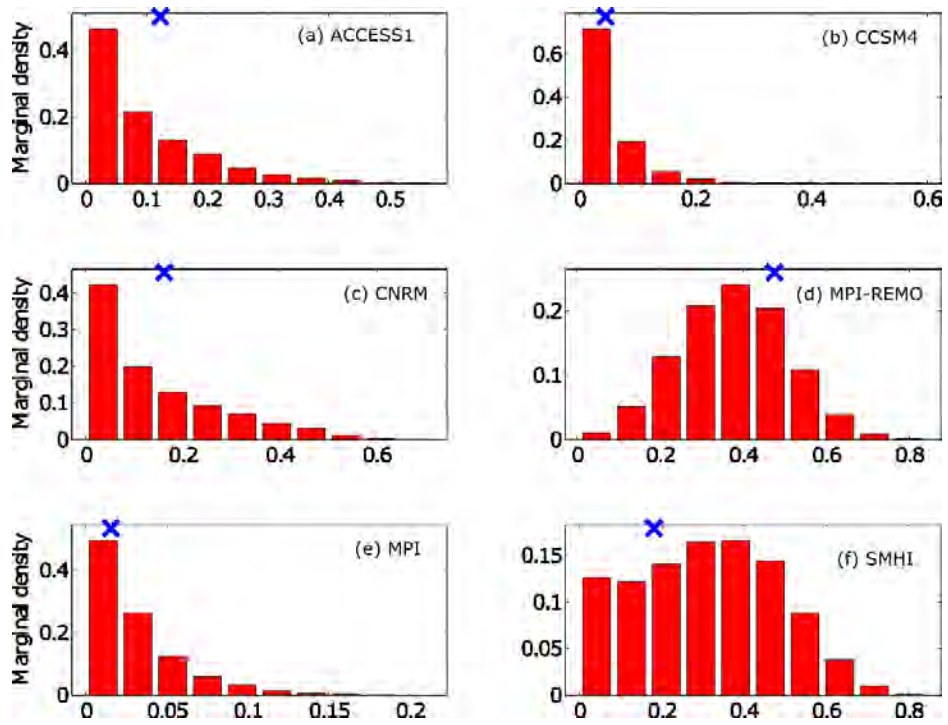


Fig B.14 Marginal posterior pdfs of the DREAM derived BMA weights of monthly rainfall totals for pre-monsoon of Bhairab Bazar station.

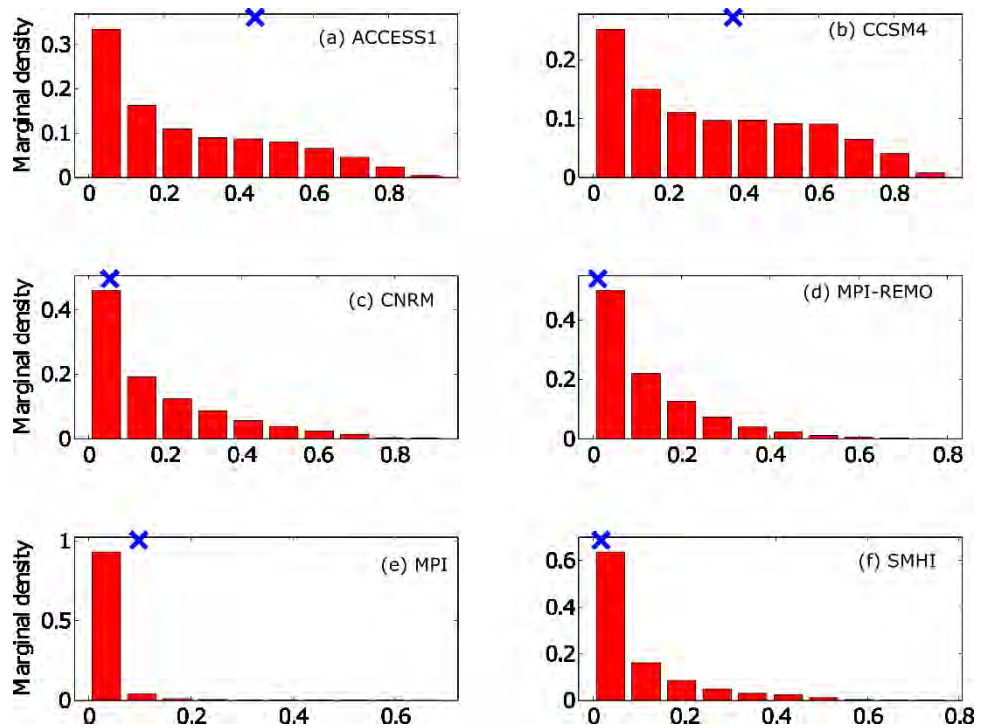
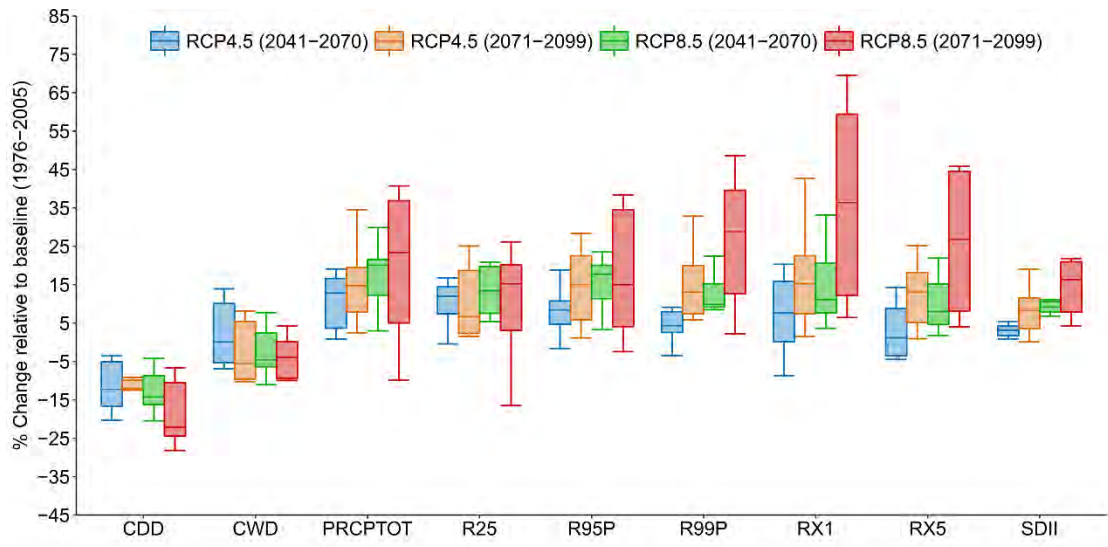
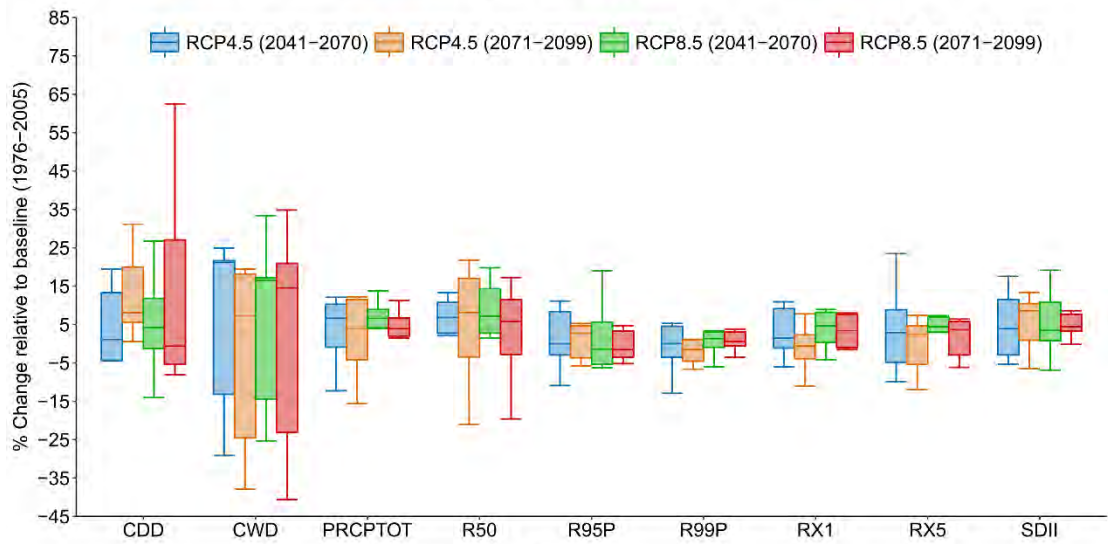


Fig B.15 Marginal posterior pdfs of the DREAM derived BMA weights of monthly rainfall totals for the monsoon of Bhairab Bazar station.

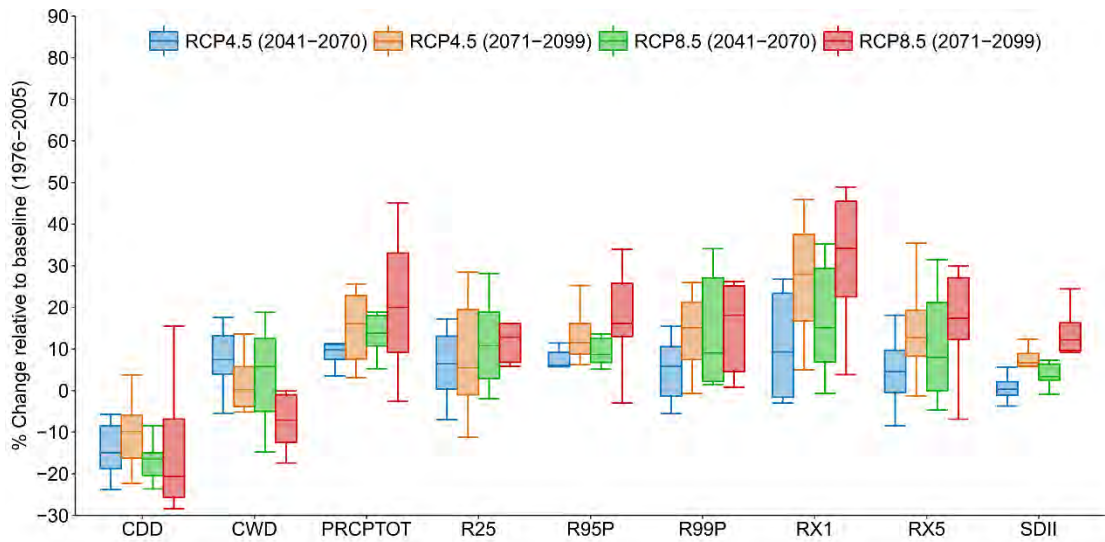


(a) Pre-monsoon

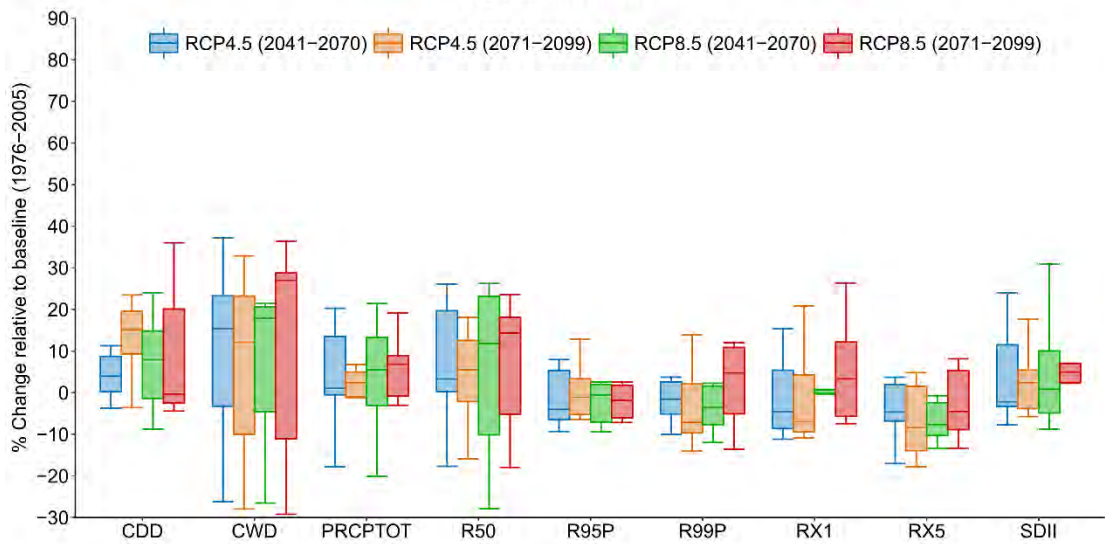


(b) Monsoon

Fig B.16 Box and whisker plots for changes of rainfall extremes of Sunamganj station considering all RCMs for two future time slices (2041-2070 and 2071-2099) relative to the baseline period (1976-2005) under RCP 4.5 and RCP 8.5 scenarios: (a) Pre-monsoon and (b) Monsoon.

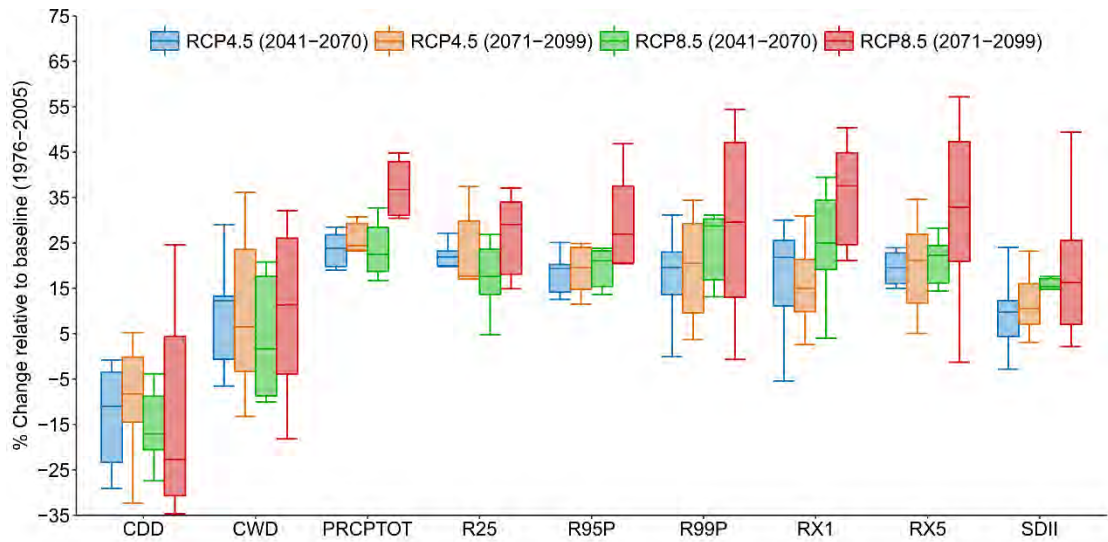


(a) Pre-monsoon

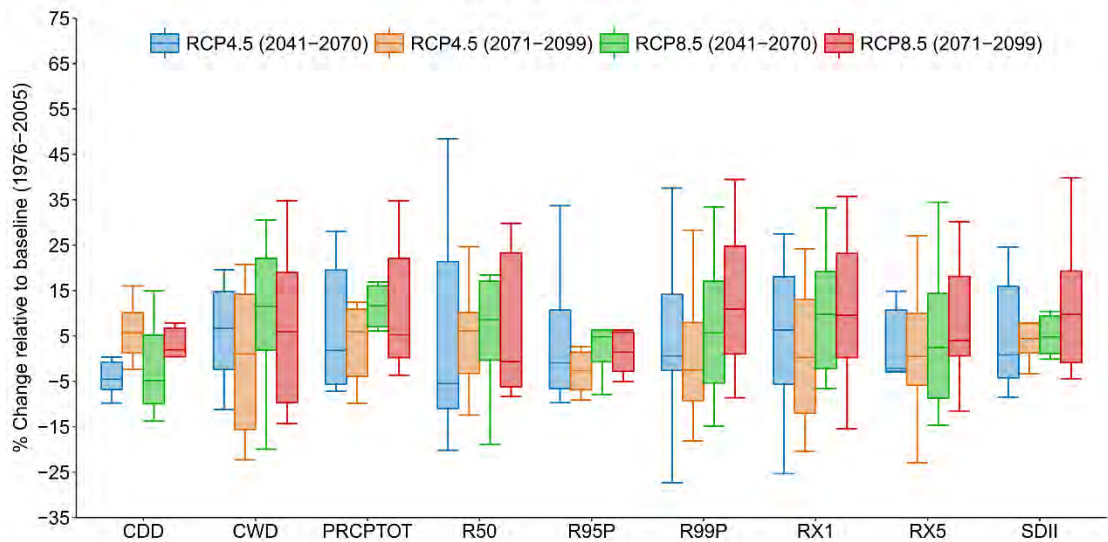


(b) Monsoon

Fig B.17 Box and whisker plots for changes of rainfall extremes of Netrokona station considering all RCMs for two future time slices (2041-2070 and 2071-2099) relative to the baseline period (1976-2005) under RCP 4.5 and RCP 8.5 scenarios: (a) Pre-monsoon and (b) Monsoon.

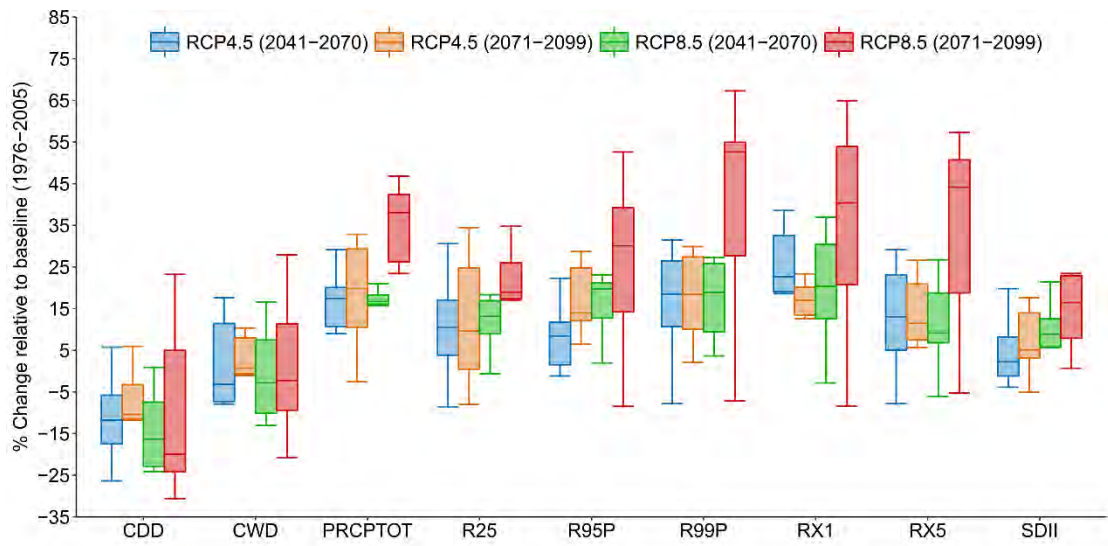


(a) Pre-monsoon

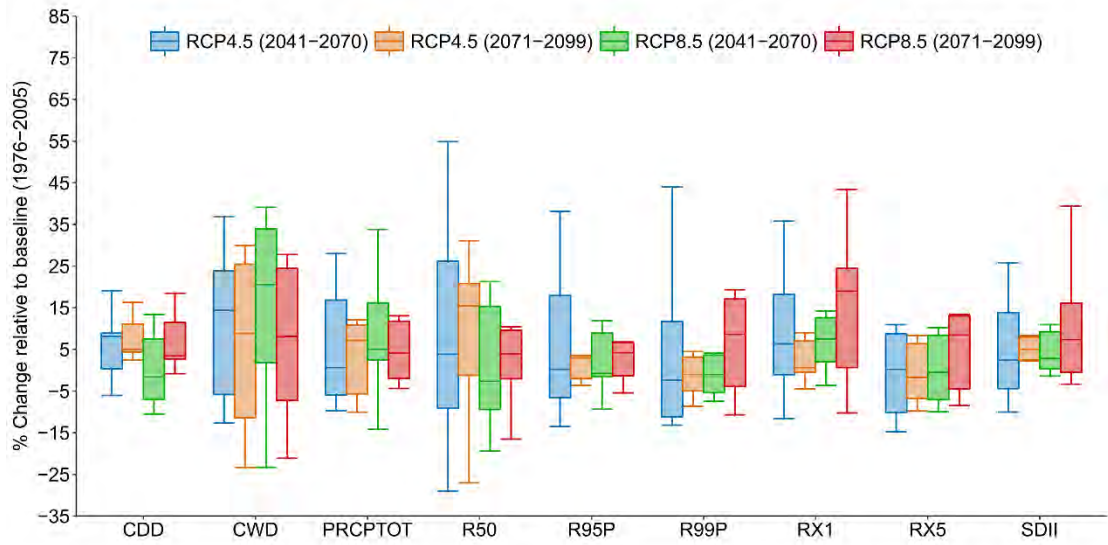


(b) Monsoon

Fig B.18 Box and whisker plots for changes of rainfall extremes of Moulvibazar station considering all RCMs for two future time slices (2041-2070 and 2071-2099) relative to the baseline period (1976-2005) under RCP 4.5 and RCP 8.5 scenarios: (a) Pre-monsoon and (b) Monsoon.

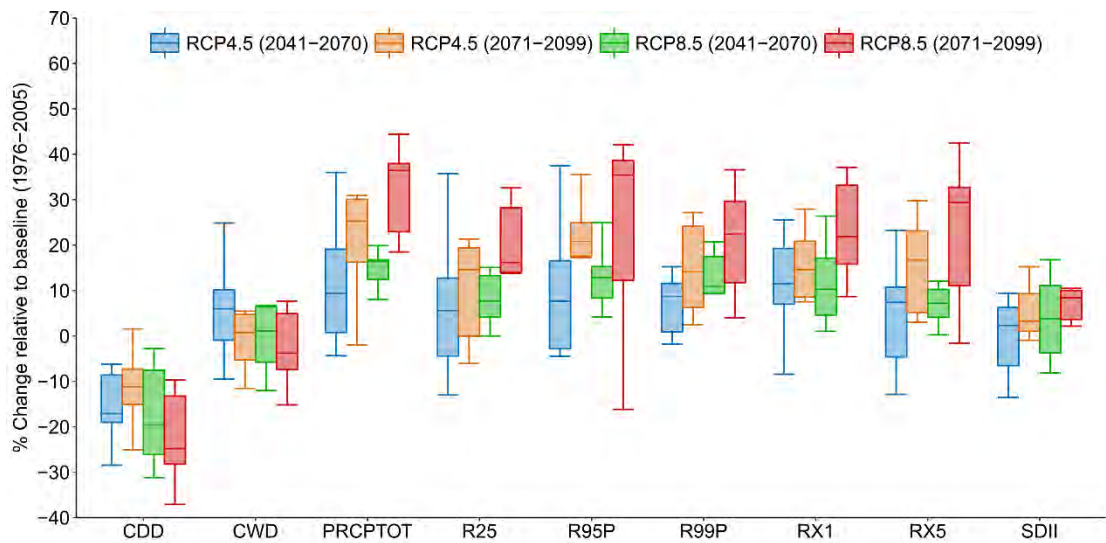


(a) Pre-monsoon

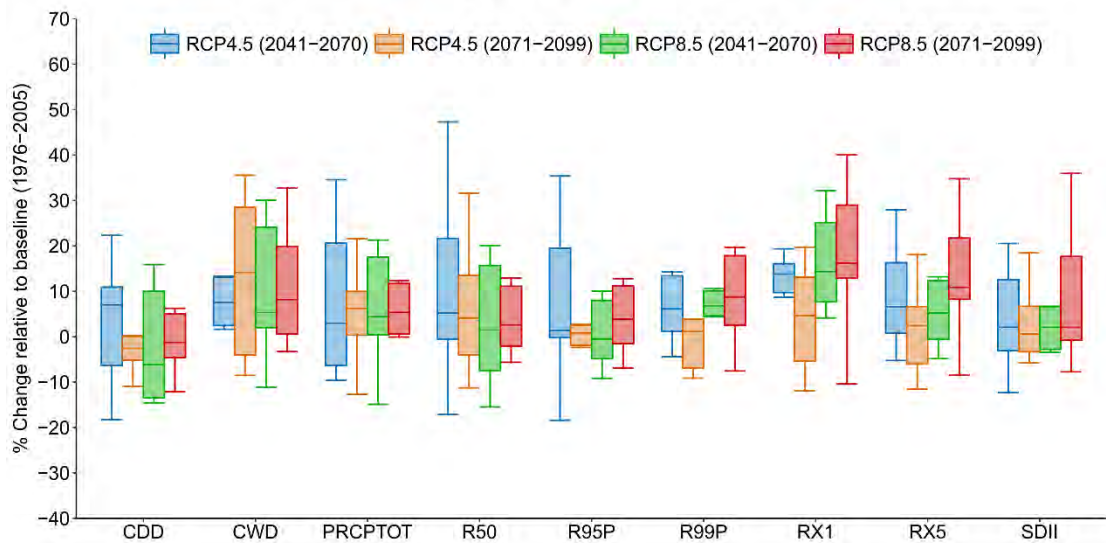


(b) Monsoon

Fig B.19 Box and whisker plots for changes of rainfall extremes of Habiganj station considering all RCMs for two future time slices (2041-2070 and 2071-2099) relative to the baseline period (1976-2005) under RCP 4.5 and RCP 8.5 scenarios: (a) Pre-monsoon and (b) Monsoon.



(a) Pre-monsoon



(b) Monsoon

Fig B.20 Box and whisker plots for changes of rainfall extremes of Bhairabbazar station considering all RCMs for two future time slices (2041-2070 and 2071-2099) relative to the baseline period (1976-2005) under RCP 4.5 and RCP 8.5 scenarios: (a) Pre-monsoon and (b) Monsoon.